TÉCNICO LISBOA

Vibro-Acoustic Source Localization Using the Transmissibility Concept

Duarte Miguel Salvado Pereira

Thesis to obtain the Master of Science Degree in

Aerospace Engineering

Supervisors: Prof. Nuno Manuel Mendes Maia
Prof. Hugo Filipe Diniz Policarpo

Examination Committee

Chaiperson: Prof. Fernando José Parracho Lau
Supervisor: Prof. Nuno Manuel Mendes Maia
Member of the committee: Prof. Miguel António Lopes de Matos Neves

January 2021

Declaration

I declare that this document is an original work of my own authorship and that it fulfills all the requirements of the Code of Conduct and Good Practices of the Universidade de Lisboa.

Resumo

O principal foco deste trabalho consiste em estudar respostas vibro-acústicas utilizando o conceito de transmissibilidade, com o intuito de identificar fontes vibro-acústicas. Para tal, procede-se à adaptação de metodologias numéricas desenvolvidas por outros autores, com o propósito de obter transmissibilidades em estruturas, sistemas acústicos e vibro-acústicos com menor esforço computacional. Complementarmente, este trabalho apresenta métodos experimentais para estimar respostas em sistemas acústicos e vibro-acústicos.

As metodologias numéricas utilizam o método de elementos finitos (implementado no software comercial ANSYS) para discretizar o sistema. Em seguida, as matrizes globais são importadas para o Matlab®, onde são estimadas as transmissibilidades. Usando o conceito de transmissibilidade, são criados códigos Matlab® para a localização de fontes em sistemas vibro-acústicos. Com os modelos experimentais avalia-se a sua próximidade em relação aos modelos numéricos, com o propósito de determinar quais as modificações necessárias para aproximar os dois modelos.

Concluindo, pretende-se que as metodologias desenvolvidas e os resultados obtidos constituam uma contribuição para o campo da transmissibilidade vibro-acústica, que se encontra ainda relativamente pouco desenvolvido.

Palavras Chave: Vibro-Acústica, Conceito de Transmissibilidade, Localização de Fontes, Método de Elementos Finitos, Esforço Computacional

Abstract

This work focuses on the study of vibro-acoustic responses using the transmissibility concept with the purpose of identifying vibro-acoustic sources. To do so, numerical methodologies developed by previous authors are updated to obtain transmissibility functions in structural, acoustic and vibro-acoustic systems with lower computational effort. Additionally, this work features experimental procedures to estimate responses in acoustic and vibro-acoustic systems.

The numerical methodologies use the finite element method (implemented in commercial software ANSYS) to discretize the system. Then, the global matrices are imported to Matlab®, where the transmissibility functions are estimated. Using the transmissibility concept, a Matlab® routine is created to perform source localization in vibro-acoustic systems. The experimental procedures allow evaluating the proximity to the numerical models, as well as determining how these models may be updated.

In conclusion, it is intended that the developed methodologies and obtained results present a contribution to the field of vibro-acoustic transmissibility, which is still relatively undeveloped.

Keywords: Vibro-Acoustics, Transmissibility Concept, Source Localization, Finite Element Method, Computational Effort

Contents

List of Tables

List of Figures

Nomenclature

Acronyms

APDL ANSYS Parametric Design Language.

BEM Boundary Element Method.

CPU Central Processing Unit.

DOF Degree of Freedom.

FE Finite Element.

FEA Finite Element Analysis.

FEM Finite Element Method.

FRF Frequency Response Function.

FSI Fluid Structure Interaction.

MDOF Multiple Degrees of Freedom.

NVH Noise Vibration Harshness.

OTPA Operational Transfer Path Analysis.

OPAX Operational Mount Identification.

SDOF Single Degree of Freedom.

SEA Statistical Energy Analysis.

SPL Sound Pressure Level.

TPA Transfer Path Analysis.

Greek Symbols

β Ratio between excitation frequency and natural frequency.

ϵ Strain.

ϵ_{kl} Strain Tensor.

ϵ_P^s Error Function in Acoustic Source Identification.

ϵ_{VA} Error Function in Vibro-Acoustic Source Identification.

λ Wavelength.

ν Ratio Between Specific Heat Capacities.

ξ Damping Coefficient.

ρ Density.

ρ_0 Equilibrium Density.

σ_{ij} Cauchy's Stress Tensor.

ϕ Oscillation Phase.

ψ Velocity Potential.

Ω Domain Boundaries.

ω Angular Frequency, Excitation Frequency.

ω_n Natural Frequency.

Matrix Operations

-1 Inverse Matrix.

$[inv[A]]$ Inverse of an Arbitrary Matrix $[A]$.

$det[A]$ Determinant of an Arbitrary Matrix $[A]$.

$[adj[A]]$ Adjugate of an Arbitrary Matrix $[A]$.

$+$ Pseudo-Inverse Matrix.

$[cof[A]]$ Matrix of the Cofactors of an Arbitrary Matrix $[A]$.

$[I]$ Identity Matrix.

$[L], [U], [P]$ Lower Triangular, Upper Triangular and Permutations Matrices Obtained from LU Decomposition.

$n \times n$ Dimension of a Square Matrix.

Roman Symbols

A Wave Amplitude.

c Sound Speed.

C_{ijkl} Fourth Order Stiffness Tensor.

$\{F\}$ Harmonic Loads Vector.

F_i Vector of Body Forces.

F_A, F_B, F_C, F_K, F_U Harmonic Load Vectors Applied in the Sets of Coordinates A, B, C, K and U Respectively.

f_1, f_2 Nodal Forces in Spring FE.

$\{f\}$ Vector of Applied Loads.

f Frequency (Hz).

$[H]$ Receptance Matrix.

i Imaginary Unit: $i = \sqrt{-1}$.

k Spring Stiffness, Wave Number.

(k_1, k_2, k_3) Wave Number Components.

$[K], [M], [C]$ Stiffness, Mass and Damping Matrices.

K, U, C, A Known, Unknown and Set of the Remaining Coordinates Respectively. A is the Set of Coordinates where the Loads are Applied.

E, R Grouped Coordinate Sets.

L Acoustic Tube Length.

m Mass.

n Normal Direction.

p Pressure.

$\{P\}$ Harmonic Pressure Vector.

P_U, P_K, P_C Pressure at Coordinates U, K and C Respectively.

p_0 Equilibrium Pressure.

p_r Reflected Wave Pressure; Pressure at Reference DOF r.

p_i Incident Wave Pressure; Pressure at DOF i.

P_{calc} Estimated Pressure Using the Transmissibility Concept.

P_{meas} Pressure Measured in the FE Program.

$p_{imp}, \overline{P}_U$ Imposed Pressure.

p_Ω Boundary Pressure.

$\{Q\}$ Volume Acceleration Vector.

q_u Acoustic Source.

R_1, R_2 Reaction at Nodes 1 and 2 of the Mass-Spring System.

r Reflection Coefficient.

R Universal Gas Constant, Specific Acoustic Resistance.

$T_{UK}^{(A)}$ Displacement Transmissibility Matrix Between Sets U and K with Loads Applied in Set A.

T_{UK} Load Transmissibility between U and K.

T_{UE} Load Transmissibility Between Sets U and E.

T_{RU}^{Z} Acoustic Transmissibility Matrix Between Set R and U in Terms of the Dynamic Stiffness Matrix.

T_{ir}^{u} Acoustic Transmissibility Matrix Between i and r DOFs for a Pressure Imposition at DOF u.

T_{KU}^{H} Acoustic Transmissibility Matrix Between Sets K and U in Terms of the Receptance Matrix.

T_{KU}^{FS} Fluid-Structure Vibro-Acoustic Transmissibility Matrix.

T_{KU}^{SF} Structure-Fluid Vibro-Acoustic Transmissibility Matrix.

T Temperature, Period.

t Time.

T_i^n Stress Vector in the Normal Direction.

u Acoustic Velocity.

u_0 Equilibrium velocity.

u_1, u_2 Nodal Displacements in Spring FE.

u_U, u_K Displacement in Sets U and K Respectively.

V Volume.

v_n Normal Velocity in Shell Elements.

w Displacement in Shell Elements.

$\{X\}$ Harmonic Displacement Vector.

X Specific Acoustic Reactance.

X_K, X_U, X_C Harmonic Displacements in Sets K, U and C.

Z Acoustic Impedance.

$[Z]$ Dynamic Stiffness Matrix.

1 Introduction

Vibration and acoustics are important areas of study in engineering. This work focuses on the study of transmissibility functions in the frequency domain. As described in [1], in multiple degree of freedom (MDOF) systems, the transmissibility functions may be used to estimate unknown dynamical loads transmitted to the supports of a structure, in a steady state regime, from known applied loads. In fact, the transmissibility concept may be applied in many different ways, making the estimation of unknown responses in structural, acoustic and vibro-acoustic systems possible.

Transmissibility plays an important role in the study of vibro-acoustic systems. It allows the engineer to predict how vibrations or acoustic disturbances affect other parts of a structure or acoustic medium. Throughout the present work, the transmissibility analyses are conducted using the Finite Element Method (FEM) combined with Matlab® routines to estimate responses using the transmissibility concept. The FEM is used to discretize the system that is being analysed, and to obtain vibration/-pressure responses at some nodes. These FEM simulated responses are then compared with the ones obtained by using the transmissibility concept, in order to evaluate the reliability of the methodology used to estimate such responses.

This work focuses mainly on the study of transmissibility functions in acoustic and vibro-acoustic systems at low (below 400 Hz) or mid-frequency (between 400 Hz and 500 Hz). In fact, generally, the FEM is not the proper tool to analyse high frequency problems (above 500 Hz). These frequency intervals are taken from [2], and may vary depending on the behaviour of the system in analysis. With the increasing frequency, the finite element (FE) meshes need to be more refined to perform a more precise analysis. However, there are other numerical methods to analyse vibro-acoustic systems, such as:

- The Boundary Element Method (BEM), which is one alternative to the use of the FEM. Though both these methods are somehow similar, while in FEM one analyses the entire domain of the system, in BEM one considers only the outer boundary of the system. Like in the FEM, the BEM also uses nodes and elements, but the FEM is more general in applications, as in BEM the formulation needs to be adapted for the problem being treated. BEM is also not appropriate to study high frequency problems.

- The Statistical Energy Analysis (SEA) is a method suitable for studying the transmission of sound

and vibration at high frequency. As described in [3], SEA is based on the principle of energy conservation, and assumes that all the energy input through mechanical or acoustic excitation leaves the system through structural damping or acoustic radiation. SEA is also suitable to study the transmission of sound and vibration at lower frequencies.

- Hybrid methods that combine the use of FEM/BEM with SEA [2]. These hybrid methods are being developed mostly for the study of problems at the mid-frequency range.

Despite having their own advantages and disadvantages, the methods described above are beyond the scope of this work. Only the FEM is used, as it is the method used by previous authors to study the transmissibility functions in vibration, acoustic and vibro-acoustic MDOF systems. Furthermore, the ease of data transfer between the FE software and Matlab® , makes the FEM suitable to perform early studies in vibro-acoustic transmissibility. The FE software used throughout this work is ANSYS, using ANSYS Parametric Design Language (APDL) . ANSYS software allows the user to extract the global assembled matrices of the FE model. These matrices can be imported to Matlab®, allowing their use to estimate responses in the system using the transmissibility concept.

The results presented in this work are obtained using the following methodology. First, one creates a FE model in ANSYS APDL and extracts the globally assembled matrices from it. Then, the global matrices are imported to Matlab®, the transmissibility functions are computed, and the responses estimated. The loads are then applied in the FE model, and a harmonic analysis is performed to obtain the responses at specific nodes of the system. The responses obtained from ANSYS are then compared to those obtained from Matlab® using the transmissibility concept. After verifying that the transmissibility concept is producing proper results, one can use it to identify the source that creates the measured response.

Therefore, throughout this work are presented the results of steady state responses in the frequency domain using transmissibility functions, as well as the results of the identification of sources in systems with increasing complexity. The relative quality of the results dictates the potential of using the transmissibility concept in MDOF vibro-acoustic systems.

Additionally, an experimental procedure is used to obtain pressure responses in acoustic and vibro-acoustic systems. The main objective is to compare the experimental and numerical results, to evaluate the need for model updating in the numerical models.

1.1 Brief State of the Art

Research articles concerning vibration, acoustic and vibro-acoustic analyses are abundant in science literature. However, the majority of these articles are related to computational or experimental analyses of a specific component. For example, in vibro-acoustics, these papers discuss the influence of a certain vibrating component in the surrounding acoustic medium. In fact, despite the large number of articles available in the literature concerning vibration, acoustics or vibro-acoustics, the presence of the transmissibility concept is still, as mentioned in [4], quite scarce.

In the last two decades, research articles concerning transmissibility in structures or in acoustic cavities started to appear, increasing knowledge in this concept and in its properties. Yet, the transmissibility concept remains relatively undeveloped in the field of vibro-acoustics.

The transmissibility concept in a simple single degree of freedom (SDOF) mass-spring system is well-known and widely spread in the literature concerning vibration. The transmissibility concept in MDOF systems is a more recent and uncommon concept.

In [5], are presented the theoretical fundamentals for displacement and force transmissibility in MDOF structural systems. These theoretical fundamentals are relevant to the present work. Also in [5], are provided examples of application of the transmissibility concept in MDOF mass-spring systems. An example of a MDOF mass-spring system is also presented in [1], along with the problem of force identification.

The problem of using transmissibility for the estimation or identification of forces is also presented in [6, 7, 8, 9] for beams, and may also be used to perform damage detection in structures, as discussed in [10, 11].

Other studies concerning structural transmissibility in MDOF systems present an experimental evaluation of the transmissibility matrix. In [12], the validity of the transmissibility functions is tested by comparing them with those calculated through frequency response functions (FRFs).

Most of the articles quoted, mainly focus on studying vibration transmissibility for harmonic load inputs. However, the transmissibility concept is also valid for random load inputs, as described in [13].

The works and advances in acoustic transmissibility are more recent. Analytical derivations for evaluating acoustic transmissibility are presented in [14, 15]. In [16, 17], the transmissibility concept is applied to acoustics to estimate unknown pressure responses in some parts of the acoustic fluid for a given set of known pressures at other points in the acoustic domain. In [16], the author also presents a strategy for pressure identification in acoustic domains, and provides a practical computational example of a 2D aircraft enclosure. This article describes some methodologies that are used throughout the present work, regarding the transmissibility analysis of acoustic systems.

In [18], the authors use the MDOF transmissibility concept to perform Noise Vibration Harshness (NVH) source contribution analysis in an automobile, and highlight the importance of the transmissibility concept for NVH engineers. According to the authors, the importance of this method relies on the fact that transmissibility functions can be obtained from operational measurements, and do not require the computation of FRFs (experimental methods to obtain FRFs may be found in [19]). The authors also compare the results obtained for NVH source contribution using the transmissibility concept, with those obtained from a classical source substitution method.

Other studies in the field of acoustics that are not necessarily related to transmissibility, but that are relevant to the present work, are the ones performed in [20, 21]. The previously cited articles highlight the importance of having at least 36 elements per wavelength when performing finite element analysis (FEA) in acoustics. According to [20], in order to achieve a relatively small error (less than 10%) when compared to the analytical solution of a reflective tube with a unitary pressure applied at one of the ends, one will need at least 36 elements per wavelength.

As previously mentioned, the presence of vibro-acoustic transmissibility in the literature is scarce [4].

Theoretical models for MDOF transmissibility in vibro-acoustic systems can be found in [22]. In [22], the authors also discuss possible uses of the transmissibility concept in Transfer Path Analysis (TPA) and Operational Transfer Path Analysis (OTPA).

In [4], the transmissibility concept is used to estimate pressures at the mid-section of an acoustic tube with a structural elastic plate at one of the ends that is subjected to a harmonic load. The same system is also studied in the present work for verification purposes. In addition, some of the methodologies developed in the present work are adapted from the ones described in [4], making this, one of the most relevant references to the present work.

It was also mentioned earlier that despite the presence of vibro-acoustic transmissibility being scarce in the literature, there are several articles concerning vibro-acoustic analysis of MDOF systems using computational and/or experimental methods. For example, the case of vibro-acoustic systems composed of composite materials is addressed in [23], in which ANSYS is used to perform a modal analysis of a composite plate with the aim of extracting the natural frequencies. Additionally, it uses LMS Virtual Lab to estimate the acoustic responses produced by the vibrating plate in a laboratory environment. It also highlights the importance of conducting the experimental procedure in an anechoic chamber to reduce the error between the computational and experimental results.

The study of vibro-acoustics applied to vehicles and/or parts of vehicles is quite spread in the literature. In [24], the authors study the vibro-acoustic responses in a vehicle interior and exterior due to cleat impacts. In [25], a FE model is developed in ANSYS to study the acoustic and vibro-acoustic behaviour of a ship compartment. The vibro-acoustic analysis of a truck-cabin is discussed in [26]. Also, [27] uses computational simulations and experimental analyses to study an external gear pump, and in [28], the authors study the technical condition of an engine water pump by performing a vibro-acoustic analysis.

In the present work, a transmissibility analysis of a vibro-acoustic cavity is performed. Therefore, one also searched for available information in the literature concerning the acoustic and vibro-acoustic behaviour of cavities. An example of a vibro-acoustic cavity is presented in [2], in which are compared the results of computational simulations and experimental tests in a rectangular enclosure with a flexible panel. The range of frequencies at which the FEM/BEM, SEA and hybrid FEM/SEA methods are valid, is also discussed by the authors. Other interesting works are the ones presented in [29, 30]. Here, the authors use the inverse FEM to identify noise sources in acoustic cavities. These works use FE models of a wooden box cavity and of a fuselage compartment.

Since one of the models developed and studied throughout the present work is a simplified aircraft interior, it is also interesting to search for papers in which the concept of transmissibility is applied to aircraft vehicles. The study of structure-borne transmissibility in an aircraft vibration damper using FEA and SEA is presented in [31]. In addition, there are some studies in which the vibro-acoustic analysis is applied to the aerospace industry. In [32], the authors study the in-flight aero-acoustics of expandable launch vehicles, and the proper placement and design of adapters to protect the sensors during hostile conditions. Besides this, [32] also discusses the vibro-acoustic modelling of payload fairings using FEM/BEM and SEA.

Taking into account that many of the research papers previously mentioned use numerical analyses,

it is opportune to mention that methods like FEM/BEM and SEA have several limitations, specially in analysing the acoustic or vibro-acoustic behaviour of systems at the mid-frequency range. The problem of mid-frequency is briefly discussed in [33], in which it is mentioned that despite the recent works in hybrid FEM/SEA methods, the analysis at the mid-frequency range is still challenging and still needs a more appropriate method.

The previously mentioned articles are only a relatively small part of those in the literature. A detailed bibliographical revision in vibration, acoustic, vibro-acoustics and transmissibility requires many other citations. Therefore, the articles presented contain the information that the author considers to be the most relevant to his research.

1.2 Motivation

The study of the transmissibility concept in vibro-acoustic systems is still, somehow, underdeveloped. As described in section 1.1, this concept has proved to be suitable to estimate vibration in solid structures, and pressure responses in acoustic domains. Furthermore, it has proved to be able to perform source identification in structural and acoustic systems. These potentialities of the transmissibility concept make it prone to be used in mechanical, naval and aerospace industries, specially in OTPA.

TPA is defined in [34], as the test-based or simulation based procedure that allows the engineer to trace the flow of vibro-acoustic energy from a source, through a set of known structure and air-borne transfer pathways to a given receiver's location. In fact, as mentioned in [34], in complex structures such as an aircraft, the vibro-acoustic sensations experienced by an observer may have been caused by a vibration or acoustic source somewhere else in the structure or fluid domain. TPA is used to solve this problem by assessing the structure and airborne energy paths between the excitation source and the receiver's location [34].

The transmissibility-based TPA differs from the generality of other methods used to perform TPA. Since the transmissibility functions are independent of the magnitude of the applied loads, transmissibility-based TPA avoids the explicit determination of the applied loads [35]. It is also mentioned in [35] that in transmissibility-based TPA, the transfer paths are determined by using transmissibility functions between sensors that can be calculated using operational measurements.

According to [36], despite having the same mathematical formulation, OTPA and TPA are actually quite different. TPA is based on a load-response relationship and OTPA is based on a relation between responses. This means that in TPA, one can establish the effect of a certain load in the total response, and in OTPA one can only establish a similarity between the target and the input responses [36]. In addition, as described in [36], OTPA may use transmissibilities instead of noise transfer functions (used in TPA) that depend on the applied loads. So, given the conditions and properties of transmissibility, it is suitable for OTPA.

Another method called OPAX [35, 37] (Operational mount identification), is a hybrid method that combines the physical understanding gained from the TPA methodologies with the identification potential of OTPA.

As the use of transmissibility in TPA and OTPA is already being investigated, it is opportune to study transmissibility in vibro-acoustic systems so that it can also be applied in the industry for such systems. Further development and increasing knowledge in the transmissibility concept applied to MDOF vibro-acoustic systems is, therefore, one of the main motivations of the present work.

Another interesting use of transmissibility in vibro-acoustic systems is to estimate responses at coordinates of difficult access in complex systems, such as an aircraft, a train, or a car, by knowing the responses at some coordinates.

Summarizing, the author intends that the advances achieved with the present work may be used not only in the estimation of responses at coordinates that are sometimes neglected due to their difficult access, but also in the aim of TPA and OTPA methodologies.

1.3 Objectives

In the last few years, a considerable number of research work was done in the field of MDOF transmissibility. Yet, the references to vibro-acoustic transmissibility and, more specifically, to the use of vibro-acoustic transmissibility to perform source identification are quite scarce. The descriptions of the FEM for coupled and uncoupled vibro-acoustic problems have been longly available in several research papers. However, it was only in the recent past that these models started being used to study transmissibility in vibro-acoustic systems. In fact, theoretical definitions in vibro-acoustic transmissibility were only found in [4, 22].

The present work uses the methodologies developed in [4] to start obtaining some results in this area, using the FEM and the transmissibility concept. It is further intended to apply these methodologies to the problem of source identification using the transmissibility concept.

Vibro-acoustic transmissibility can be used in two ways: to estimate the displacement response in the structural part of the system for a given imposed pressure (fluid-structure transmissibility); to estimate the pressure in the acoustic medium for a given imposed displacement on the structural plate (structure-fluid transmissibility). The present work only studies coupled vibro-acoustic problems in which the thickness of the structural shell is not enough to be considered rigid, and focuses on the study of structure-fluid transmissibility.

The main purpose of the present work is to study structure-fluid transmissibility, in particular, to use transmissibility to estimate the pressure at a given set of coordinates (unknown pressures) when displacement measurements are available at a set of known coordinates (known displacements). This is done by studying vibro-acoustic systems (with fluid-structure interactions (FSI)) with increasing complexity. The present work addresses mainly the point to point (scalar) transmissibility, in which the transmissibility function corresponds to the pressure/displacement ratio. After validating the model that calculates the transmissibilities by comparing the results obtained using the transmissibility concept with the results obtained from the harmonic analysis in ANSYS APDL, it is further intended to use the transmissibility concept to study the problem of source localization. So, another major objective of the present work is to study the potential of the transmissibility concept for source identification in vibro-acoustic systems.

One major problem that arises from the transmissibility analysis in Matlab®, is the computational time spent. In fact, the computation of transmissibility matrices requires, many times, the inverse of the dynamic stiffness matrix. However, in most cases, the computation of the transmissibility matrix requires only a few entries of the receptance matrix (the inverse of the dynamic stiffness matrix). The inversion of matrices is usually a very demanding procedure that requires considerable computational power and, as a consequence, a considerable amount of time. In the present work, one also presents an approach to obtain only the required entries of the receptance matrix, without computing the entire inverse of the dynamic stiffness matrix. This allows to reduce the simulation time, and opens the door to the analysis of more complex systems that require larger FE meshes. Also, without some code optimization, the simulation times would become relatively high, and it would not be possible to approach the source identification problem.

Wrapping it up, in the present work it is intended to develop a more efficient version of the Matlab® routines that evaluate transmissibility functions in vibro-acoustic systems, and to perform source identification in these same systems. Thus, the present work has three main objectives: the first is to develop a more efficient way to obtain the desired entries of the receptance matrix; the second is to study if it is possible to estimate a pressure response for a given known displacement in a vibro-acoustic system, using the transmissibility concept; the third is to study if it is possible, giving a certain pressure response measurement, to find the correct displacement source using vibro-acoustic transmissibility in an inverse method of source identification.

1.4 Thesis Outline

The present work aims to increase knowledge in vibro-acoustic transmissibility, and to analyse vibro-acoustic systems with increasing complexity. It intends to present the necessary theoretical grounds to perform such analyses, as well as the methodologies used to obtain the presented results. A critical analysis of the obtained results is presented, and some conclusions are drawn along with future perspectives.

The first chapter is the introduction, in which is presented a brief introduction on the methods that are used to evaluate vibro-acoustic transmissibility, on the possible applications of the studies conducted in today's industry, and on the objectives intended to be achieved. A brief bibliographical revision in areas of interest such as vibration, acoustics, vibro-acoustics, and transmissibility is also presented.

The second chapter contains the theoretical definitions that are necessary to understand the problems discussed along this document. This chapter addresses several subjects concerning vibration in MDOF systems, acoustic waves, and transmissibility in structural, acoustic and vibro-acoustic systems. A brief description on the FEM in structural, acoustic and vibro-acoustic systems is also provided in this chapter.

The third chapter describes the methodologies implemented to solve several transmissibility problems. This chapter shows how the theoretical concepts introduced in the second chapter can be used to solve these problems. The methodology developed to improve the Matlab® code that computes the

transmissibility matrices is also presented in the third chapter.

Chapter four presents the results obtained with the methodologies described in the third chapter, and a critical discussion of such results. Several types of results are presented in this chapter:

- Verification results in structural, acoustic and vibro-acoustic systems. In this chapter, the results obtained with the implemented methodologies are compared with results available in the literature, in order to evaluate if these methodologies are producing correct results.
- Results of the analyses of several acoustic and vibro-acoustic systems with increasing complexity. This includes: the estimation of unknown pressures in acoustic domains for a given pressure imposition using acoustic transmissibility; the estimation of unknown pressures in acoustic domains for a given load/displacement imposition on the elastic structure of a coupled vibro-acoustic system using transmissibility; the localization of the unknown sources of disturbance in acoustic and vibro-acoustic systems using the transmissibility concept. The systems studied include an acoustic and vibro-acoustic cavity similar to the one presented in [38], and acoustic and vibro-acoustic models of a simplified aircraft interior.
- Comparison of simulation times between two different but equivalent ways of obtaining the entries of the receptance matrix. A comparison is made between the elapsed and Central Processing Unit (CPU) times obtained from both methods.

With the information presented in chapters 2, 3 and 4, one is able to understand how these results are obtained, and what is the theory behind the implemented methodologies.

Finally, the fifth chapter presents the conclusions drawn from analysing the results presented in the fourth chapter.

2 Theoretical Background

In this chapter, the theoretical fundamentals considered necessary for the present work concerning vibrations, acoustics, vibro-acoustics, transmissibility, and FE theory are presented.

2.1 Elastodynamics

When the loads applied to an elastic solid are in equilibrium, the solid remains at rest or at constant speed. However, when this equilibrium is disturbed, the solid will undergo accelerations. This is the subject of study in elastodynamics [39].

A body that is subjected to external loads develops a state of inner stresses that may be quantified by the Cauchy's stress tensor. The Cauchy's stress tensor relates the stress vector with the unit vector normal to the boundary surface of the solid element in the following manner [4]:

$$T_i^n = \sigma_{ij} n_j \tag{2.1}$$

where T_i^n is the stress vector, σ_{ij} is the Cauchy's stress tensor and n_j is the vector along the normal direction to the reference surface.

When a volume V with a boundary surface S undergoes surface stresses T_i^n, and body forces F_i, the equation of conservation of momentum can be derived, as in [40], by applying Newton's second law.

$$\frac{d}{dt}\int\int\int_V \frac{\partial u_i}{\partial t}\rho dV = \int\int\int_V F_i dV + \int\int_S \sigma_{ij} n_j dS \tag{2.2}$$

By applying the divergence theorem to the surface integral in equation 2.2, and assuming that ρ is approximately constant, one can obtain [40]:

$$\frac{\partial \sigma_{ij}}{\partial x_j} + F_i = \rho \frac{\partial^2 u_i}{\partial t^2} \tag{2.3}$$

where ρ is the mass density of the solid and u is the displacement vector.

The strains ϵ can be related to the displacements by the following linearised equation [40]:

$$\epsilon_{ij} = \frac{1}{2}\left(\frac{\partial u_i}{\partial x_j} + \frac{\partial u_j}{\partial x_i}\right) \tag{2.4}$$

and the stress tensor is related to the strain tensor by the constitutive equations. For elastic materials, the generalization of Hooke's law is used to relate the stresses and strains. The constitutive equation is, therefore, given by:

$$\sigma_{ij} = C_{ijkl}\epsilon_{kl} \tag{2.5}$$

where C_{ijkl} is the fourth order stiffness tensor.

2.2 Spring Element

The spring FE is one of the most common FEs in discrete systems. It can be characterized as illustrated in figure 2.1, which involves only stiffness (k), forces (f_1, f_2) and displacements (u_1, u_2). No inertias are involved in this element.

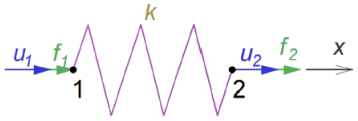

Figure 2.1: Spring FE [41].

Using Hooke's law and performing static equilibrium, one can get [4]:

$$\begin{bmatrix} k & -k \\ -k & k \end{bmatrix} \begin{Bmatrix} u_1 \\ u_2 \end{Bmatrix} = \begin{Bmatrix} f_1 \\ f_2 \end{Bmatrix} \tag{2.6}$$

where the matrix concerning the k values is the stiffness matrix $[K]$.

2.3 Vibration in MDOF Systems

The original form of the equation of motion of a MDOF system may be written as follows [42]:

$$[M]\{\ddot{x}(t)\} + [C]\{\dot{x}(t)\} + [K]\{x(t)\} = \{f(t)\} \tag{2.7}$$

where $[M]$ is the mass matrix, $[C]$ is the damping matrix, $[K]$ is the stiffness matrix, $\{x(t)\}$ is the vector of displacements, and $\{f(t)\}$ is the vector of applied loads. The first and second time derivatives of $x(t)$ are $\dot{x}(t)$ and $\ddot{x}(t)$, respectively. Considering that in steady state regime, the displacement and dynamic load are harmonic functions, and using complex algebra, the previous equation becomes

$$(-\omega^2[M] + i\omega[C] + [K])\{X\} = \{F\} \tag{2.8}$$

where ω is the angular frequency. The previous equation can be rewritten as

$$[Z]\{X\} = \{F\} \tag{2.9}$$

where $[Z]$ is the dynamic stiffness matrix given by the following equation.

$$[Z] = [K] + i\omega[C] - \omega^2[M] \tag{2.10}$$

Having defined the dynamic stiffness matrix, one can now define the system's FRF. These FRFs describe the dynamic behaviour of the system in the frequency domain. The receptance matrix $[H]$ appears in this context, and relates the dynamic displacements with the dynamic loads applied to the system in the following manner [4].

$$\{X\} = [H]\{F\} \tag{2.11}$$

Analysing the previous equation, it is clear that the receptance matrix is the inverse of the dynamic stiffness matrix.

Considering now an undamped MDOF system in free vibration, one obtains the following equation [42].

$$([K] - \omega^2[M])\{X\} = 0 \tag{2.12}$$

This equation has one trivial solution ($\{X\} = 0$), and the remaining solutions are given by the solution of the following eigenvalue and eigenvectors problem.

$$det([K] - \omega^2[M]) = 0 \tag{2.13}$$

By solving the problem one obtains the natural frequencies (ω_n) and the corresponding mode shapes, given by the eigenvectors $\{X\}$.

2.4 The Transmissibility Concept

The transmissibility concept is presented in many classic textbooks on vibrations, associated to simple fixed-free or guided-free systems. For the case illustrated in figure 2.2, the differential equation of motion becomes

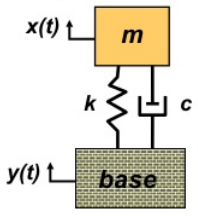

Figure 2.2: SDOF system with its base moving harmonically [43].

$$m\ddot{x} + c(\dot{x} - \dot{y}) + k(x - y) = 0. \tag{2.14}$$

The displacement of the base is harmonic and can be written as

$$y = Ye^{i\omega t} \tag{2.15}$$

and the response can be expressed in the following manner

$$x = Xe^{i(\omega t - \phi)} \tag{2.16}$$

where ϕ is the oscillation's phase. Replacing the two previous equations in 2.14 and with some more algebra, one obtains [42]:

$$\frac{X}{Y} = \sqrt{\frac{1 + (2\xi\beta)^2}{(1-\beta^2)^2 + (2\xi\beta)^2}} \tag{2.17}$$

where $\xi = c/2m\omega_n$ is the damping coefficient and $\beta = \omega/\omega_n$. The ratio between the magnitude of the response X and the magnitude of the imposed displacement Y, is the transmissibility.

In a SDOF system it is also possible to talk about force transmissibility. Considering the same system as before, but with a fixed base and a harmonic load applied to the mass, the ratio between the magnitudes of the transmitted and applied loads is given by the following expression [42].

$$\frac{F_{Tr}}{F_{ap}} = \sqrt{\frac{1 + (2\xi\beta)^2}{(1-\beta^2)^2 + (2\xi\beta)^2}} \tag{2.18}$$

This ratio is the force transmissibility in SDOF systems, where F_{ap} is applied to the SDOF and F_{T_r} is the reaction at the fixed degree of freedom (DOF). One can state that the previous equation is similar to equation 2.17, but the systems have different boundary conditions. Summarizing, the transmissibility concept in "two-point" systems can be defined as the ratio between the amplitude of the response and the amplitude of the imposed disturbance.

In the last two decades, this concept has been generalized to the MDOF systems. As mentioned in [5], such generalization has been not only developed in terms of a relation between two sets of harmonic responses for a given loading, but also between applied forces and corresponding reactions.

2.4.1 Transmissibility of Motion

Here, the main definitions of vibrational transmissibility are presented as in [5].

2.4.1.1 Fundamental Formulation

This formulation is based on harmonically applied forces and uses relations between forces and responses in terms of receptance. Defining a vector F_A of magnitudes of applied forces at a set of coordinates A, a vector X_U of unknown response amplitudes at coordinates U, and a vector X_K of known response amplitudes at coordinates K, as represented in figure 2.3,

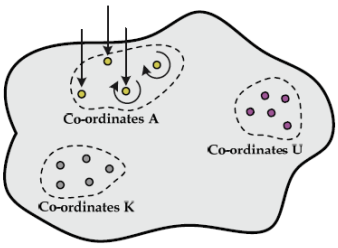

Figure 2.3: System with coordinates A where the forces are applied, coordinates U of unknown response amplitudes, and coordinates K of known response amplitudes [5].

one may write the following equations:

$$X_U = H_{UA} F_A \tag{2.19}$$

$$X_K = H_{KA} F_A \tag{2.20}$$

where H_{KA} and H_{UA} are submatrices of $[H]$. Relating the two previous equations, it is possible to eliminate F_A and obtain the following relation.

$$X_U = H_{UA} H_{KA}^{+} X_K \tag{2.21}$$

Defining the transmissibility matrix as

$$T_{UK}^{(A)} = H_{UA} H_{KA}^{+} \tag{2.22}$$

the relation between the known responses and unknown responses using the transmissibility matrix may be obtained as follows.

$$X_U = T_{UK}^{(A)} X_K \tag{2.23}$$

It is important to notice that: the set of coordinates A does not need to coincide with the set of coordinates K; in order for the pseudo-inverse to exist, K must be equal or greater than A; the transmissibility matrix does not depend on the magnitude of the applied forces.

2.4.1.2 Alternative Formulation

One alternative approach consists of evaluating the transmissibility matrix from the dynamic stiffness matrix.

The dynamic behaviour of a MDOF system is given, in the frequency domain, by equation 2.9. From the set of dynamic responses, it is possible to define two subsets of coordinates U and K; from the set of dynamic loads, it is possible to define two sets of coordinates A and B, in which A is the subset of coordinates where the loads may be applied, and B is the set of the remaining coordinates where the

loads are never applied. Thus, $\{X\}$ and $\{F\}$ can be written as follows.

$$\{X\} = \begin{Bmatrix} X_K \\ X_U \end{Bmatrix}, \{F\} = \begin{Bmatrix} F_A \\ F_B \end{Bmatrix} \tag{2.24}$$

Replacing equation 2.24 in 2.9, one can obtain the following relation:

$$\begin{bmatrix} Z_{AK} & Z_{AU} \\ Z_{BK} & Z_{BU} \end{bmatrix} \begin{Bmatrix} X_K \\ X_U \end{Bmatrix} = \begin{Bmatrix} F_A \\ F_B \end{Bmatrix} \tag{2.25}$$

as the subset of coordinates B is the one where the loads are never applied, then $F_B = 0$. Considering that B is equal or greater than U, the vector of unknown responses can be obtained:

$$X_U = -Z_{BU}^{+} Z_{BK} X_K \tag{2.26}$$

and the transmissibility matrix can be defined as presented below, with forces applied at A but not at B.

$$T_{UK}^{(A)} = -Z_{BU}^{+} Z_{BK} = H_{UA} H_{KA}^{+} \tag{2.27}$$

2.4.2 Transmissibility of Forces

In a "two point" system, the transmissibility of forces is defined as the ratio between the transmitted load and the applied one. For a more generic case of MDOF systems, it is necessary to relate the known applied loads F_K to the unknown reactions F_U. This can be achieved in two different approaches.

2.4.2.1 In Terms of Frequency Response Functions

Considering X_K and X_U to be the responses corresponding to F_K and F_U respectively, and X_C to be the responses at the remaining coordinates then:

$$\begin{Bmatrix} X_K \\ X_U \\ X_C \end{Bmatrix} = \begin{bmatrix} H_{KK} & H_{KU} \\ H_{UK} & H_{UU} \\ H_{CK} & H_{CU} \end{bmatrix} \begin{Bmatrix} F_K \\ F_U \end{Bmatrix}. \tag{2.28}$$

Assuming that the responses at the reaction coordinates are equal to zero ($X_U = 0$), one can obtain

$$F_U = -H_{UU}^{-1} H_{UK} F_K. \tag{2.29}$$

Thus, the transmissibility matrix can be defined in the following manner.

$$T_{UK} = -H_{UU}^{-1} H_{UK} \tag{2.30}$$

2.4.2.2 In Terms of Dynamic Stiffness

Regarding this approach, one can write:

$$\begin{Bmatrix} F_K \\ F_U \end{Bmatrix} = \begin{bmatrix} Z_{KK} & Z_{KU} & Z_{KC} \\ Z_{UK} & Z_{UU} & Z_{UC} \end{bmatrix} \begin{Bmatrix} X_K \\ X_U \\ X_C \end{Bmatrix} \tag{2.31}$$

and assuming a set of fictitious loads F_C at the remaining coordinates, the previous equation can be rewritten as follows.

$$\begin{Bmatrix} F_K \\ F_C \\ F_U \end{Bmatrix} = \begin{bmatrix} Z_{KK} & Z_{KC} & Z_{KU} \\ Z_{CK} & Z_{CC} & Z_{CU} \\ Z_{UK} & Z_{UC} & Z_{UU} \end{bmatrix} \begin{Bmatrix} X_K \\ X_C \\ X_U \end{Bmatrix} \tag{2.32}$$

Assuming, as before, that $X_U = 0$ and defining

$$X_E = \begin{Bmatrix} X_K \\ X_C \end{Bmatrix}, F_E = \begin{Bmatrix} F_K \\ F_C \end{Bmatrix} \tag{2.33}$$

it is possible to obtain:

$$F_U = Z_{UE} Z_{EE}^{-1} F_E \tag{2.34}$$

and, therefore, the transmissibility matrix is defined in the next equation.

$$T_{UE} = Z_{UE} Z_{EE}^{-1} \tag{2.35}$$

2.5 Acoustic Waves

The field of acoustics studies the propagation of sound waves. The propagation of sound waves corresponds to compressions and rarefactions of the acoustic fluid.

Sound waves may be characterized by some definitions regarding wave mechanics such as [16]:

- Frequency, f (Hz) - Is defined as the number of cycles per unit of time. As an alternative, a sound wave may be characterized by the angular frequency (ω) (rad/s). The two frequencies are related by the following equation.

$$\omega = 2\pi f \tag{2.36}$$

- Oscillation period, T (s) - Refers to the time elapsed between two complete oscillations. It may be related to the frequency by the following expression.

$$T = f^{-1} = \frac{2\pi}{\omega} \tag{2.37}$$

- Wavelength, λ (m) - Is the length of a complete wave. May be computed as follows:

$$\lambda = \frac{2\pi c}{\omega} \tag{2.38}$$

where c is the sound speed.

Sound waves are created by vibrating objects and the way they propagate is deeply related to the medium where they are immersed. Sound speed is one of the properties that changes the most depending on the medium. Sound speed varies from fluid to fluid according to its properties. This work studies the propagation of sound waves through air. The theoretical fundamentals to obtain the sound speed in air are presented as described in [44].

Considering the air to be an ideal gas, the equation of state can be given by:

$$p = \rho R T \tag{2.39}$$

where T is the absolute temperature, R is a constant of the gas, and ρ is the density of the gas. Considering an isentropic process one can write:

$$\frac{p}{\rho^{\nu}} = \frac{p_0}{\rho_0^{\nu}} \tag{2.40}$$

where p is the pressure and ν is the ratio between the specific heat capacities. The speed of sound can be defined with the following equation.

$$c^2 = \frac{dp(\rho_0)}{d\rho} \tag{2.41}$$

Relating 2.41 with 2.40 and 2.39, one can obtain the equation for the speed of sound in the air.

$$c = \sqrt{\nu R T} \tag{2.42}$$

The propagation of sound waves is also influenced by the opposition that a certain medium offers to the sound propagation. This resistance to the sound propagation is called acoustic impedance. The acoustic impedance has the symbol Z, and is described by the ratio between the acoustic pressure (p) and the acoustic flow velocity (u). Therefore, the acoustic impedance can be defined by the following expression [44].

$$Z = \frac{p}{u} \tag{2.43}$$

The acoustic impedance can also be written in the complex form [16]:

$$Z = R + iX \tag{2.44}$$

where the real part, R, is the specific acoustic resistance, and the imaginary part, X, is the specific acoustic reactance.

2.5.1 Equations of Mass and Momentum Conservation

As mentioned in [44], the changes caused by a sound disturbance in a medium at rest ($\vec{U} = 0$) are characterized by disturbances in velocity ($\vec{u}$), pressure (p) and density (ρ).

$$u_t(x, y, z, t) = U + u(x, y, z, t) \tag{2.45}$$

$$p_t(x, y, z, t) = p_0 + p(x, y, z, t) \tag{2.46}$$

$$\rho_t(x, y, z, t) = \rho_0 + \rho(x, y, z, t) \tag{2.47}$$

Considering one-dimensional sound waves, the velocity, the pressure and the density are functions of one single space variable. As the pressure does not change in the y and z direction, then the speed has only one component in the x direction [44].

By studying the mass and momentum variation in a volume element, and considering the product of perturbations to be negligible, one can get the equation of conservation of mass and momentum respectively [44].

$$\frac{\partial \rho}{\partial t} + \rho_0 \frac{\partial u}{\partial x} = 0 \tag{2.48}$$

$$\rho_0 \frac{\partial u}{\partial t} + \frac{\partial p}{\partial x} = 0 \tag{2.49}$$

2.5.2 Tri-Dimensional Sound Waves

The equations derived in section 2.5.1 can be generalized to a 3D sound wave. In order to do so, one has to consider that the acoustic wave is now able to move in every direction.

As described in [44], considering an element of volume δV, the variation of the mass is due to the mass flow that passes through the delimiting surface S. In this manner, the equation of mass conservation can be written as follows.

$$\frac{\partial \rho}{\partial t} + \rho_0 \nabla \vec{u} = 0 \iff \frac{\partial \rho}{\partial t} + \rho_0 \frac{\partial u_i}{\partial x_i} = 0 \tag{2.50}$$

In the same manner, the momentum varies with the loads applied by the acoustic fluid that surrounds the volume element. With this in mind, one can obtain the equation of conservation of momentum [44].

$$\rho_0 \frac{\partial \vec{u}}{\partial t} + \nabla p = 0 \iff \rho_0 \frac{\partial u_i}{\partial t} + \frac{\partial p}{\partial x_i} = 0 \tag{2.51}$$

By combining the two previous equations and knowing that, for plane waves $p = c^2 \rho$, one can get the 3D wave equation [44].

$$\frac{1}{c^2} \frac{\partial^2 p}{\partial t^2} - \nabla^2 p = 0 \tag{2.52}$$

The acoustic fluid is an irrotacional fluid. This can be explained by the fact that the forces applied act along the center of mass of the volume element. In these conditions, one can define a scalar velocity

potential that depends solely on the coordinates.

$$\vec{u} = \nabla\psi \tag{2.53}$$

Making some more derivations (see [44]), one can get a new wave equation.

$$\frac{1}{c^2}\frac{\partial^2\psi}{\partial t^2} - \nabla^2\psi = 0 \tag{2.54}$$

2.5.2.1 Plane Wave

As described in [44], the solution for a plane wave is one of the possible solutions for the wave equation that was derived in section 2.5.2. A plane wave is a wave that travels harmonically in a certain direction through a plane. This kind of waves do not exhibit any variations in the angular frequency, and travel along one single direction in which the properties of the acoustic fluid remain unchanged [4]. One solution to this wave is in the following form [44]:

$$p(x_i, t) = f(x_i - ct) + g(x_i + ct) \tag{2.55}$$

or in the complex form:

$$p(x_i, t) = Ae^{i(\omega t - kx_i)} \tag{2.56}$$

where k is the wave number, ω is the frequency and A is the amplitude. The wave number is given by the following expression.

$$k = \frac{\omega}{c} \tag{2.57}$$

Generally, one can state that one plane wave travels along the direction $\vec{k}$, and the previous equation can be rewritten in the following manner [44]:

$$p(\vec{x}, t) = Ae^{i(\omega t - \vec{k}\cdot\vec{x})} \tag{2.58}$$

where $\vec{k}$ is the wave vector defined by

$$\vec{k} = (k_1, k_2, k_3). \tag{2.59}$$

2.5.3 Effects of Temperature and Humidity

The way sound propagates through air is influenced by the temperature and humidity of the air mass.

According to equation 2.42, the sound speed in the air increases with the increasing temperature. When the temperature is constant throughout the entire fluid domain, its effects in the acoustics are minimal. However, when there are differences in the temperature between several regions of the acoustic fluid, the sound speed will vary between them, and there will be distortion in the acoustic waves.

As the density of water vapor is lower than the density of the air, whenever there is moisture in the air (which is the most common scenario in real life situations), the density of the air mass decreases. This

produces changes in the sound speed. In addition, the presence of water vapor in the air decreases its absorption, making the medium less absorbent the higher the humidity [45].

2.5.4 Helmholtz's Equation

The Helmholtz's equation is derived from the wave equation using the separation of variables. So, as described in [46], assuming that the wave function is separable, one may define:

$$p(\vec{x}, t) = P(\vec{x})T(t) \tag{2.60}$$

Substituting in equation 2.52, one can obtain the following expression.

$$\frac{\nabla^2 P}{P} = \frac{1}{c^2 T}\frac{\partial^2 T}{\partial t^2} \tag{2.61}$$

One can now notice that in the previous equation, the term on the first member depends only on $\vec{x}$, and the term on the second member depends only on t. Therefore, this equation is only valid if both sides of the equation are equal to a constant. Thus, one can write the following expression:

$$\frac{\nabla^2 P}{P} = -k^2 \tag{2.62}$$

where the value of the constant is chosen to be $-k^2$. This previous equation is the Helmholtz's equation. This equation is important for acoustic FEA, once the previous form of the Helmholtz's equation is the initial strong form of the FE problem.

2.5.5 Acoustic Boundary Conditions

As in many problems in physics, also in the field of acoustics it is necessary to define boundary conditions.

Concerning the boundary of the medium in which the acoustic waves travel, by relating the pressure of the reflected wave (p_r) with the pressure of the incident wave (p_i), one may define the reflection coefficient as follows [16]:

$$r = \frac{p_r}{p_i}. \tag{2.63}$$

According to the previous equation, the medium boundaries may reflect and absorb part of the wave. However, there are two extreme types of boundaries that can be defined:

- Anechoic boundary - An anechoic boundary is a type of boundary that is able to absorb all the sound. In other words, if an acoustic wave encounters an anechoic wall, it will be entirely absorbed by this wall, which means that there will not be a reflected wave. This type of boundary condition can be used to simulate an infinite chamber where the sound travels to infinity without being reflected. In an anechoic boundary, the reflection coefficient will be equal to zero, once there is no reflected wave.

- Reflective boundary - A reflective boundary is able to reflect completely the sound wave. This means that if a sound wave encounters a fully reflective wall, there will be no transmitted wave through the wall. Only a reflected wave will be observed. In this case, the reflection coefficient will be equal to 1, since the pressure of the reflected wave is equal to the pressure of the incident wave.

Regarding imposed boundary conditions, let us consider a boundary surface $\Omega = \Omega_p \cup \Omega_v \cup \Omega_Z$, where the boundary conditions are imposed. In that situation, it is possible to have the following cases [4, 47]:

- Imposed pressure - In this case the pressure in the boundary surface is equal to the imposed pressure.

$$p_\Omega = p_{imp} \text{ ,on } \Omega_p \tag{2.64}$$

- Imposed normal velocity - The velocity in the boundary surface is equal to the imposed velocity.

$$u_{\Omega_n} = u_{imp} = \frac{i}{\rho_0 \omega} \frac{\partial p}{\partial n} \text{ ,on } \Omega_v \tag{2.65}$$

- Imposed normal impedance - The impedance in the boundary surface is equal to the imposed one.

$$p = \overline{Z} u_{\Omega_n} = \frac{i\overline{Z}}{\rho_0 \omega} \frac{\partial p}{\partial n} \text{ ,on } \Omega_Z \tag{2.66}$$

2.5.6 Transmissibility in Acoustics

Previously, the transmissibility concept was applied to the analysis of structural systems. In these systems, there are, usually, applied loads or displacements that are transmitted to other points in the structure. Now, one has to extend the equations derived for the structural dynamics case, to the acoustic case, where there are no displacements or loads applied, but applied pressures or imposed volume accelerations. Therefore, in the field of acoustics, transmissibility studies how an imposed pressure at a certain point of the acoustic fluid is transmitted to another in the form of a pressure response [4].

It was stated earlier that linear structural mechanical systems could be modelled by equation 2.8. In the same manner, acoustic systems can be modelled in the frequency domain by the following equation [16]:

$$(-\omega^2[M] + i\omega[C] + [K])\{P\} = \{Q\} \tag{2.67}$$

where $[M]$ is the acoustic mass matrix, $[C]$ is the acoustic damping matrix, $[K]$ is the acoustic stiffness matrix, $\{P\}$ is the vector of pressure amplitudes, and $\{Q\}$ is the volume acceleration vector.

In the field of acoustics, the scalar transmissibility functions can be defined as the ratio between the scalar pressure response and the scalar pressure input. As defined in [14], assuming one single acoustic source (q_u) applied at a known DOF u, the transmissibility function is the ratio between the pressure measured at a reference DOF r, and the pressure measured at DOF i. This model can be

described by the following equation.

$$T_{ir}^{u} = \frac{p_i(\omega)}{p_r(\omega)} = \frac{H_{iu} q_u(\omega)}{H_{ru} q_u(\omega)} \tag{2.68}$$

The previous equation can be generalized for the case of multiple acoustic sources [15]:

$$T_{ir}^{u} = \frac{p_i(\omega)}{p_r(\omega)} = \frac{\sum_{u=1}^{n} H_{iu} q_u(\omega)}{\sum_{u=1}^{n} H_{ru} q_u(\omega)}. \tag{2.69}$$

Similarly to the case of structural dynamics transmissibility for MDOF systems, there are two different but equivalent approaches to the study of acoustic transmissibility. The definitions regarding these approaches are taken from [16], and are presented below.

2.5.6.1 Transmissibility from Dynamic Stiffness Matrix

The linear dynamic acoustic system can be modelled, in the frequency domain, in terms of the dynamic stiffness matrix in the following manner:

$$[Z]\{P\} = \{F\} \tag{2.70}$$

where $[Z] = -\omega^2[M] + i\omega[C] + [K]$, $\{P\}$ is the vector of nodal pressures, and $\{F\}$ is the vector of acoustic loads. Considering that the acoustic fluid is inviscid, the matrix $[C]$ can be set to zero.

Defining a set of coordinates U of unknown pressures, a set of coordinates K where the pressure is known, and a set C for the remaining coordinates, one may rewrite the previous equation, obtaining:

$$\begin{bmatrix} Z_{KK} & Z_{KC} & Z_{KU} \\ Z_{CK} & Z_{CC} & Z_{CU} \\ Z_{UK} & Z_{UC} & Z_{UU} \end{bmatrix} \begin{Bmatrix} P_K \\ P_C \\ P_U \end{Bmatrix} = \begin{Bmatrix} F_K \\ F_C \\ F_U \end{Bmatrix} \tag{2.71}$$

Considering a null vector of acoustic loads, and grouping the sets K and C in the same set of coordinates R, for a given imposed pressure amplitude $\overline{P}_U$, the previous equation becomes:

$$\begin{bmatrix} Z_{RR} & Z_{RU} \\ Z_{UR} & Z_{UU} \end{bmatrix} \begin{Bmatrix} P_R \\ \overline{P}_U \end{Bmatrix} = \begin{Bmatrix} 0 \\ 0 \end{Bmatrix} \tag{2.72}$$

and the pressure at coordinates R can be described as:

$$P_R = -(Z_{RR})^{-1} Z_{RU} \overline{P}_U \tag{2.73}$$

from which it is possible to define the transmissibility matrix.

$$T_{RU}^{Z} = -(Z_{RR})^{-1} Z_{RU} \tag{2.74}$$

2.5.6.2 Transmissibility from the Receptance Matrix

One alternative approach for evaluating transmissibility in the field of acoustics, is by using the receptance matrix. Using the same sets of coordinates K, U, and C, as in the dynamic stiffness matrix method, one can establish the following relationship in the frequency domain:

$$\{P\} = [H]\{F\} \tag{2.75}$$

and thus obtain

$$\begin{Bmatrix} P_K \\ P_U \\ P_C \end{Bmatrix} = \begin{bmatrix} H_{KK} & H_{KU} \\ H_{UK} & H_{UU} \\ H_{CK} & H_{CU} \end{bmatrix} \begin{Bmatrix} F_K \\ F_U \end{Bmatrix} \tag{2.76}$$

where it was assumed that there are no loads applied in set C. Again, assuming an imposed pressure $\overline{P}_U$ and expanding the previous equation, the following expressions are obtained.

$$P_K = H_{KK}F_K + H_{KU}F_U \tag{2.77}$$

$$\overline{P}_U = H_{UK}F_K + H_{UU}F_U \tag{2.78}$$

Solving for F_U in equation 2.78 and substituting in equation 2.77, the following equation is obtained.

$$P_K = [H_{KK} - H_{KU}(H_{UU})^{-1}H_{UK}]F_K + H_{KU}(H_{UU})^{-1}\overline{P}_U \tag{2.79}$$

Now assuming that the forces F_K are equal to zero, the previous equation can be rewritten as:

$$P_K = H_{KU}(H_{UU})^{-1}\overline{P}_U \tag{2.80}$$

and the transmissibility matrix can be defined by the following equation.

$$T^H_{KU} = H_{KU}(H_{UU})^{-1} \tag{2.81}$$

One can notice that the transmissibility is independent of the pressure amplitudes. If it is considered an imposed harmonic pressure at set U, it can be assumed that this formulation is independent of the amplitude of the sources.

2.6 Vibro-Acoustic Fundamentals

Here, one presents the theoretical fundamentals for vibro-acoustic analysis, either by using the FEM or the transmissibility concept. The FE model description presented here is based on [4]. The descriptions in [4] are taken from [47]. For detailed derivations on the methods presented the reader should see [47].

2.6.1 Problem Definition

Vibro-acoustics is usually a coupled problem in which the structural and acoustic problems are solved simultaneously. The approach to solve this problem consists of a FEM in which the acoustic FEM is coupled with the structural FEM.

Like the acoustic problem, the vibro-acoustic problem is also defined in a volume V, enclosed by a boundary Ω, but in this case a new segment, Ω_s, must be created on the boundary to correspond to the elastic structure. Regarding this, a new boundary condition concerning continuity of normal velocity must be imposed. This condition represents the vibro-acoustic coupling, and establishes equality between the normal fluid velocity and normal structural velocity. This new boundary condition can be defined by the following expression, where w_n is the normal displacement imposed to the structure, and v_n is the normal velocity [4, 47].

$$v_n = \frac{i}{\rho_0 \omega} \frac{\partial p}{\partial n} = i\omega w_n \text{ ,on } \Omega_s \tag{2.82}$$

2.6.2 Structural Displacement

Although any type of elastic structure can be a part of a vibro-acoustic coupled problem, the elastic structure is chosen to be a shell type structure with a small thickness, because significant vibro-acoustic coupling effects occur mainly for structures with small stiffness and mass [47].

The displacement in these structures is usually characterized by the displacement components in the plane of the mid-surface of the shell, and is described by a coordinate system at the centre of the shell's surface, as illustrated by figure 2.4.

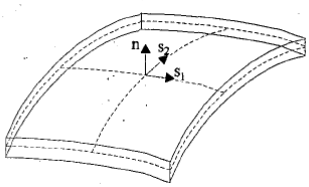

Figure 2.4: Shell coordinate system (from [4, 47]).

Regarding the coordinate system presented in figure 2.4, the displacement field is regulated by the following linear dynamic equation [4, 47]:

$$([\hat{L}_s] - \omega^2[\hat{M}_s]) \begin{Bmatrix} w_{s_1}(r) \\ w_{s_2}(r) \\ w_n(r) \end{Bmatrix} = \begin{Bmatrix} \tilde{f}_{s_1}(r) \\ \tilde{f}_{s_2}(r) \\ \tilde{f}_n(r) \end{Bmatrix} + \begin{Bmatrix} 0 \\ 0 \\ p(r) \end{Bmatrix}, r \in \Omega_s \tag{2.83}$$

where (w_{s_1}, w_{s_2}, w_n) is the displacement field, $[\hat{L}_s]$ is the matrix of differential operators of the shell structure that rules elastic and damping forces, and the $[\hat{M}_s]$ matrix governs the inertial parameters of the same structure. The first term of the second member of equation 2.83 represents the forces applied

to the structure. The second term of the second member of equation 2.83 represents the acoustic pressure loading.

2.6.3 Eulerian Coupling Formulation

Although there are several coupling formulations, in this work only the Eulerian formulation is presented.

In the Eulerian formulation the acoustic response is defined by a single scalar function, usually the pressure, and the structural response is described by the displacement vector. The following definitions are taken from [4, 47].

2.6.3.1 Acoustic FE Model

The FE approximation of the steady-state pressure p can be described in the bounded volume V, as an expansion $\hat{p}$ in terms of a set of global shape functions N_i [4, 47]:

$$\hat{p}(x,y,z) = \sum_{i=1}^{n_a} N_i(x,y,z) \cdot p_i + \sum_{i=1}^{n_p} N_i(x,y,z) \cdot \overline{p}_i \tag{2.84}$$

which can be rewritten as:

$$\hat{p}(x,y,z) = [N_a]\{p_i\} + [N_p]\{\overline{p}_i\}, (x,y,z) \in V \tag{2.85}$$

where n_p is the number of constrained DOFs where a pressure $\overline{p_i}$ is imposed. These nodes are located on the boundary Ω_p and are associated with the vector $\{\overline{p}_i\}$ and the set of shape functions $[N_p]$. The number of unconstrained nodes is given by n_a, and these are related with the vector $\{p_i\}$ and to the set of shape functions $[N_a]$. The FE model for the unconstrained DOFs can be defined as:

$$([K_a] + i\omega[C_a] - \omega^2[M_a])\{p_i\} = \{F_a\} \tag{2.86}$$

where the term $\{F_a\}$ contains the contributions of the constrained DOFs, the contributions of the acoustic sources applied in the fluid domain V, and the contributions from the prescribed velocity input imposed on the boundary surface Ω_v. Being $\overline{v}_n$ the prescribed normal velocity, with positive orientation away from the volume V, the latest contribution can be defined by the following expression.

$$\int_{\Omega_v} (-i\rho_0\omega[N_a]^T\overline{v}_n)d\Omega \tag{2.87}$$

2.6.3.2 Structural FE Model

The FE approximation of the steady-state dynamic displacement of the mid-section of an elastic shell can be defined as [4, 47]:

$$\begin{Bmatrix} \hat{w}_x(x,y,z) \\ \hat{w}_y(x,y,z) \\ \hat{w}_z(x,y,z) \end{Bmatrix} = [N_s]\{w_i\} + [N_w]\{\overline{w}_i\} \tag{2.88}$$

where $[N_s]$ comprises the global shape functions corresponding to the unconstrained DOFs $\{w_i\}$ on the shell structure. The $[N_w]$ comprises the global shape functions corresponding to the constrained DOFs $\{\overline{w}_i\}$. The FE model for the unconstrained DOFs can be defined as:

$$([K_s] + i\omega[C_s] - \omega^2[M_s])\{w_i\} = \{F_s\} \tag{2.89}$$

where, as for the acoustic FE model, $\{F_s\}$ contains the terms in the constrained DOFs, the contributions of the prescribed forces and moments applied on the shell boundary, and the contributions from the external load p applied normal to the shell surface Ω_s. The latter contributions can be defined as:

$$\sum_{e=1}^{n_{se}} (\int_{\Omega_{se}} ([N_s]^T \{n^e\} p) d\Omega) \tag{2.90}$$

where n_{se} is the number of flat plate elements, Ω_{se}, in the shell discretization, and where the unit vector normal to a plate element is represented in the vector $\{n^e\}$.

2.6.3.3 Coupled FE Model

The force loading of the acoustic pressure on the elastic shell structure along the fluid structure interface may be regarded as an additional normal load. As a consequence of this, another term must be added to the structural FE formulation, and, therefore, the previous model is written as follows.

$$([K_s] + i\omega[C_s] - \omega^2[M_s])\{w_i\} + [K_c]\{p_i\} = \{F_{si}\} \tag{2.91}$$

In the previous equation, $[K_c]$ corresponds to the number of acoustic and structural unconstrained DOFs.

The continuity of the normal shell velocities and the normal fluid velocities may be regarded as an additional velocity input on the Ω_s part of the boundary surface of the acoustic domain. Therefore, an additional term must be added to the acoustic FE model. As a consequence, the acoustic FE model becomes:

$$([K_a] + i\omega[C_a] - \omega^2[M_a])\{p_i\} - \omega^2[M_c]\{w_i\} = \{F_{ai}\}. \tag{2.92}$$

By combining equations 2.91 and 2.92, one can now define the vibro-acoustic FE model [4, 47].

$$\left(\begin{bmatrix} K_s & K_c \\ 0 & K_a \end{bmatrix} + i\omega \begin{bmatrix} C_s & 0 \\ 0 & C_a \end{bmatrix} - \omega^2 \begin{bmatrix} M_s & 0 \\ -\rho_0 K_c^T & M_a \end{bmatrix} \right) \begin{Bmatrix} w_i \\ p_i \end{Bmatrix} = \begin{Bmatrix} F_{si} \\ F_{ai} \end{Bmatrix} \tag{2.93}$$

Although the coupled mass and stiffness matrices are still frequency independent, these matrices are no longer symmetrical. This is due to the fact that the force loading of the fluid on the structure is proportional to the pressure. This results in a cross-coupling matrix $[K_c]$ in the vibro-acoustic stiffness matrix. As the force loading of the structure on the fluid is proportional to the acceleration, then the cross-coupling matrix $[-\rho_o K_c^T]$ appears in the coupled mass matrix.

An alternative to the previous coupled formulation is to describe the fluid as the fluid velocity potential ψ, of which the gradient vector equals the fluid velocity vector $\vec{v}$.

$$\vec{v} = \frac{i}{\rho_0 \omega} \nabla p = \nabla \psi \tag{2.94}$$

Using this, it is possible to achieve a symmetrical formulation for the vibro-acoustic coupled FE model [47].

$$\begin{bmatrix} K_s & 0 \\ 0 & -\rho_0 K_a \end{bmatrix} + i\omega \begin{bmatrix} C_s & -\rho_0 K_c \\ -\rho_0 K_c^T & -\rho_0 C_a \end{bmatrix} - \omega^2 \begin{bmatrix} M_s & 0 \\ 0 & -\rho_0 M_a \end{bmatrix} \begin{Bmatrix} w_i \\ \psi_i \end{Bmatrix} = \begin{Bmatrix} F_{si} \\ \frac{F_{ai}}{i\omega} \end{Bmatrix} \tag{2.95}$$

For damped systems, this formulation is obtained without any penalty. For undamped systems ($C_a = C_s = 0$), the use of this formulation involves the introduction of a complex artificial damping matrix. This is disadvantageous since solving a non symmetrical but real model, requires less computational effort than solving a symmetrical but complex model. This is due to the fact that solving complex models involves more arithmetical operations than solving real systems [47].

In ANSYS APDL, when the system is undamped, the program does not retrieve a damping matrix when the matrices are extracted. This shows that, most likely, ANSYS uses the non symmetrical model to solve these problems.

2.6.3.4 Limitations of the FE Model in Acoustics and Vibro-Acoustics

One of the most common limitations in acoustic FEs is choosing the proper element size. As mentioned in [48], in acoustics, there is a strong relationship between the element size and the wavelength. According to [48], in order to obtain acceptable results for the first order elements, the size of the element must be chosen such that the biggest element is at least six times smaller than the acoustic wavelength. For second order elements this requirement is twice smaller. In [20], is stated that in order to have an error smaller than 10% with respect to the analytical solution of an acoustic tube with reflective boundaries, one should have at least 36 elements per wavelength. In addition, when there is reflection and interference between waves in the model, it gets more difficult to predict what the ratio between the size of the element and the acoustic wavelength must be, as it is not possible to predict the frequency of the resultant wave [48].

It is also mentioned in [48] that the imposition of absorptive boundary conditions is another limitation of the FEM in acoustics. According to [48], the results of numerical analyses in acoustics are relatively sensitive to the boundary conditions, and this becomes a problem because the absorption at the boundary is nonlinearly dependent on frequency. So, the absorption coefficients should be frequency dependent, and generally, this is not implemented in commercial FE software.

Acoustic problems can be divided in three different groups according to the wave frequency [48]: into low frequency problems, in which the response has a strong modal behaviour; into medium frequency problems, in which the response spectra exhibits high irregularities, indicating irregular modal density; into high frequency problems, in which the response spectra is smooth, indicating high modal density. As previously mentioned, the FEM is suitable for the analysis of low frequency problems, and becomes unable to accurately predict the acoustic behavior of a system at high frequency. However, this is not entirely accurate. In fact, the FE model stays valid as long as the spectral density does not become high. However, the spectral density usually tends to grow higher with the frequency, making FEM unable to predict acoustic responses in these situations. The strong relationship between the FE size and the acoustic wavelength also makes the FEM more suitable to analyse low frequencies. With the increasing frequency, the discretization must have a larger refinement, leading to large models at high frequencies. These models require a considerable amount of memory and computational effort, and, as a consequence, they are time costly and inefficient.

Once coupled vibro-acoustic FE models use acoustic FEs, then, the limitations that affect the acoustic FEM are also valid for the coupled vibro-acoustic FEM. However, coupled vibro-acoustic FE models also present their own limitations.

One of the biggest limitations of the coupled FEM, is that it usually requires larger models that need more computational effort and more memory when compared with uncoupled models. This is mainly due to the following aspects [47]:

- In coupled FEM the structural and acoustic problems must be solved simultaneously in order to incorporate the vibro-acoustic coupling effects. This does not happen in uncoupled models, in which the structural and acoustic problem may be solved with a sequential procedure.
- In addition to being larger, coupled FEMs have smaller computational efficiency. The coupled vibro-acoustic FEM is no longer symmetrical, and its bandwidth is significantly higher.

It is also mentioned in [47] that for coupled vibro-acoustic problems, just like in acoustic problems (as mentioned before), the number of FEs in the FE discretization must increase as the frequency increases. Such increase in the number of elements leads to a larger model, that requires a considerable amount of computational effort and memory resources to be solved. As a consequence, the applicability of the coupled vibro-acoustic FEM becomes restricted to a certain frequency range.

2.6.4 Vibro-Acoustic Transmissibility

Previously, several approaches to study transmissibility in structural and acoustic MDOF systems have been presented. Now, one intends to extend the previous approaches, namely the one presented for acoustic systems, to a vibro-acoustic MDOF system. In this case, only the approach based on the receptance matrix is presented due to implementation easiness.

Regarding vibro-acoustic transmissibility, two different cases can occur [4]. The first case concerns a pressure imposition leading to a structural response with dynamic displacement. The other case is

the opposite of the previous one, and concerns a dynamic load or displacement imposition leading to an acoustic response in the form of a pressure response in the fluid. As defined in section 2.5.6, the sets of coordinates U and K correspond to the coordinates where the imposition is set, and to the coordinates where the responses are measured, respectively.

As mentioned in [4], regarding a pressure imposition and the previously mentioned sets of coordinates, one can write:

$$\begin{Bmatrix} u_K \\ P_U \end{Bmatrix} = \begin{bmatrix} H_{KK} & H_{KU} \\ H_{UK} & H_{UU} \end{bmatrix} \begin{Bmatrix} F_K \\ F_U \end{Bmatrix} \tag{2.96}$$

and writing F_U as a function of P_U, the following relation is obtained.

$$F_U = (H_{UU})^{-1}(P_U - H_{UK}F_K) \tag{2.97}$$

Considering $F_K = 0$ and replacing the previous equation in the equation of the first line of equation 2.96, one obtains:

$$u_K = H_{KU}(H_{UU})^{-1}P_U \tag{2.98}$$

and therefore, the transmissibility matrix for the vibro-acoustic system with an imposed pressure can be defined by the following equation.

$$T_{KU}^{FS} = H_{KU}(H_{UU})^{-1} \tag{2.99}$$

Now considering the second case, in which an imposed force or displacement in the structure creates a pressure response in the acoustic fluid, one can write [4]:

$$\begin{Bmatrix} u_U \\ P_K \end{Bmatrix} = \begin{bmatrix} H_{UU} & H_{UK} \\ H_{KU} & H_{KK} \end{bmatrix} \begin{Bmatrix} F_U \\ F_K \end{Bmatrix} \tag{2.100}$$

and defining F_U as a function of u_U, the following relation is obtained.

$$F_U = (H_{UU})^{-1}(u_U - H_{UK}F_K) \tag{2.101}$$

By substituting the previous equation in the P_K equation and setting $F_K = 0$, one obtains:

$$P_K = H_{KU}(H_{UU})^{-1}u_U \tag{2.102}$$

and the transmissibility function can be defined by the following equation.

$$T_{KU}^{SF} = H_{KU}(H_{UU})^{-1} \tag{2.103}$$

3 Methodology

In this chapter, the methodologies used to obtain the results contained in the following chapter are presented.

Once the main focus of this work is to estimate the localization of a vibro-acoustic source using the transmissibility concept, one first needs to understand this concept in simpler examples, such as vibrational and acoustic transmissibility. Then, numerical and experimental vibro-acoustic analyses are conducted.

The methodologies (Matlab® and ANSYS APDL) used to obtain the results in vibrational and acoustic transmissibility are similar to those presented in [4]. The main objective is to reproduce some of the results available in the literature recurring to these methods, with the purpose of gaining knowledge and understanding in the subject. In addition, the verification of results is important in computational simulations to evaluate if the methodologies are producing proper results. The methodologies used in vibro-acoustic transmissibility analysis are based on the ones described in [4], and modified in order to analyse systems with increasing complexity.

3.1 Vibrational Transmissibility

Here, the theoretical fundamentals presented in 2.4 are applied to the case of a MDOF mass-spring system. The results obtained are compared to the results presented in [5].

3.1.1 MDOF Mass-Spring System

Let us consider the MDOF mass-spring system presented in figure 3.1, with a set of known harmonic loads applied at certain nodes of the structure. The problem to be solved consists of estimating the reactions at the supports of the MDOF system using force transmissibility.

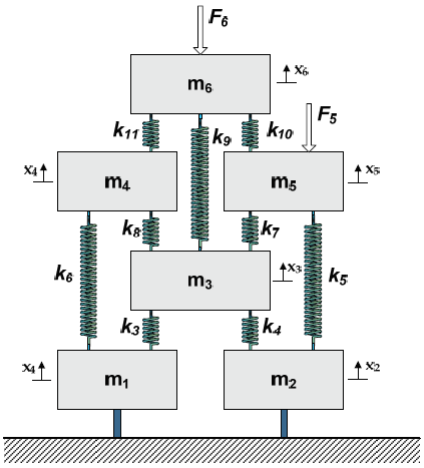

Figure 3.1: MDOF mass-spring system [5].

The current problem is solved numerically, by discretizing each spring as a two node FE, as shown in section 2.2. Having the local stiffness matrix of each element, and using a connectivity table, one can assemble the global stiffness matrix of the system. The mass and stiffness matrices are $n \times n$ symmetric matrices where n is the number of DOFs of the system.

The Maltlab® routine developed in [4] is in accordance with the following steps:

- The variables concerning the mass and springs stiffness are introduced along with the mass and stiffness matrices. The force vector is also introduced in this step;
- A cycle is created to evaluate the force transmissibility over a previously defined range of frequencies. The cycle ends when all the interest frequencies have been analysed;
- Inside the cycle, the dynamic stiffness matrix is computed using equation 2.10, and the receptance matrix is obtained through the inverse of $[Z]$. Then, the submatrices of $[Z]$ and $[H]$ that relate the coordinates between which the transmissibility matrix is computed, are defined according to equations 2.35 and 2.30, respectively. Finally, the transmissibility matrix is obtained using equations 2.35 or 2.30, and the unknown reactions are obtained from equations 2.34 or 2.29.
- The transmissibility and the loads are then plotted as a function of the frequency.

The obtained results are compared with the results presented in [5] for verification.

3.2 Acoustic Transmissibility

In this example, an acoustic tube is studied. One intends to model a 3D tube filled with an acoustic fluid, and compare the numerical results with available theoretical solutions for verification purposes. To do so, a 1 Pa pressure is applied to one end of the tube and the pressure distribution is measured along the length of the tube for two possible cases: in the first case, the second end of the tube is considered to be a fully reflective boundary; in the second case, the second end of the tube is considered to be anechoic.

Then, a transmissibility analysis takes place. The goal is to use the concept of acoustic transmissibility to estimate the unknown pressure at the mid-section of the tube, for a given imposed pressure at one of the ends (see figure 3.2). Finally, a measurement of the pressure response is taken from the FE model at the mid-section of the tube. This measurement is compared to several pressure responses estimated using the transmissibility concept for some possible locations of the imposed pressure, with the purpose of finding the correct source.

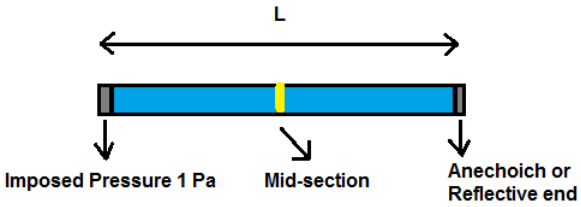

Figure 3.2: Illustration of the acoustic tube with an imposed pressure at one end, and a reflective/anechoic boundary at the other.

To solve this problem, one has to create an APDL model [49] of a 3D tube filled with an acoustic fluid. The created model is similar to the one in [4].

In order to verify if the results obtained by the FE model are correct, one has to take the following steps:

- Create the geometry and meshes. To model the geometry, one starts by creating a square using the commands *Modeling/Create/Areas/Rectangle/By dimensions*. Then, after specifying the dimensions of the square, the area is extruded along the normal direction to the specified length. The commands *Modeling/Operate/Extrude/Areas/Along Normal* are used to achieve this goal. Finally, the commands *Meshing/Size Cntrls/Manual Size/Lines/Picked Lines* are used to specify the size of the FEs, and a mesh of FLUID30 elements is created using the *Volume Sweep* command.;
- Apply a pressure of 1 Pa to all the nodes of one end of the tube;
- In the other end, choose between a reflective or anechoic boundary. When the boundary admittance of the FE is set to 0, the boundary stays reflective if no boundary conditions are applied to it. To create the anechoic boundary, one has to select the elements on the boundary and impose a unit impedance in them. The definition of the anechoic end is completed when these elements are changed to a second material with a unitary boundary admittance [4];
- Perform a harmonic analysis and obtain the pressure as a function of the tube's length;
- Compare the results obtained from the FE model with the analytical solutions available. The analytical solutions for the reflective and anechoic boundaries with an imposed pressure of 1 Pa are given by the following equations respectively [20]:

$$p(z) = cos(kz) + tan(kL)sin(kz) \tag{3.1}$$

$$p(z) = cos(kz) \tag{3.2}$$

where $k = \omega/c$, z is the coordinate along the tube's length, and L is the tube's length.

The harmonic analysis is also used to obtain the pressure at the reference nodes along an imposed frequency range. These results are later compared with those obtained from the transmissibility functions in order to identify the correct acoustic source.

With the purpose of obtaining the transmissibility functions, one has to perform a modal analysis. Once this is done, the global mass and stiffness matrices may be extracted from ANSYS (if one used an anechoic boundary, the damping matrix would also be extracted).

Once the APDL solution is finished and the matrices are extracted using the *hbmat* command [50], the post processing needs to be done in Matlab® to obtain the transmissibility functions. The Matlab® routine is similar to the one presented for the mass-spring system, featuring the following steps [4]:

- Import the global matrices from ANSYS using the *hb_to_msm* Matlab® function [51];
- Create a cycle that increments the frequency and, inside the cycle, compute $[Z]$ using equation 2.10, and obtain $[H]$ using the inverse of $[Z]$ for every frequency of interest;
- Compute the sub-matrices H_{KU} and H_{UU}, and obtain the transmissibility matrix using equation 2.81 in the imposed frequency range;
- Obtain the pressure as a function of the frequency using equation 2.80.

Once the Matlab® routine is finished and able to obtain the transmissibility functions, one can use transmissibilities to locate the acoustic source. First, an acoustic pressure is imposed at a node of the fluid, and the response is measured at the reference node using the FE model. Then, the pressure responses are obtained with the transmissibility concept (between the reference node and many possible sources), and compared with the ones obtained with the FE model. The pressure response at the correct source is the one that matches the values obtained in the FE model, therefore minimizing the following function [16]:

$$\epsilon_P^s = \sum_{i=1}^{nfreq} [(P_{meas})_i - (P_{calc})_i]^2 \tag{3.3}$$

where $nfreq$ is the number of frequencies to evaluate, P_{meas} is the pressure obtained from the FE model, and P_{calc} is the pressure obtained from the transmissibility concept using the following expression:

$$P_{calc} = T_{KU} \cdot \overline{P}_U \tag{3.4}$$

where $\overline{P}_U$ is an arbitrated amplitude. In this case $\overline{P}_U$ is set to 1 Pa.

3.3 Vibro-Acoustic Transmissibility

With the purpose of creating a complex vibro-acoustic system, first it is necessary to study a simpler one in order to verify the obtained results, and then, evaluate if the developed FE model and Matlab® post processing routine are working properly.

Here, it is intended to analyse vibro-acoustic transmissibility in the model of the tube described in section 3.2. For this case, the model described in 3.2 is modified, and a steel plate is inserted at one end of the tube as described in [4]. Then, a harmonic load is imposed at the center of the plate, and a harmonic analysis is conducted to measure the displacement at the center of the plate and the pressure response at the mid-section of the tube (see figure 3.3).

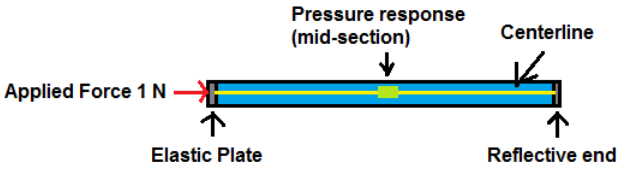

Figure 3.3: Illustration of the geometry and boundary conditions of the vibro-acoustic tube.

The methodology used to create the APDL model and to obtain the results from it is as follows:

- Use the methodology described in 3.2 to create the discretized model of the tube;
- Select the nodes of one end of the tube and insert the structural plate;
- Change the elements that are touching the plate to FSI elements using the procedure in [52];
- Fix the DOFs on the edges of the plate;
- Perform a modal analysis and extract the $[M]$, $[K]$, and $[C]$ (only if there is an anechoic end) matrices in the Harwell-Boeing format;
- Perform a harmonic analysis with an applied load of 1 N at the center of the plate (along the direction normal to the plate's surface), and measure the pressure at the mid-section of the tube and the displacement at the center of the plate. Dividing the measured pressure by the displacement created by the applied load gives the transmissibility function.

These results are compared with the ones presented in [4] to verify if the model is working correctly. Like in the previously studied models, the post-processing is done using a Matlab® routine that is based on the one described in [4]:

- Import the Harwell-Boeing matrices [53] to Matlab® and create a cycle to compute the dynamic stiffness matrix $[Z]$;
- Inside the cycle, use the inverse of $[Z]$ to obtain the receptance matrix, and then, compute the submatrices H_{UK}^T and H_{UU};
- Use equation 2.103 to obtain the transmissibility function (substitute H_{KU} by H_{UK}^T);
- Obtain the pressure responses and plot the results.

The results of the Matlab® routine obtained using the MDOF transmissibility concept can be compared to the ones obtained in ANSYS to verify if the Matlab® routine is working properly.

3.4 Wooden Cavity Characterization

One of the main objectives of this work is to study acoustic and vibro-acoustics transmissibility in a wooden box cavity. The wooden box where the numerical and experimental procedures are conducted is the same as in [38]. In addition, the numerical and experimental procedures that are implemented, are based on the ones presented in [38]. It is intended to conduct several analyses:

- Perform an acoustic transmissibility analysis in order to estimate unknown pressure responses at specific coordinates for a given set of applied pressures;
- Given a certain pressure response obtained from the harmonic analysis conducted in ANSYS, it is intended to use the transmissibility concept to identify the pressure source in the acoustic cavity;
- Perform a vibro-acoustic transmissibility analysis to estimate unknown pressure responses at specific coordinates for a given imposed displacement on the elastic shell;
- Given certain pressure responses obtained from the harmonic analysis conducted in ANSYS, it is intended to use the vibro-acoustic transmissibility concept to find the correct sources of displacement.
- Compare the numerical and experimental results in order to evaluate the amount of updating required in the acoustic and vibro-acoustic FE models.

The wooden cavity is composed by several elements [38]:

- A wooden box with inner dimensions of 700$\times$500 mm, a thickness of 18 mm, and 45 degrees by 100 mm corners. The box is made of pine wood boards;
- Two acrylic plates: one with a 5 mm thickness and the other with a 6 mm thickness. These plates are 740 by 540 mm;
- A steel U plate with 1 mm thickness. This plate is 500 mm by 100 mm with 45 mm side bends, and is inserted on the right side of the box, 100 mm from the board where $S2$ is located (see figure 3.4). This plate is only used in the vibro-acoustic experimental setup.

As described in [38], several holes were drilled in the wooden box to fit the speakers and microphones needed for the acoustic and/or vibro-acoustic experimental setup. The position of the holes along with their designation may be seen in figure 3.4, and the coordinates of the holes are presented in table 3.1

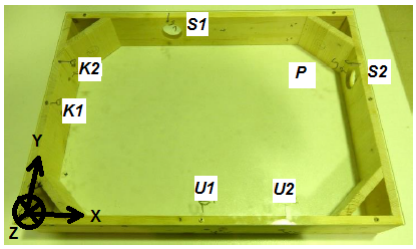

Figure 3.4: Acoustic cavity [38].

Point	x (mm)	y (mm)	z (mm)
$S1$	250	500	50
$S2$	700	350	50
$K1$	0	250	50
$K2$	0	350	50
$U1$	350	0	50
$U2$	500	0	50

Table 3.1: Coordinates of the points of interest [38].

In table 3.1, the points $S1$ and $S2$ correspond to the location of the speakers (acoustic sources), and the remaining points correspond to the locations where the pressure responses are measured by the microphones.

3.4.1 Analysis of the Acoustic Cavity

3.4.1.1 Numerical Analysis

In this section one intends to describe the methodology used to model the acoustic cavity presented in figure 3.4, and to perform a modal analysis in ANSYS in order to obtain the global matrices that are imported to Matlab®. Then, a transmissibility analysis is conducted, and the pressure responses are obtained by using the methodology described in section 3.2.

Since this model has two dimensions that are somewhat larger than the third one, one will primarily test if a 2D model can be used to solve the problem, as was done in [38]. This hypothesis is tested by performing a modal analysis in a 2D and in a 3D model of the acoustic cavity. The results of the natural frequencies are then compared, in order to evaluate if the 2D model offers enough precision to study this case.

The geometry is modelled in ANSYS APDL by creating a set of keypoints located at the vertices of the inner part of the wooden cavity (table 3.2), using the sequence of commands *Modeling/Create/Keypoints/In active CS*.

	Coordinates	
Keypoint nº	x (m)	y (m)
1	0.1	0
2	0.6	0
3	0.7	0.1
4	0.7	0.4
5	0.6	0.5
6	0.1	0.5
7	0	0.4
8	0	0.1

Table 3.2: Coordinates of the keypoints in the APDL model of the acoustic cavity.

Then, lines are created to connect the several keypoints using the command sequence *Modeling/Create/Lines/Lines/Straight Line*. The 2D geometry is completed when the cavity area is created within the lines by using the commands *Modeling/Create/Areas/By lines*. If a 3D model of the cavity is to be created, the sequence of commands *Modeling/Operate/Extrude/Areas/Along Normal* is selected, and the area must be extruded along 0.1 m, therefore creating the inner volume of the acoustic cavity.

The 2D and 3D meshes are created using FLUID29 and FLUID30 ANSYS Fluid elements respectively. The element dimension is defined by using the commands *Meshing/Size Cntrls/Manual Size/Lines* or *Areas*, and then selecting the maximum element size. If a 2D mesh is to be created, the sizing of the elements is done by using all the lines of the model. In the 3D model, the areas are used to size the elements. After defining the element size, the mesh is created by using the *free* meshing option. After analysing the data from the modal analyses, one of the two models is picked, and used to extract the $[M]$ and $[K]$ matrices. These matrices are then imported to Matlab® routines (see section 3.2) that extract the transmissibility functions, estimate the pressure responses, and identify the acoustic sources.

3.4.1.2 Experimental Analysis

The experimental analysis uses speakers placed at points $S1$ and $S2$ to create a signal. The responses are then measured by microphones placed at points $U1$, $U2$, $K1$ and $K2$. The goal is to compare the responses obtained experimentally with the ones obtained numerically in order to validate both models.

The experimental setup (based on the one described in [38]) uses the wooden cavity presented in figure 3.4 with the two acrylic plates placed on both tops. To produce the signal and measure the responses, the following hardware is required:

- Two FoneStar SQ-2143 speakers;
- Four Behringer ECM8000 condenser microphones;
- Two Behringer U-Phoria UMC2002HD audio interfaces;
- Two Velleman VM114 power amplifiers (one for each speaker);

- Four SM6BK XLR cables (one for each microphone);
- Two USB cables;
- Two double head Jack cables;
- A computer with LabVIEW [54] for sound emission and acquisition;
- An EATON 5E Essential UPS - Despite having no direct purpose, this object provides protection against energy failures such as current peaks, and helps reducing the noise in the results.

The experimental procedure requires the following steps:

- Assemble the wooden box cavity and the acrylic plates, and place the microphones and the speakers. The speakers must be fixed using tape;
- Connect the SM6BK XLR cables to the microphones and to the Behringer audio interfaces (two microphones per box) at input 1 and input 2 (see figure 3.5 (a))

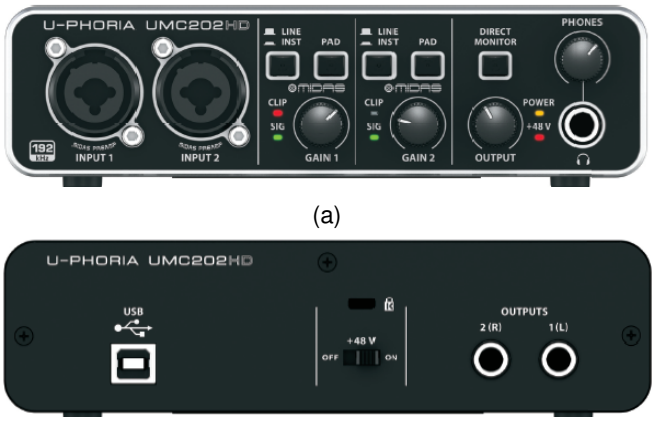

(a)

(b)

Figure 3.5: Behringer U-Phoria UMC2002HD audio interface.

- Connect the audio interfaces to the computer using the USB cables. The cables must be connected between the USB entry in the audio interface (see figure 3.5 (b)) and the USB entries in the computer;
- Connect the audio interfaces to the power amplifier using the Jack cables. These cables must be connected between the power amplifier and the output entry (see figure 3.5 (b)) of the audio interface;
- Turn the audio interface +48V switch to the ON position, and control the gains in order to produce proper results;
- Connect the speakers to the power amplifier;

After taking these steps, one is ready to conduct the experiment. To do so, one needs to import a signal to LabVIEW and to play it. The signal is then passed on to the audio interface, and from it to the

power amplifier that will magnify the signal to the speakers. Then, the responses are measured in the microphones and conveyed to the audio interface, which sends them to the computer where they are processed in LabVIEW. The acoustic experimental setup can be seen in figure 3.6.

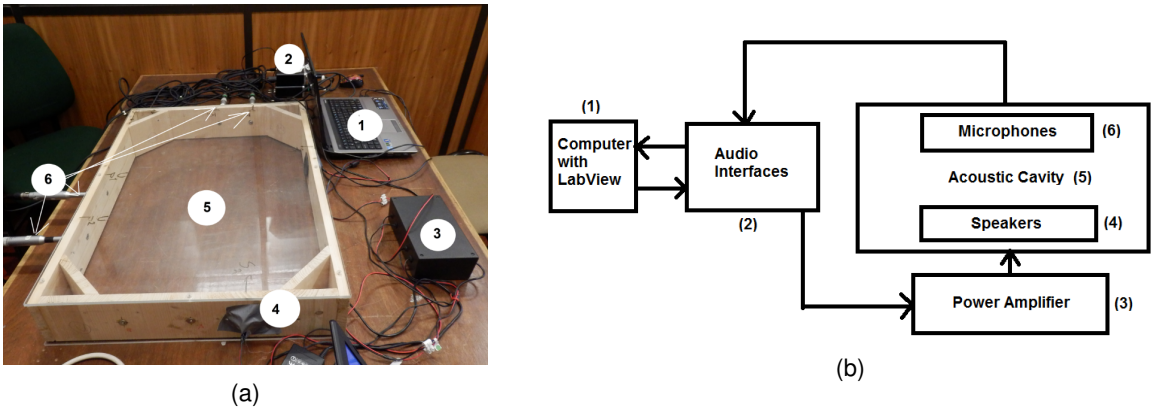

(a) (b)

Figure 3.6: a) Illustration of the acoustic experimental setup; b) Simple schematic of the connections in the acoustic experimental setup.

To verify that all the equipment is working properly, a signal with constant frequency is generated and the response is then measured by the microphones. In this case, the responses obtained by the microphones must have only one peak in the same frequency of the original signal. Otherwise, there may exist problems with the equipment and/or wire connections that must be fixed.

3.4.2 Analysis of the Vibro-Acoustic Cavity

3.4.2.1 Numerical Analysis

In this numerical analysis, the methodology described in section 3.3 is updated to analyse the vibro-acoustic cavity of a wooden box.

A new ANSYS APDL model is created with the geometry of the vibro-acoustic cavity described in [38]. Then, a mesh of FLUID30 3D acoustic elements is generated, and a structural steel plate is introduced in the cavity (see figure 3.7) using SHELL181 2D FEs. The acoustic fluid elements that are touching the plate are changed to FSI elements. The plate's displacement and rotation DOFs are fixed around the edges of the plate, and then, modal (to extract the global matrices) and harmonic analyses (with a load applied at an arbitrary point P of the plate) are conducted.

The geometry of the vibro-acoustic cavity is created by using the same set of commands as described in section 3.4.1.1. The coordinates of the defined keypoints are presented in table 3.3.

	Coordinates	
Keypoint nº	x (m)	y (m)
1	0	0
2	0.5	0
3	0.6	0.1
4	0.6	0.4
5	0.5	0.5
6	0	0.5

Table 3.3: Coordinates of the keypoints in the APDL model of the vibro-acoustic cavity.

Lines connecting these keypoints are defined, and an area is created using those lines. The area is extruded 0.1 m along the normal direction, completing the definition of the vibro-acoustic cavity geometry.

The sizing of the FLUID30 FE is done using the modelled areas, with the set of commands described in section 3.4.1.1. The mesh is then generated using the commands *Meshing/Mesh/Volume Sweep/Sweep*, and selecting the modelled volume as the volume to mesh.

After completing the solution of the modal analysis, the global assembled matrices may be imported to Matlab®. Then, these matrices are used to compute the transmissibility functions that are used to estimate the pressure responses (as described in section 3.3), and to perform the identification of sources.

3.4.2.2 Experimental Analysis

In this experiment, the previously described steel plate is inserted at $x = 600$ mm (see figure 3.7). Then, a shaker excites the plate at a point P of coordinates $(x, y, z) = (600, 350, 50)$ mm and the pressure responses are measured by the microphones.

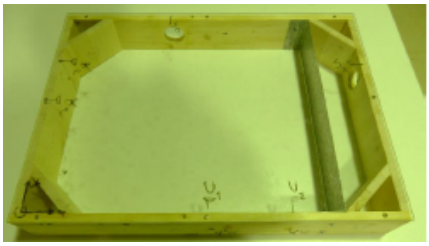

(a)

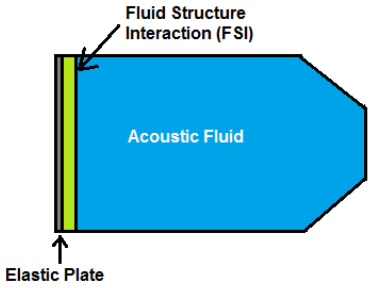

(b)

Figure 3.7: a) Experimental vibro-acoustic cavity [38]; b) Geometry of the numerical vibro-acoustic cavity.

The hardware and experimental procedures are similar to the ones described in [38].

The hardware used in the experimental setup is the following:

- Four Behringer ECM8000 condenser microphones;
- Two Behringer U-Phoria UMC2002HD audio interfaces;
- Four SM6BK XLR cables (one for each microphone)
- Two USB cables;
- A computer with LabVIEW for sound acquisition;
- Bruel & Kjaer Vibration Exciter Type 4809;
- Bruel & Kjaer Power Amplifier Type 2712;
- Bruel & Kjaer Signal Analyser Type 3160-A-042;
- A computer with Pulse LabShop Version 22 Software;
- Three Bruel & Kjaer Accelerometers Type 4508;

The experimental procedure is as follows:

- Secure the steel plate to the wooden box, and hang the box on the stand using nylon strings to simulate free-free conditions;
- Place the microphones in the respective holes, and connect them to the audio interfaces using the SM6BK XLR cables (as described in the acoustic cavity experimental procedure);
- Connect the audio interfaces to the computer using the USB cables;
- Fix the magnet of the vibration exciter on the steel plate (at point P), and connect it to the power amplifier;
- Connect the power amplifier to the signal analyser;
- Connect the signal analyser to the computer;
- Place the accelerometers on the plate and wooden cavity using wax to secure them;
- Use Pulse LabShop software to generate a swept sin wave. This signal is conveyed to the signal analyser, and from it to the power amplifier. Then, the power amplifier amplifies the signal and passes it to the vibration exciter.
- When the plate starts to vibrate, run the LabVIEW program for sound acquisition, and obtain the pressure responses in the frequency domain.
- Import the data of the accelerometers and check for vibration peaks in the structures.

Three accelerometers are placed in the vibro-acoustic setup: Two of them are placed on the wooden box (at points A and B in figure 3.8); the third one is placed on the steel plate where the vibration exciter is connected (point C in figure 3.8). Figure 3.8 shows the experimental vibro-acoustic setup.

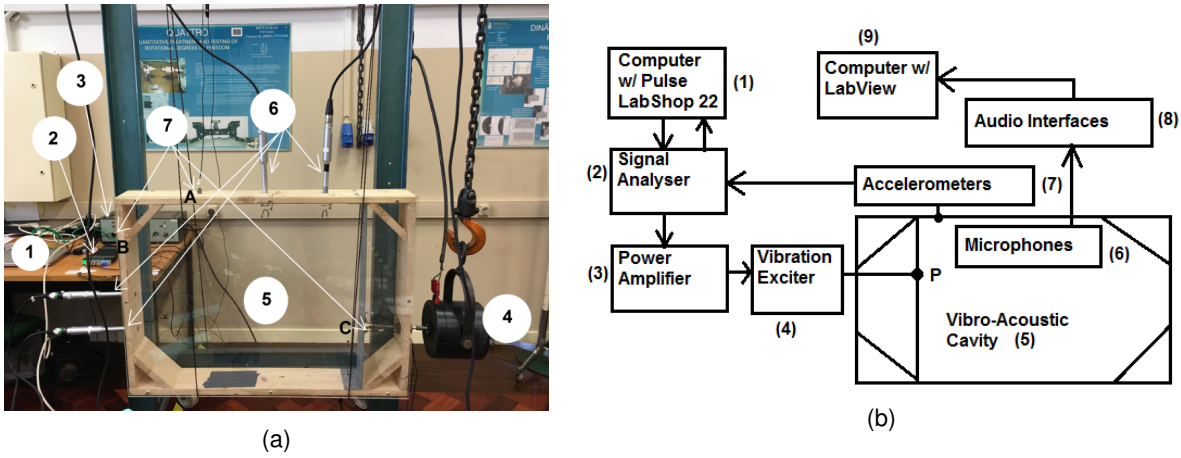

(a) (b)

Figure 3.8: a) Illustration of the vibro-acoustic experimental setup; b) Simple schematic of the connections in the vibro-acoustic experimental setup (numbers 9 and 8 correspond to numbers 1 and 2 respectively, in figure 3.6).

After conducting this experiment, the obtained pressure responses are compared with the ones obtained using the numerical procedure.

3.4.3 Matlab® Code Optimization

So far, the receptance matrix $[H]$ was computed with the entire inverse of $[Z]$. However, the analyses that have been conducted so far, only required a few entries of $[H]$. This means that the described method computes many unnecessary data, thus decreasing code performance and increasing simulation time.

One possible solution for this, is to use the adjugate matrix to compute only the necessary entries of the recepance matrix $[H]$. The adjugate of an $n \times n$ matrix $[A]$ is defined as

$$[adj[A]] = [cof[A]]^T, \tag{3.5}$$

where $[cof[A]]$ is, as described in [55], the cofactor matrix of $[A]$ that can be defined in the following manner

$$(cof[A])_{ij} = (-1)^{i+j} \cdot B_{ij} \tag{3.6}$$

where B_{ij} is the ij-minor of $[A]$. For any $n \times n$ matrix one can write [55]:

$$[A] \cdot [cof[A]]^T = (det[A])[I]. \tag{3.7}$$

Then, the required entries of the inverse of $[A]$ can be computed using the following equation.

$$[A]^{-1} = (det[A])^{-1} \cdot [adj(A)] \tag{3.8}$$

To implement this method in a Matlab® routine, one has to take the following steps:

- Obtain the determinant of $[Z]$ using the *det* command in Matlab®. In some cases it might happen that Matlab® returns the determinant of $[Z]$ as 0 or as *inf*. This happens because the determinant of $[Z]$ becomes too small or too large and surpasses the precision of Matlab® (overflow occurs). This problem can be solved by multiplying $[Z]$ with a constant, and determining the determinant of the resulting matrix. If the determinant is returned as zero, the constant must be higher than one. If the determinant is returned as infinite, then the constant must be lower than one.

- Create a set of new matrices equal to the dynamic stiffness matrix to perform the next computations. The number of matrices created must be equal to the number of the required entries of $[H]$.

- In the new matrices, remove row j and column i. The indexes i, j are the indexes of the required entry of $[H]$.

- Compute the determinant of this new matrix. In this case, it might also be necessary to multiply this matrix with a constant, because the determinant of the matrix obtained from removing the row j and column i will probably overflow.

- Create a selection condition that evaluates if $i + j$ is an odd or even number. If the sum retrieves an odd number, the cofactor must be multiplied by -1.

- Divide the cofactor by the determinant of $[Z]$ to obtain the required entry of $[H]$. When doing this operation, one must keep in mind that $det(c[A]) = c^n det[A]$, and take this into account when performing the division. Therefore, the required entry of $[H]$ is given by the following expression:

$$H_{ij} = \frac{\pm det[Z_{aux}]}{det[Z]} = \frac{\pm c \cdot det(c[Z_{aux}])}{det(c[Z])} \tag{3.9}$$

  where $[Z_{aux}]$ is the matrix obtained when row j and column i are eliminated from $[Z]$, and c is the arbitrary constant.

This new method of obtaining the entries of $[H]$ can save both time and computational power when using Matlab® to compute transmissibility functions. The results for the elapsed and CPU times are presented for several systems in analysis.

3.4.4 Vibro-Acoustic Source Localization

The main purpose of this work is to use the transmissibility concept to find the location of a vibro-acoustic source. This is done by using a Matlab® routine that implements the following algorithm:

- Import a file containing the measurements of the pressure response at the desired node, obtained from ANSYS harmonic analysis;

- Import the $[K]$, $[C]$, and $[M]$ matrices and the mapping file obtained from ANSYS in the modal analysis;
- Read the mapping file, evaluate the several nodes and DOFs, and choose the ones where the source might be located;
- For every possible source, a cycle is launched in which $[Z]$ is computed over the intended range of frequencies, and the entries of the adjugate matrix of $[Z]$ are used to extract the necessary entries of $[H]$. Then, the transmissibility functions are computed, and equation 2.102 is used to estimate the pressure responses;
- The correct source is the one that minimizes the error function defined by the following equation:

$$\epsilon_{VA} = \sum_{i=1}^{freq} [(P_{meas})_i - (P_{calc})_i]^2 \tag{3.10}$$

where P_{meas} is the measured pressure response obtained in ANSYS, and P_{calc} is the estimated pressure response obtained in Matlab® by using the following expression:

$$P_{calc} = T_{KU} \cdot u_U \tag{3.11}$$

where u_U is the displacement imposed by an arbitrary dynamic load of constant amplitude (in this case $F = 1$), and T_{KU} is given by the following equation.

$$T_{KU} = H_{UK}^T H_{UU}^{-1} \tag{3.12}$$

As the force is unitary the imposed displacements may be estimated (when there is no cross-talk) using the sum of the lines of the submatrix H_{UU}.

One may notice that equation 3.12 differs from equation 2.103. This has to do with the global matrices that are extracted from ANSYS and imported to Matlab®. These matrices are assembled in a manner that requires an adaptation on the theoretical equations. Without such adaptations, the analysis of transmissibility functions would not retrieve the correct results, and therefore, the source identification routine would not work either.

Usually, the measurements obtained experimentally are polluted with noise. In order to simulate this, one can add noise to the signal obtained in ANSYS, and analyse how the source localization results vary with it. The addition of white Gaussian noise can be done in Matlab® using the command *randn*.

3.5 Aircraft Interior Analysis

The previously presented methodologies can be applied to the analysis of a simplified aircraft interior. The goal is to use the transmissibility concept to evaluate transmissibilities, to determine unknown pres-

sures at certain locations of the aircraft, and to use the source localization algorithm to find the source of the measured disturbances.

3.5.1 Acoustic Analysis

This analysis is conducted using a simplified model of an aircraft interior. The model has the shape of a half circular tube with 3 m in length. This model is created in ANSYS APDL by defining a half circle with a radius of 2.5 m, using the commands *Modeling/Create/Areas/Circle/By dimensions*. Then, this half circle is extruded along the normal axis using the command sequence *Modeling/Operate/Extrude/Areas/Along Normal*.

The discretization of the domain is done by using the FLUID30 3D acoustic FE. Using the *manual size* command, the maximum length of the elements is set to 0.175 m in all areas of the model. Then, a swept mesh is generated with the desired dimensions.

Once the modelling and meshing are completed, a modal analysis is conducted, and the mass and stiffness matrices (no absorption is considered so there is no damping matrix) are extracted from ANSYS using the *hbmat* command. The harmonic analysis is conducted with an imposed pressure at a node of the domain, and after measuring the pressure response at another node, this result is compared to the one obtained in Matlab® by using the methodology described in 3.2.

With the purpose of studying the presence of chairs in the aircraft interior, another model is created with the same geometry as before. The model of the chairs can be seen in the following figure.

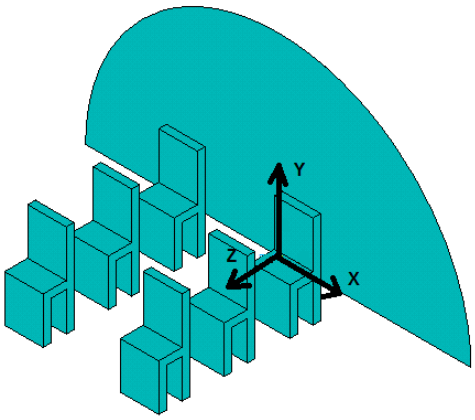

Figure 3.9: Model of the chairs of the aircraft interior.

These chairs are 1.25 m height, the thickness of the back, legs and sit is 0.1 m, the height of the sit is 0.6 m, the length of the chairs is 0.4 m and the width is of 0.5 m. The distance between chairs is of 0.45 m in the Z direction, and of 1 m in the X direction. These chairs are considered to be rigid and reflective (for modelling simplicity), and their geometry is subtracted to the geometry of the cabin by using the commands *Modeling/Operate/Booleans/Subtract/Volumes* of ANSYS APDL.

The discretization is, again, done by using the FLUID30 FE and, on the manual size command, the maximum length of the elements is set to 0.25 m in all the areas. This allows the mesh to be coarser

away from the chairs, and more refined in the vicinity of the chairs. Due to the geometry of the problem, it is not possible to define a swept mesh. As a consequence, a free mesh is defined.

After the modelling and meshing are concluded, the same procedure is conducted as for the model without chairs.

This analysis includes the localization of acoustic sources in the models described above. This is done with the methodology described in 3.2

3.5.2 Vibro-Acoustic Analysis

The vibro-acoustic analysis of the simplified aircraft interior uses the same models as the acoustic analysis. However, for the vibro-acoustic analysis, SHELL181 FEs are used for coating the outer surface of the model. To introduce the shell and define the FSIs in the model, one has to take the following steps:

- Select the nodes of the boundary surfaces, and change the material properties of these nodes in order to introduce the structural plate;
- Select the elements attached to these nodes, and make these elements the FSI elements by using the procedure in [52]. In this case, it is necessary to change the active coordinate system to cylindrical coordinates in order to select the nodes on the cylindrical wall. In this case, the X coordinate is equivalent to the R coordinate of the cylindrical coordinate system.

The rotation and displacement DOFs of the structural shell are considered to be fixed around the shell's edges.

After defining the model, the meshes, and the boundary conditions, a modal analysis is performed in order to extract the stiffness and mass matrices from ANSYS. After concluding this analysis, a harmonic load of 1 N is imposed at a node of the shell to simulate an imposed displacement. After running the harmonic analysis, transmissibility functions can be obtained by dividing the pressure responses by the imposed displacements over a previously defined frequency range. These results are then compared with the ones obtained in Matlab® using the routine for transmissibility analysis.

The vibro-acoustic analysis of this system is done in several steps:

- First, the two vertical walls at the ends are inserted, and the harmonic and modal analyses are conducted;
- Then the floor is inserted and the procedure is repeated;
- Then the ceiling is inserted, completing the entire shell, and the analyses are conducted once more;
- Lastly, the chairs are inserted along with the entire shell, and the modal and harmonic analyses are conducted.

Given the large increase in the number of DOFs when the shell is inserted, the analyses without chairs used a coarser mesh with a maximum length per FE of 0.5 m. The length of the elements in the vibro-acoustic analysis of the model with chairs is the same as in the acoustic analysis.

3.5.3 Matlab® Transmissibility Analysis

The procedures to conduct the transmissibility analysis and source localization in Matlab® for the aircraft interior are similar to those described in sections 3.2, 3.3 and 3.4.4. However, due to the large dimension of the $[Z]$ matrix, for some analyses it is not possible to solve the overflow in the determinants used to obtain the entries of the adjugate of $[Z]$. Multiplying the $[Z]$ matrix by a constant and computing the determinant of the resultant matrix proved to be ineffective in the vibro-acoustic analysis. As a consequence of this, a new strategy to avoid overflow is created.

Overflow occurs because the value of the determinant exceeds the limits of Matlab®'s precision. One possible way to avoid this is to work with the logarithm of the determinant.

As described in [56], using LU decomposition of a matrix $[A]$, the determinant of $[A]$ can be given by

$$det[A] = det[L] \cdot det[U] \tag{3.13}$$

where $[L]$ and $[U]$ are both triangular matrices. Once the terms in the diagonal of $[L]$ are all equal to 1, the determinant of $[L]$ is equal to one. This means that the determinant of $[A]$ may be rewritten as follows:

$$det[A] = u_{11} \cdot u_{22} \cdot ... \cdot u_{nn} \tag{3.14}$$

or, if permutations are necessary, the determinant of $[A]$ is given by

$$det[A] = \pm u_{11} \cdot u_{22} \cdot ... \cdot u_{nn} \tag{3.15}$$

where the determinant of the permutations matrix $[P]$ is either given by 1 or by -1. Using the properties of logarithms it is possible to obtain the logarithm of the absolute value of the determinant of $[A]$ as

$$log(|det[A]|) = log(|u_{11}|) + ... + log(|u_{nn}|). \tag{3.16}$$

Using these previous equations and applying them to the case in analysis, one can get the absolute value of the entry of $[H]$ using the following expression:

$$H_{ij} = 10^{log(|det[A]|) - log(|det[Z]|)} \tag{3.17}$$

where $[A]$ is the matrix obtained from eliminating row j and column i of the $[Z]$ matrix.

This method can be implemented in Matlab® using the following algorithm:

- Obtain the $[Z]$ matrix and create several matrices equal to $[Z]$. One should create as many matrices as the number of intended entries of the $[H]$ matrix;
- Eliminate row j and column i of the previously defined matrices. The indexes i and j are the indexes of the intended entry of $[H]$;
- Perform LU decomposition in all of these matrices and in the $[Z]$ matrix using the Matlab® com-

mand *[L,U,P]=lu(Z)*;

- Store the elements of the diagonal of $[U]$ in a vector using the command *x=diag(U)*;
- Create a cycle where the logarithms of all the entries of the vector that contains the diagonal of $[U]$ are obtained. Still inside this cycle, one must perform the summation of all the logarithms.
- Repeat the last two steps for all the matrices including the $[Z]$ matrix.
- Obtain the absolute value of the entry of $[H]$ using equation 3.17.

One major problem of this method is related to the loss of the signal of the desired entry. In order to track the signal, one has to compute the determinants of the several $[P]$ matrices and count the number of negative entries in the diagonal of $[U]$. Then, taking this into consideration, the signal of the entry can be easily determined.

This method produces results similar to those described in 3.4.3, and is more effective in avoiding overflow. Therefore, this method is more suitable to analyse problems with larger matrices. Despite becoming unstable with larger matrices, the method described in 3.4.3 is faster than this new one, and keeps the signal of the intended entry of $[H]$. Regarding this, one should first evaluate if it is possible to solve the problem with the method described in 3.4.3, and if not, then use this new approach.

4 Results and Discussion

In this chapter the results obtained following the methodologies previously described are presented. Whenever possible, the obtained results are compared with those available in the literature.

4.1 Transmissibility in a Mass-Spring System

In the present section, it is intended to apply the methodology introduced in section 3.1.1 to study the system presented in figure 3.1. The verification of the obtained results is done by comparing them with the results presented in [5]. The assembly of the stiffness matrix is based on the connectivity table presented in table 4.1.

Element	Stiffness (10^5)(N/m)	Corresponding Nodes
3	4	1 2
4	5	2 3
5	7	2 5
6	2	1 4
7	8	3 5
8	3	3 4
9	6	3 6
10	3	5 6
11	5	4 6

Table 4.1: MDOF mass-spring system connectivity table.

The mass of the several masses is presented in table 4.2. As the displacements x_1 and x_2 are fixed (see figure 3.1), the masses of m_1 and m_2 are set to 0. So the mass matrix is a diagonal matrix, and the entries of the diagonal are $(0, 0, m_3, m_4, m_5, m_6)$.

Masses	kg
m_3	4
m_4	3
m_5	6
m_6	8

Table 4.2: Masses of the mass-spring system.

With the material properties defined, the mass and stiffness matrices are assembled. Then, the dynamic stiffness and the receptance matrices are obtained, and used to compute the transmissibility matrix.

The results obtained for the entries T_{11} (equivalent to T_{15}) and T_{12} (equivalent to T_{16}) of the transmissibility matrix are presented in figures 4.1 and 4.2 respectively.

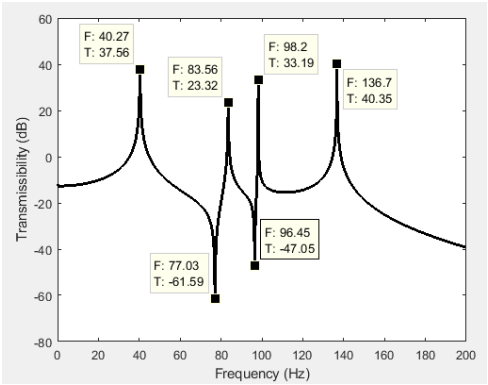

(a)

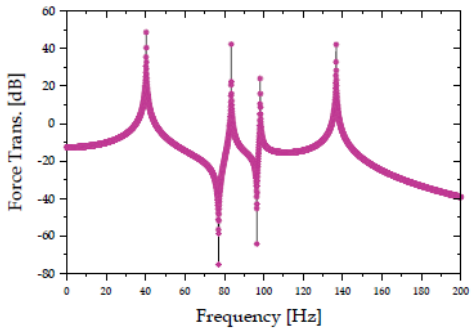

(b)

Figure 4.1: Comparison between the obtained results (a), and the results in [5] (b), for the entry T_{11} of the transmissibility matrix in dB.

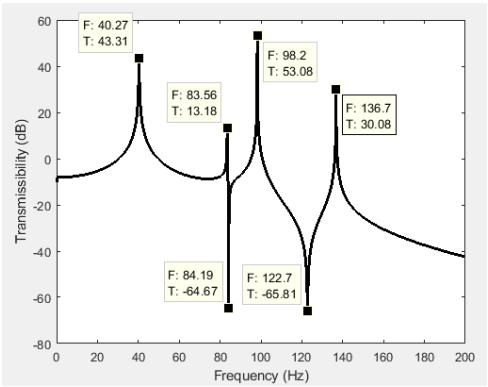

(a)

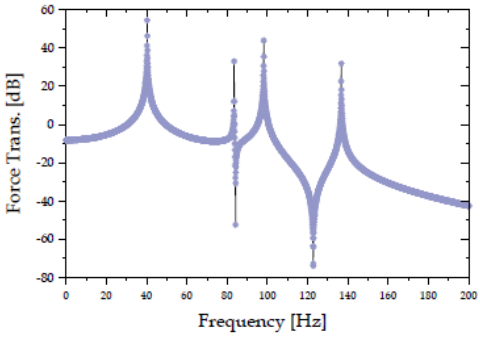

(b)

Figure 4.2: Comparison between the obtained results (a), and the results in [5] (b), for the entry T_{12} of the transmissibility matrix in dB.

By observing figures 4.1 and 4.2, one can notice an almost perfect match between the obtained results and the results in [5]. The transmissibility peaks and the overall shape of the curves are the

same. However, sometimes the amplitude of the peaks is not exactly the same. This difference in terms of amplitude may be caused by a different number of evaluated frequencies within the frequency range. The results in figure 4.1 are obtained using the dynamic stiffness matrix approach, while the results in figure 4.2 are obtained using the receptance matrix approach. It can be seen that both approaches are equally appropriate to evaluate transmissibility in a mass-spring system.

In order to obtain the transmitted loads at the supports, it is considered that the applied forces have a magnitude of 10 N. The transmitted loads are shown in figure 4.3 and are obtained using the receptance matrix approach.

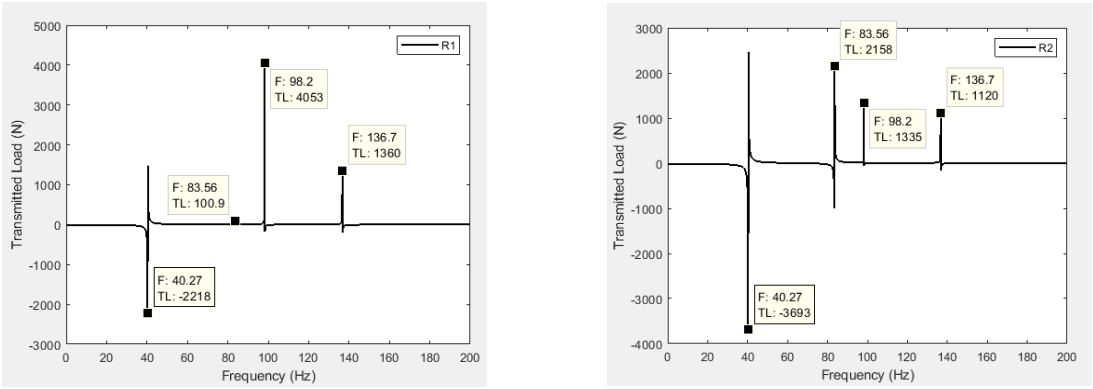

(a) (b)

Figure 4.3: Results obtained for the transmitted load in node 1 (a), and in node 2 (b) of the mass-spring system.

As expected, the frequency of the peaks of the transmitted loads presented in figure 4.3, is coincident with the frequency of the peaks of the transmissibility functions shown in figures 4.1 and 4.2.

As an alternative, the transmissibility functions presented in figures 4.1 and 4.2 can be computed as described in 3.4.3. The CPU and elapsed times of the simulations are presented in table 4.3.

Method		Elapsed Time (s)	CPU Time (s)
$[adj[Z]]$	1	0.1957	0.4212
	2	0.2070	0.4680
	3	0.1895	0.3744
$[inv[Z]]$	1	0.1416	0.3120
	2	0.1588	0.3744
	3	0.1247	0.2496

Table 4.3: Simulation times obtained in the transmissibility analysis of the mass-spring system.

Analysing table 4.3, one can conclude that, for this analysis, using the complete inverse of $[Z]$ is faster than using its adjugate to compute only the necessary entries. This happens because $[Z]$ is a 6×6 matrix. In addition, in this case, 8 entries of $[H]$ are required. Therefore, trying to compute only these entries of $[H]$ requires more instructions and increases the simulation time. Despite the difference in the simulation time, the results obtained from both methods are similar, as shown in figure 4.4.

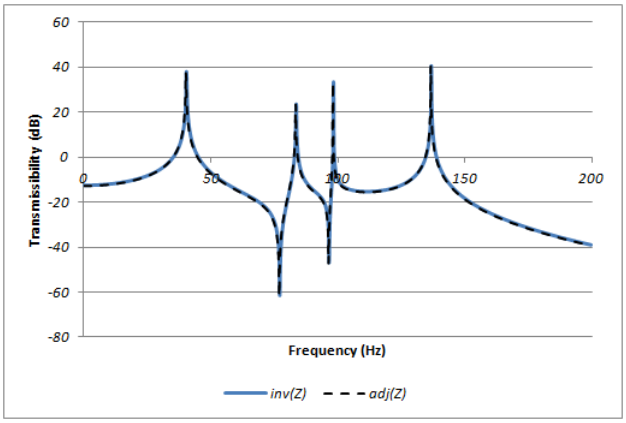

Figure 4.4: Results obtained from both methods for the entry T_{11} of the mass-spring system's transmissibility matrix. The results obtained using the adjugate of $[Z]$ are presented in black, and the results obtained using the inverse of $[Z]$ are presented in blue.

4.2 Acoustic Transmissibility

This section presents the results obtained with the methodology described in section 3.2. The system studied is a 3D model of a tube with rectangular cross section, filled with an acoustic fluid. The properties of the acoustic fluid and the dimensions of the tube are presented in table 4.4.

Sound Speed	344 m/s
Mass density	1.21 kg/m^3
Reference Pressure	20×10^{-6} Pa
Length	4 m
Height and Width	0.1 m

Table 4.4: Acoustic Tube Properties [4].

As mentioned before, the tube is modelled in ANSYS APDL. As the tube's length is relatively larger than the width and height, then, it can be considered, as an approximation, that the tube is 1D. Analytical solutions for a 1D tube with an imposed pressure of 1 Pa at one end, and a reflective or anechoic boundary at the other are available. So, for both cases, one modelled tubes with different mesh refinements using the FLUID30 FE, and a harmonic solution was conducted for a frequency of 200 Hz. The obtained results and comparison with the analytical solutions are presented in figure 4.5.

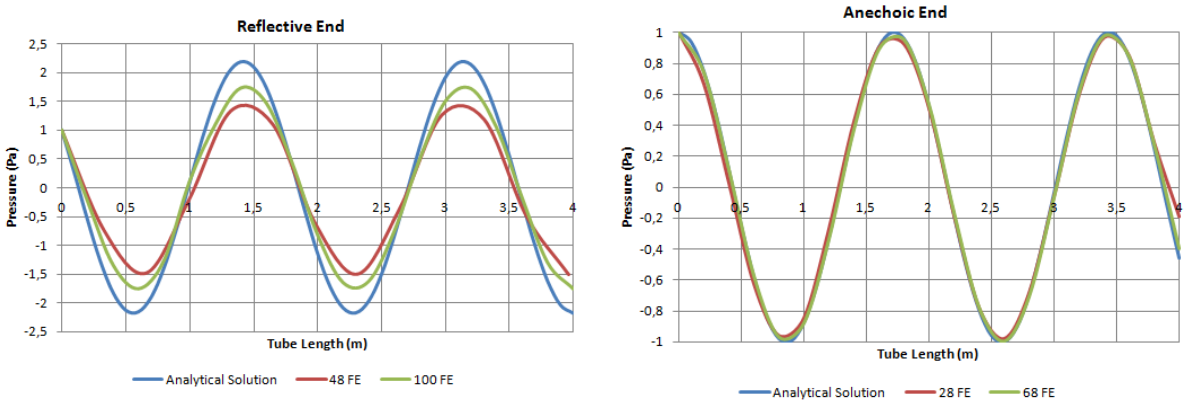

(a) (b)

Figure 4.5: Comparison between the analytical solution and the numerical solution for an acoustic tube with an imposed pressure of 1 Pa at $z = 0$ and: a) a reflective end; b) an anechoic end.

The number of FEs presented in the legend of the plots in figure 4.5 corresponds to the number of FEs along the length of the tube. By observing the plots in figure 4.5, it can be stated that for an anechoic end, the solution converges rapidly to the analytical one, being able to create a precise solution for a relatively small number of FEs. However, for the case of a reflective end, the refinement needs to be larger, but it can be seen in figure 4.5 that the solution is converging to the analytical one. From the results obtained in the verification process, one can conclude that the FE model is properly defined and obtaining correct results.

From this point forward, only results concerning a reflective end are presented. The methodology for obtaining the transmissibilities for an anechoic end is similar to the one used for a reflective end. In addition, since the main focus of this work is performing source localization, the case with a reflective end is enough to provide an example of the source localization method introduced in section 3.2. Once the mesh of 100 FEs was not sufficiently close to the analytical solution for a reflective end, in the further analyses, a mesh with 200 FEs will be used.

In this analysis, a 200 FE mesh is used. The mesh only presents refinement in the longitudinal direction because, in this case, as the wave is plane and there are no obstacles in the tube, the transverse refinement is not necessary. In order to simulate an imposed pressure at $z = 0$, a pressure of 1 Pa is applied at each one of the four nodes of the element that is contained in $z = 0$. Then, the pressure is measured at one of the nodes of the mid-section of the tube. Once the wave is plane, the pressure at the mid-section is the same for all the four nodes located in this area.

The transmissibility function between the source and the mid-section is calculated using the equations presented in section 2.5.6.2, and using the methodology described in 3.2. In this analysis, one has to consider the transmissibility between the four source nodes at the beginning of the tube, and the four reference nodes at the mid-section of the tube. Therefore, both H_{KU}, H_{UU} and T_{KU} are 4×4 matrices. After adapting the methodology to the case under study and performing the necessary calculations, one obtains the transmissibility matrix and the pressure at the reference nodes. In the following figure, the results obtained for the pressure as a function of the frequency are presented.

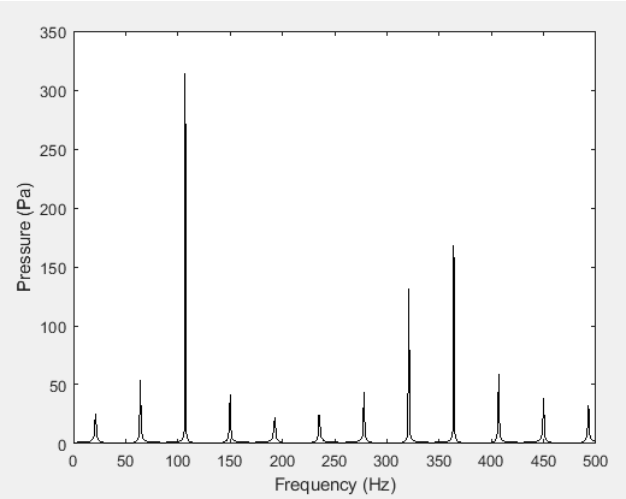

Figure 4.6: Pressure response at the reference node, in the acoustic tube.

Now, one will obtain the pressure response at the reference node while varying the location of the source, and use equation 3.3 to evaluate which one of the possible sources is the correct one. It is considered that the source comprises the pressure imposed at four nodes of the same element belonging to the same plane. Eight different sources are considered at different locations along the tube's length, and it is known that the eighth location is the correct one. The pressure is calculated using the transmissibility concept, and is compared with the results obtained from the FE model. The results of the source localization problem are presented in figure 4.7

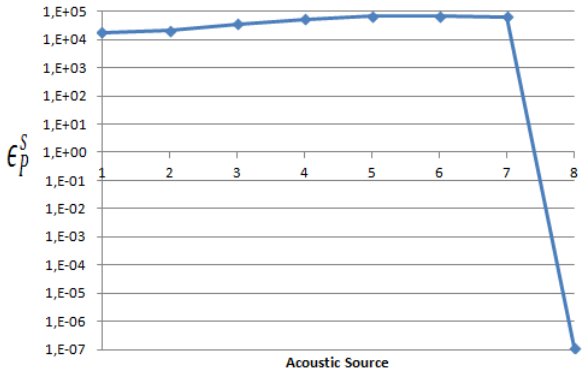

Figure 4.7: Results obtained with the source localization algorithm applied to an acoustic tube.

As it can be observed in figure 4.7, the source that minimizes the error function (ϵ_p^s) corresponds to the location number eight. So, it can be concluded that the transmissibility concept is able to accurately locate the acoustic source.

Now, a new system is created with a new arrangement of FEs in order to create a center-line along the acoustic tube. This means that each section of the tube is composed by 4 FEs. The tube is divided in 100 sections, giving a total of 909 nodes. So, the new dynamic stiffness matrix is a 909×909 matrix. In this case, a pressure of 1 Pa is imposed at one end of the tube (at the center) and the pressure response is measured at the mid-section along the center-line. Using the method of the entire inverse of $[Z]$ to compute the transmissibility function between these two nodes, and the method of the adjugate

matrix to compute only the necessary entries of $[H]$ and then the transmissibility function, the following simulation times are measured.

Method		Elapsed Time (s)	CPU Time (s)
$[adj[Z]]$	1	3.688	3.759
	2	3.679	3.713
	3	3.687	3.713
$[inv[Z]]$	1	424.151	423.933
	2	428.396	427.895
	3	426.517	426.039

Table 4.5: CPU and elapsed times obtained in the transmissibility analysis of an acoustic tube.

The results presented in table 4.5 prove that for larger matrices, the method of the adjugate matrix can become significantly faster. Then, this method enables the analysis in Matlab® of larger or more refined systems.

4.3 Vibro-Acoustic Transmissibility

Applying the methodology described in 3.3, a tube with a length of 4 m and a square cross section of 0.1 m width is created. Then, a structural steel plate is inserted at one of the ends. The properties of the acoustic fluid are presented in table 4.4, and the properties of the structural steel plate are described in table 4.6.

Young's Modulus	210 GPa
Density ρ	7800 kg/m^3
Thickness	0.001 m
Poisson's Ratio	0.3

Table 4.6: Steel plate properties [4].

The model is discretized with 24 elements per wavelength with a reference frequency of 200 Hz, and the dynamic load is applied at the node of the center of the plate. The pressure at the mid-section of the tube and the imposed displacement are then measured, and the P/u ratio is computed as a function of the frequency. The obtained results and the results presented in [4] are displayed in the following figure.

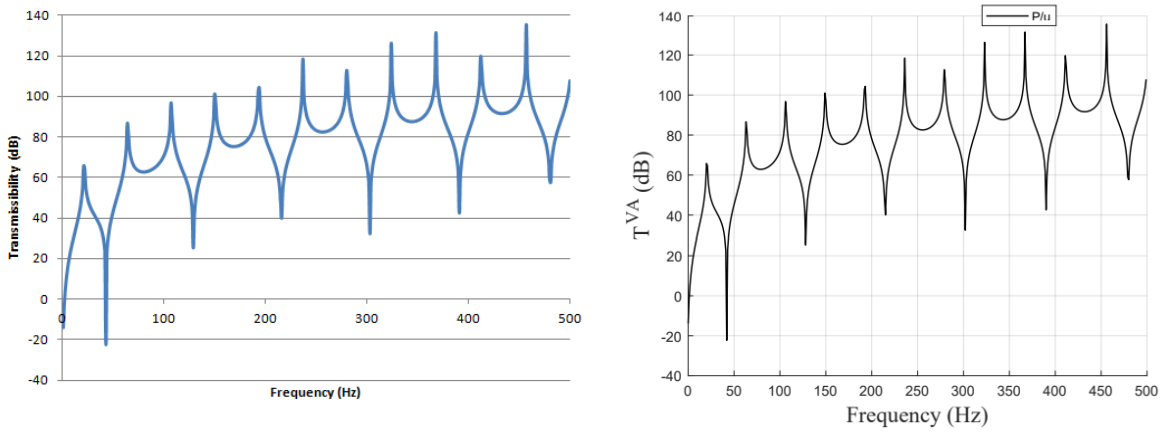

(a) (b)

Figure 4.8: Comparison between the obtained results (a), and the results presented in [4] (b), for a vibro-acoustic tube.

It can be seen in figure 4.8 that the results are similar, therefore, the verification was successful and the APDL model is working properly.

Now that the APDL model is verified, one needs to evaluate if the Matlab® routine is defined properly.

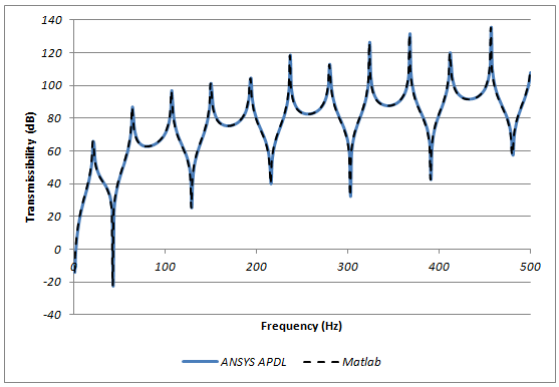

Figure 4.9: Comparison between the results obtained using Matlab®'s transmissibility analysis, and those obtained using the FEM for a vibro-acoustic tube.

Analysing the results in figure 4.9, one can conclude that the results obtained in Matlab® using the transmissibility concept, are similar to those obtained through ANSYS harmonic analysis. This concludes the verification of results in vibro-acoustics.

As mentioned before, the two different methods implemented for evaluating transmissibility functions present different simulation times. Table 4.7 presents the simulation times obtained from both methods.

Method		Elapsed Time (s)	CPU Time (s)
$[adj[Z]]$	1	2.072	2.090
	2	2.088	2.153
	3	2.065	2.121
$[inv[Z]]$	1	48.394	47.564
	2	43.390	43.399
	3	44.061	44.008

Table 4.7: Simulation times obtained in the transmissibility analysis of a vibro-acoustic tube.

Again, it becomes clear that for large matrices ($[Z]$ is 501×501), computing only the required entries of $[H]$ using the adjugate matrix of $[Z]$, can save a considerable amount of simulation time and computational power.

4.4 Acoustic Cavity Analysis

4.4.1 Numerical Analysis

The modelled cavity has the geometry of the inner part of the wooden box described in section 3.4. The properties of the acoustic fluid inside the cavity are the same as in table 4.4.

To evaluate this problem, two models, a 2D and a 3D model, are created, and a modal analysis is conducted. The geometry and meshes of these FE models are presented in figure 4.10.

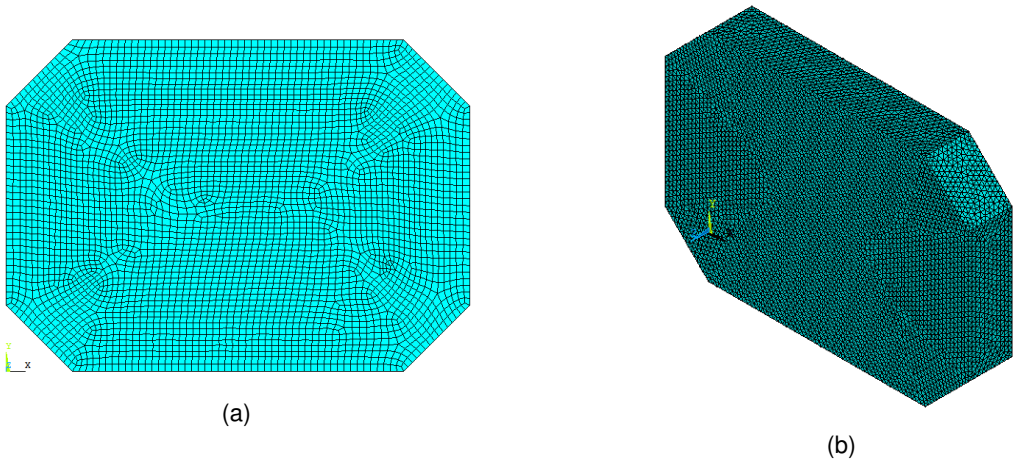

(a) (b)

Figure 4.10: FE models of the acoustic cavity. On the left (a), the 2D model, and on the right (b), the 3D model.

Both meshes have elements with a 10 mm side. This is done to ensure that for the studied range of frequencies there are at least 36 elements per wavelength. The results of the modal analyses for both models are presented in table 4.8.

Natural Frequencies (3D) (Hz)	Natural Frequencies (2D) (Hz)
0	0
259.30	259.30
360.07	360.07
466.47	466.43

Table 4.8: Comparison between the natural frequencies obtained with the 2D and 3D models of the acoustic cavity.

It can be seen in table 4.8 that the results of the modal analyses are practically the same for both models. In addition, the results presented in [38] show that from 0 to approximately 600 Hz, the solution of the harmonic analysis retrieves the same results for both models. Therefore, and in order to save computational power, the 2D model is used to compute the transmissibility functions. Also, a coarser mesh is used in order to use less computational effort between simulations. The used mesh has elements with a 25 mm side. The coordinates of the points where the pressure may be imposed/measured are presented in table 3.1. The pressure is imposed at points $S1$ and/or $S2$ and the pressure response is measured at point $K2$ (see figure 3.4). The results obtained for the pressure responses using the transmissibility concept are presented in figure 4.11.

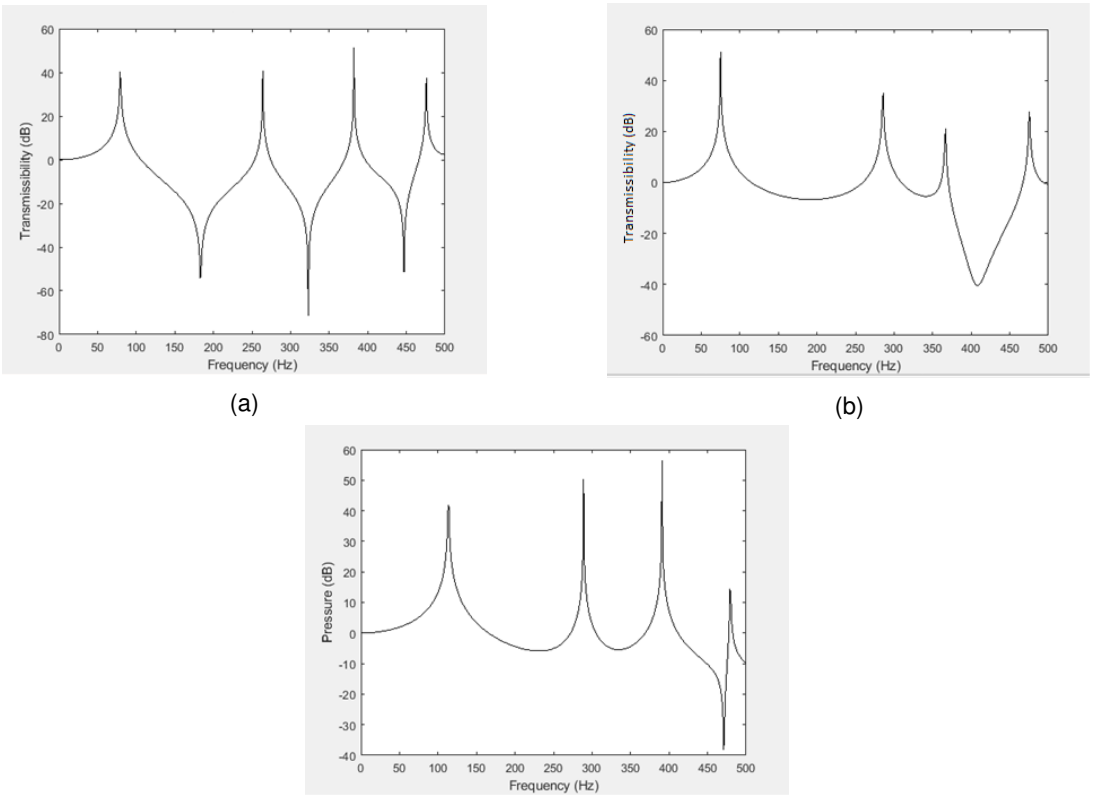

Figure 4.11: Pressure responses obtained using the transmissibility concept applied to an acoustic cavity. In (a), the pressure of 1 Pa is imposed at $S1$ and the response is measured at $K2$. In (b), the pressure is imposed at $S2$ and the response is measured at $K2$. In (c), the pressure is imposed at $S1$ and $S2$ and the response is measured at $K2$.

In fig.4.11.(a) and fig.4.11.(b), the transmissibility as a function of the frequency is equal to the pressure response function because a 1 Pa pressure is imposed only at one point. As a consequence, once the transmissibility function may be obtained, in this case, by dividing the pressure response by the imposed pressure, it is obvious that the transmissibility function is equal to the pressure response function. For the case in fig.4.11.(c) this is no longer true and the graph only presents the pressure response function.

The source localization algorithm can also be applied to this system. To do so, a model is created with an imposed pressure at point $S1$, and the measurements of the pressure response are taken at point $K1$. The obtained results can be seen in figure 4.12.

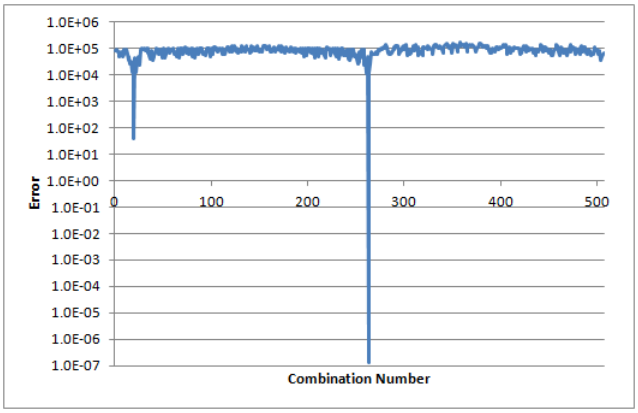

Figure 4.12: Accumulated error for every possible source in the acoustic cavity.

Figure 4.12 shows that the minimum error occurs in combination number 263. This combination corresponds to node 66. As $S1$ is located at node 66, then the program was able to identify the correct source.

4.4.2 Experimental Analysis

Applying the methodology described in 3.4.1.2, a frequency sweep signal with a range from 0 Hz to 1000 Hz is applied at the speaker positioned at $S2$ (see table 3.1). The responses are then measured on the microphones placed at points $U1$, $U2$, $K1$ and $K2$ (see table 3.1), and the results between 200 and 600 Hz are recorded. This range of frequencies is chosen because below 200 Hz, the amount of noise picked by the microphones is very high, and above 600 Hz, the FE model produced would require larger meshes and, therefore, higher simulation times. Since the speaker placed at point $S1$ has exhibited signs of malfunction (increasing noise and interference), no signal is sent to this speaker.

The comparison between the experimental and numerical results is presented in figure 4.13.

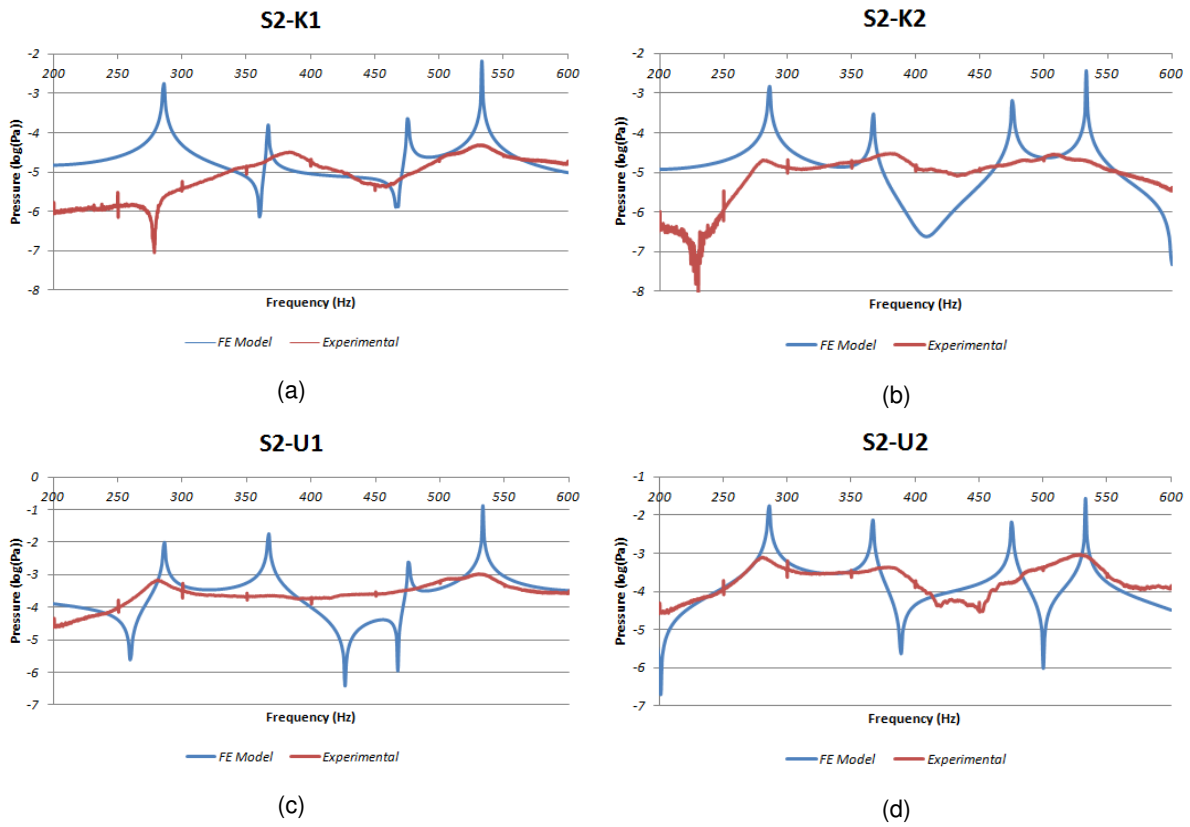

Figure 4.13: Comparison between the experimental and numerical results obtained in the acoustic cavity analysis.

It is clear that the differences between the numerical and experimental data are quite significant. First, not all the resonances of the numerical model are present in the experimental measurements, and, in addition, the resonances and anti-resonances that are present in both models exhibit some deviations.

The measurements taken at $U2$ and $K2$ are the ones that show more similarity when compared to the numerical results. In these experimental measurements, one can clearly relate the two first resonances and the first anti-resonance to the resonances and anti-resonances calculated by the FE model, making the results obtained between 200 Hz and 400 Hz quite reasonable when compared to the numerical model. At $K1$ there are also some resonances and anti-resonances identified by both numerical and experimental models with small deviations, and between 350 and 600 Hz, one can observe some similarities between the curves of both models. At $U1$, the model presents two resonances that also appear in the numerical model. Yet, in this case, the experimental response does not show 2 resonances and 3 anti-resonances that are present in the results of the FE model.

The differences between the numerical and experimental results, despite being significant, are expected. Some assumptions of the numerical model are not present in the experimental model such as:

- The assumption of fully reflective boundaries. The experimental model is made of pine wood boards and acrylic plates. These materials are not fully reflective, and, in addition, have different

absorption coefficients. As a consequence, the boundary conditions adopted in the FE model are a rough approximation.

- The fact that no acoustic damping is considered in the numerical model - The absorption of sound by the air is neglected in the FE model.

In addition, the approximation to a 2D model is not able to simulate the reflective behaviour of all the boundaries. Since the sides of the cavity are made of wood, and the tops made of acrylic plates with different thicknesses, the introduction of all these reflective boundaries would only be possible if a 3D model was used. However, some characteristics of the experimental setup also contribute to the differences presented in figure 4.13. The existence of background noise and of noise related to the interaction between electrical components, also create errors in the measurements.

4.5 Vibro-Acoustic Cavity Analysis

4.5.1 Numerical Analysis

This section presents the results obtained with the methodologies described in section 3.4.2.1. The discretized model with a 50 mm element mesh and boundary conditions can be seen in figure 4.14.(a). The properties of the acoustic fluid are the same as in table 4.4 and the properties of the steel plate are presented in table 4.9

Young's Modulus	205 GPa
Density ρ	7800 kg/m^3
Thickness	0.001 m
Poisson's Ratio	0.3

Table 4.9: Material properties of the steel U plate [38].

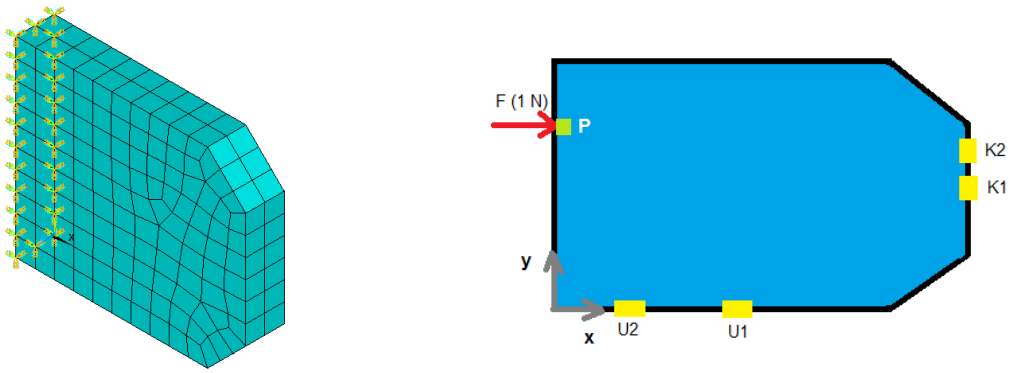

(a) (b)

Figure 4.14: Illustration of the FE model of the vibro-acoustic cavity (a); Illustration of the imposed load, and points where the pressure responses are obtained (b).

This model has the rotation and displacement DOFs fixed around the edges of the plate, and reflective boundary conditions. The harmonic analysis is performed with an applied load at point P of coordinates $(x, y, z) = (0, 350, 50)$ (mm) and the pressure responses are measured at $U1$, $U2$, $K1$ and $K2$ (see figure 4.14(b)).

Given the applied boundary conditions, by evaluating the transmissibility functions between the pressure responses at $U1$, $U2$, $K1$ and $K2$, and the displacement at point P, one obtains the following results (figure 4.15).

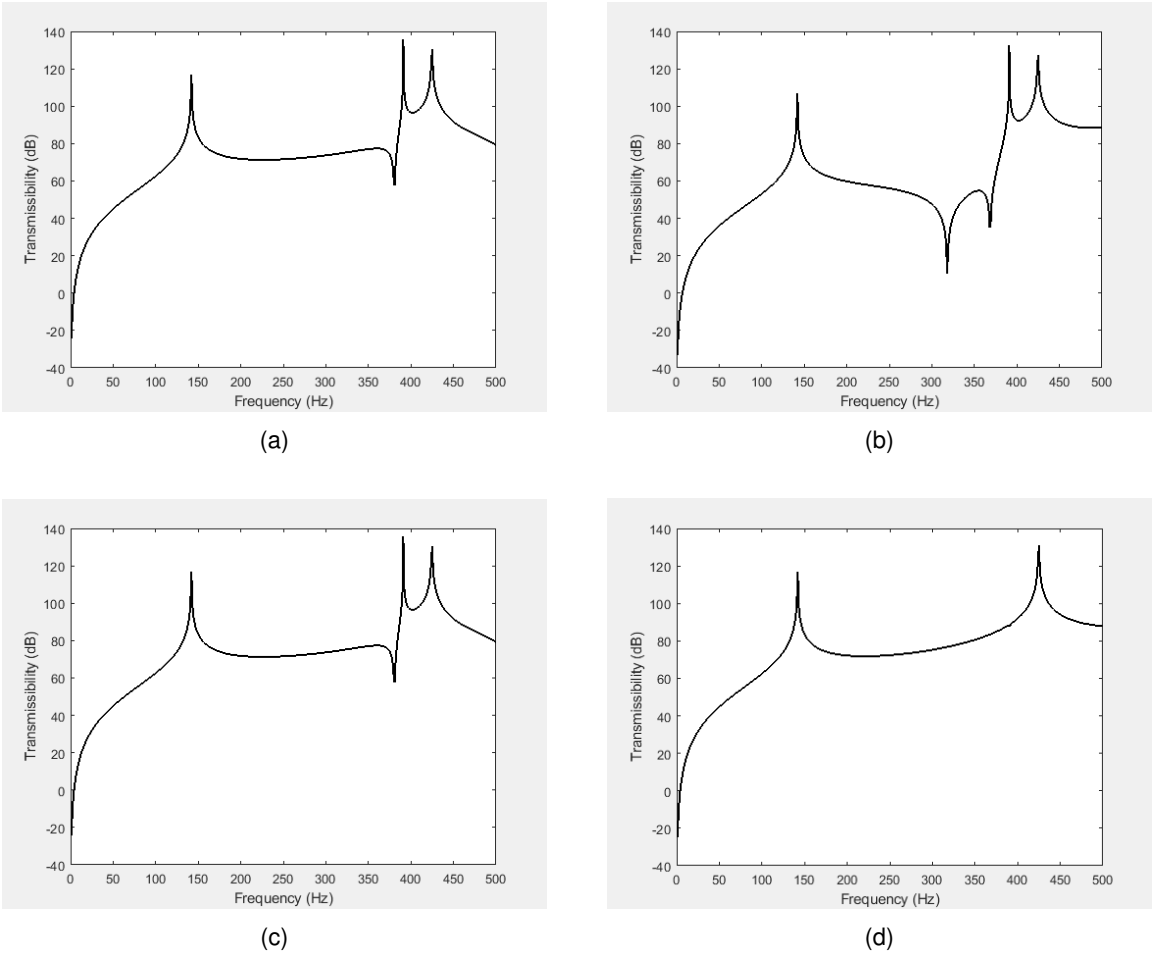

Figure 4.15: Vibro-acoustic cavity's transmissibilities. The load is applied at point P, and the pressure is measured at $K1$ (a), $K2$ (b), $U1$ (c) and $U2$ (d).

These results are obtained by using the adjugate matrix of $[Z]$ to calculate only the necessary entries of $[H]$. By doing so, the Matlab® simulation run significantly faster. Table 4.10 presents the simulation times for the optimized Matlab® code (using the adjugate matrix) and for the non-optimized code (using the entire inverse of $[Z]$).

Method		Elapsed Time (s)	CPU Time (s)
$[adj[Z]]$	1	11.168	11.123
	2	11.063	11.014
$[inv[Z]]$	1	54.088	54.288
	2	53.687	54.304

Table 4.10: Simulation times obtained in the transmissibility analysis of a vibro-acoustic cavity.

As it can be seen in table 4.10, by using only the necessary entries of $[H]$, one can save a significant amount of simulation time. For this simulation, the time needed to obtain the results using the adjugate matrix of $[Z]$, is approximately five times smaller. For the vibro-acoustic source localization routine, this optimized method can give the results faster and with the same precision.

As mentioned in section 3.4.4, the Matlab® code developed to perform the localization of a vibro-acoustic source is able to receive the mapping file and select the nodes where the source might be located. Knowing that the plate is fixed around the edges, and that the dimensions of the plate are 100$\times$500 mm, for the 50 mm element mesh generated (see figure 4.14.(a)), there are 9 possible nodes for the displacement to be imposed. For this case in particular, it is known that the number of the node that corresponds to point P is 259. The pressure response is measured at node 460, which corresponds to the location of point $K2$. After comparing the pressure estimation with the measured pressure for all the possible sources, the error is plotted as a function of the evaluated nodes. The obtained results are presented in figure 4.16.

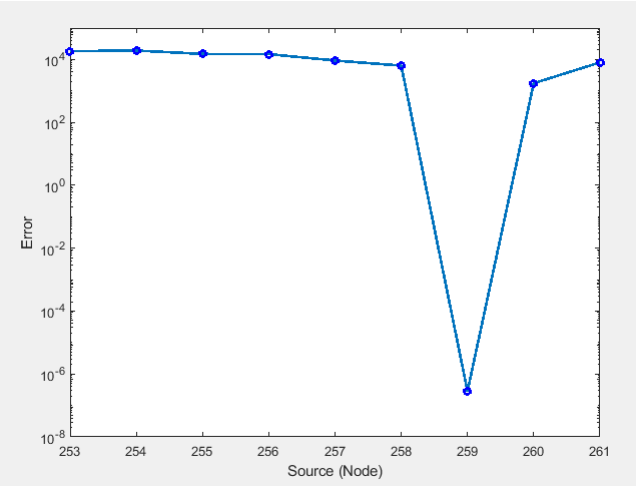

Figure 4.16: Accumulated error for every possible source in the vibro-acoustic cavity.

It can be seen in figure 4.16 that the program was able to properly identify the 9 nodes where the source could be located. It is also shown in figure 4.16 that the minimum of the error function occurs when the source is located at node 259, the node where the actual source is located.

Once experimental measurements are usually polluted with noise, it is interesting to see if adding noise to the measured signal compromises the obtained results. In order to evaluate the noise influence in the obtained results, several levels of additive noise are added to the signal. The goal is to discover

if the program is still able to identify the source node when the signal is polluted with noise. Figure 4.17 presents the results obtained for the several levels of noise, and compares them with the results obtained for the clean signal.

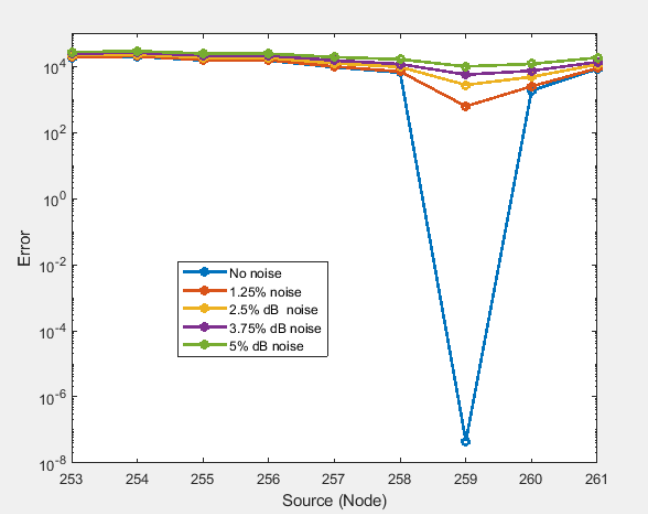

Figure 4.17: Results of the vibro-acoustic cavity's source identification algorithm with noise in the measured signal.

By analysing the results in figure 4.17, it becomes clear that exists a significant increase in the accumulated error when the noise is introduced. It is also clear that the minimum of the error function becomes less prominent. This means that eventually, the presence of noise in a signal can introduce larger errors, making the program unable to accurately predict the source location.

All the analyses conducted in this section had only one dynamic load applied to the steel plate, and, furthermore, so far only problems using scalar transmissibility have been analysed. Now, it is considered an additional source (1 N dynamic load) somewhere else on the plate. In this analysis, the second source is located at the point of the plate with coordinates (0,100,50) (mm), and the first source is located, as before, at point P. The pressure measurements are taken at points $K1$ and $K2$, and the obtained results are presented in figure 4.18.

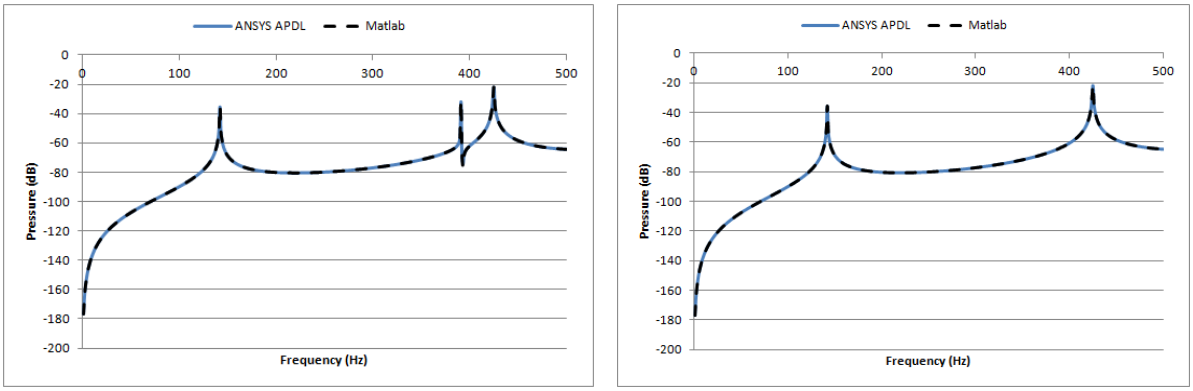

(a) (b)

Figure 4.18: Comparison between the results obtained using Matlab® 's transmissibility analysis, and those obtained using the FEM. The pressure responses at $K1$ and $K2$ are presented in (a) and (b) respectively.

The results presented above prove that the transmissibility concept also works when multiple sources are applied to the plate. In the present example, the displacements are applied in such a way that there is no cross-talk between both sources, and the results obtained from both the harmonic analysis and the transmissibility analysis are a perfect match. However, as it will be presented later in this work, the presence of cross-talk can produce differences in the results obtained from both methods.

When there are two sources applied on the plate, the source localization algorithm has to test all the possible combinations of two sources in the structure. This makes the identification of multiple sources more demanding computationally.

As mentioned before, in section 3.4.4, a possible way to estimate the displacements caused by 1 N dynamic loads applied to the structural plate in vibro-acoustic systems, is to estimate the displacement by assuming that it is equal to the summation of the terms in the lines of the H_{UU} matrix. So, in this case, as the H_{UU} matrix is a 2×2 matrix, the estimated displacements are given by

$$\begin{cases} u_1 = a_{11} + a_{12} \\ u_2 = a_{21} + a_{22} \end{cases} \tag{4.1}$$

where u_n are the estimated displacements and a_{ij} are the entries of H_{UU}. This estimation also carries an error associated to it, but it is small enough for the identification process to work properly. When there is cross-talk, this associated error becomes larger and the displacement on the plate cannot be estimated in this manner.

The results obtained using this method for displacement estimation are presented in figure 4.19. These results also contain the accumulated error for single sources applied on the plate (combination 37 to 45). The pressure measurement is taken at $K2$.

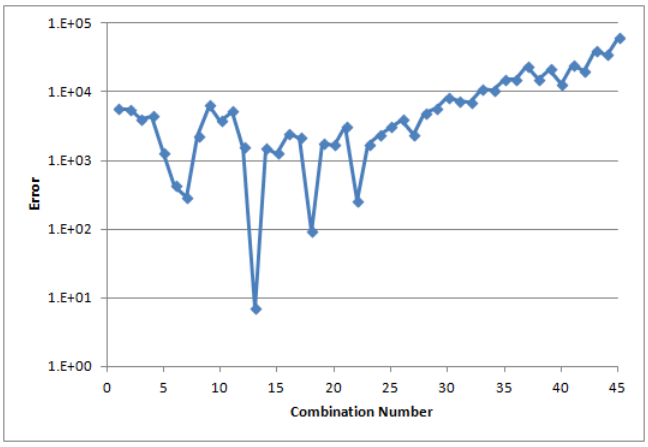

Figure 4.19: Results obtained in the identification of multiple sources in a vibro-acoustic cavity.

The minimum error occurs in combination 13. This combination refers to the sources applied at nodes 254 and 259. These two nodes are the nodes where the sources are actually located, meaning that the program was able to identify the correct pair of sources.

In the previous example, with only one source, one studied the influence of noise addition to the

measured signal in the quality of the results. The same procedure is conducted in this example, and several levels of noise (in %) are added to the measured signal. The results of the source identification problem with noise addition are presented in the figure below.

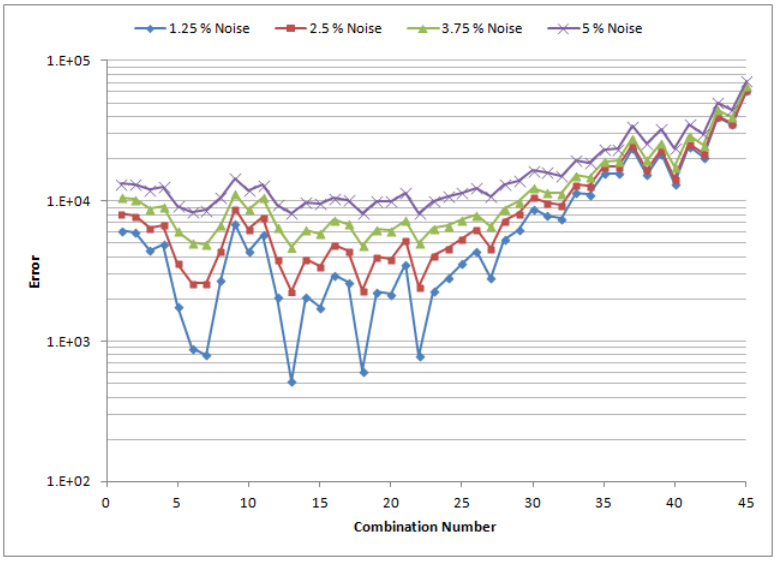

Figure 4.20: Results obtained in the identification of multiple sources in a vibro-acoustic cavity, with noise in the measured signal.

Analysing the data in figure 4.20, one can state that for the higher levels of noise addition, it is no longer possible to clearly identify the correct combination from direct observation of the results. In table 4.11 it is presented the accumulated error of the four more pronounced minimums for every level of noise addition.

	Combination Number			
	7	13	18	22
Error (1.25 % Noise)	798.47	518.95	614.34	781.45
Error (2.5 % Noise	2586.66	2274.93	2323.19	2464.97
Error (3.75 % Noise)	4917.65	4688.19	4809.95	5001.59
Error (5 % Noise)	8519.30	8154.62	8124.29	8221.53

Table 4.11: Accumulated error of the more pronounced minimums in the identification of multiple sources in the vibro-acoustic cavity, with noise in the measured signal.

Table 4.11 shows that for a 5% noise addition, the program is no longer able to pick the correct combination of sources. For this level of noise, the absolute minimum is located in combination 18, while the correct combination of sources is combination 13. So, in this case, the addition of noise compromises the correct functioning of the Matlab® routine.

4.5.2 Experimental Analysis

Using the procedures described in 3.4.2.2, a swept sine wave is generated and conveyed to the vibration exciter connected to point P. The created signal analyses the frequencies from 100 to 700 Hz with 10 Hz substeps. Then, the pressure responses between 200 and 600 Hz are measured by the microphones at points $U1$, $U2$, $K1$ and $K2$ (see figure 4.14(b)), and processed in LabVIEW. The obtained results are compared with the numerical ones.

Changes had to be made in the FE model so that it could predict the behaviour of the experimental vibro-acoustic cavity more accurately. First, since the plate in the experimental setup is connected only to the wooden boards, the boundary conditions of the plate have been changed. Now, the plate's displacement and rotation DOFs are considered to be fixed only on the edges that are touching the wooden boards. In addition, the meshes have been refined to increase the accuracy of the model.

The results obtained with both experimental and numerical models are presented in figure 4.21.

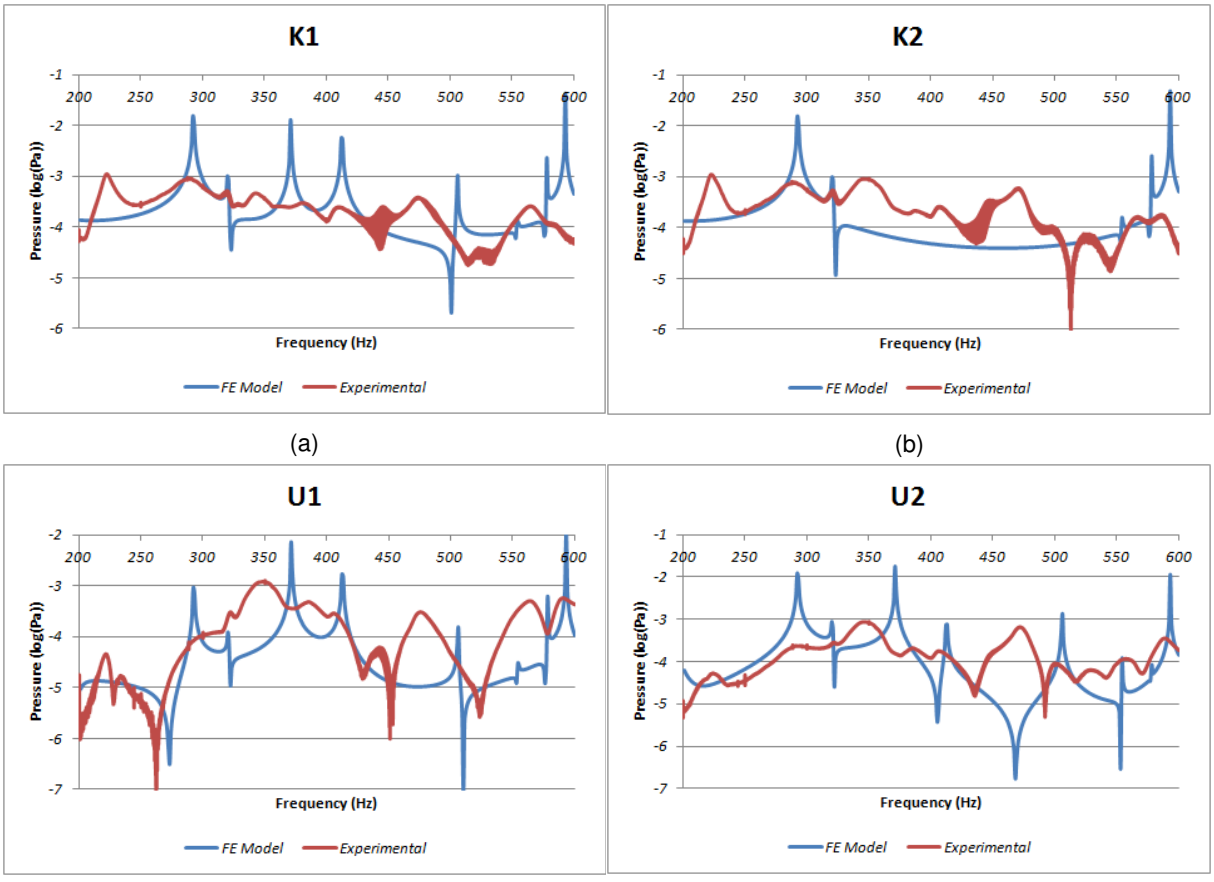

Figure 4.21: Comparison between the experimental and numerical results obtained in the vibro-acoustic cavity analysis.

It is clear that there are some significant differences between the numerical and experimental results. One that is quite clear, is the presence of acoustic damping and absorption in the experimental results, something that is neglected in the FE model. It is also clear that not all the resonances of the numerical model appear in the experimental results, and that there are some deviations between the

resonances and anti-resonances in the experimental and numerical results. These differences are due to the assumptions of a fully reflective boundary and no acoustic damping in the FE model. Furthermore, the results obtained experimentally are polluted with noise, something that may also be responsible for some of the differences presented in figure 4.21. Nevertheless, one can establish some similarities between the numerical and experimental behaviour, particularly in the responses at $U1$ and $U2$, in the frequencies between 200 and 400 Hz. In these cases, despite some deviations, the pressure responses exhibit a somehow similar behaviour.

The vibration in the wooden boards is also measured. The results obtained by the accelerometers are presented in figure 4.22.

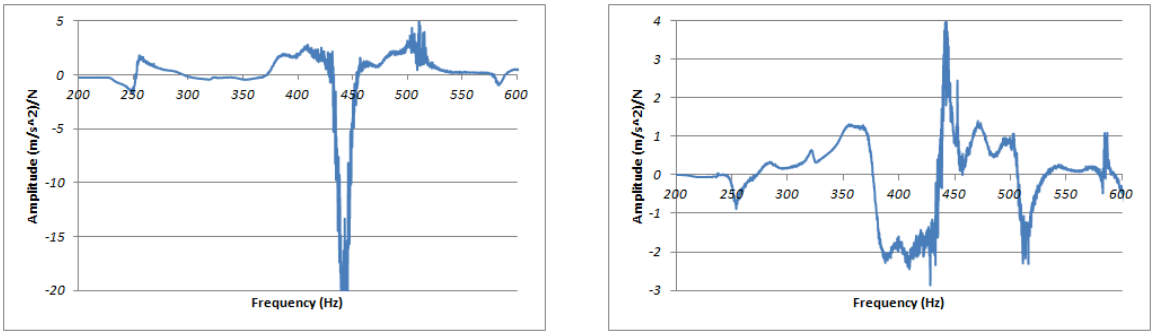

(a) (b)

Figure 4.22: FRFs measured by the accelerometers at the wooden boards at point A (a), and point B (b) (see figure 3.8).

These results show that the wooden boards undergo small vibrations during the experimental procedure. However, there is a significant peak at point A that may be responsible for some of the differences between the numerical and experimental results.

A third accelerometer is placed at point P (point C in figure 3.8) to analyse the vibration of the plate. The numerical and experimental results for the vibration peaks are presented in table 4.12.

Frequency of the Steel Plate Vibration Peaks	Experimental (Hz)	Numerical (Hz)
1	249	292
2	503	412
3	580	578

Table 4.12: Experimental and numerical vibration peaks of the steel plate at point P.

The differences between the results presented in table 4.12 are, most likely, due to the differences in boundary conditions. In the FE model the plate is considered to be fixed along the entire edge, but in the experimental model, the plate is connected to the wooden boards by two small bolts. Therefore, the FE model boundary conditions are more restrictive than the experimental ones.

4.6 Aircraft Interior Analysis

In this section, the results obtained with the methodologies described in section 3.5 are presented. As mentioned before, the acoustic fluid is discretized with FLUID30 FEs, and the shell elements are discretized with SHELL181 FEs. The material properties of the several elements used are presented in the following tables. The coordinates of the points presented throughout this section are related to the coordinate axes presented in figure 3.9.

SHELL181 Finite Elements	
Young's Modulus	205 GPa
Mass Density	7800 kg/m^3
Poisson Ratio	0.3
Thickness	0.002 m

Table 4.13: Material properties of the shell elements used in the FE models of the simplified aircraft interior.

FLUID30 Finite Elements (No FSI)	
Speed of Sound	344 m/s
Mass Density	1.21 kg/m^3
Boundary Admitance	0
Reference Pressure	20×10^{-6} Pa

Table 4.14: Material Properties of the acoustic FEs used in the FE models of the simplified aircraft interior.

FLUID30 Finite Elements (FSI)	
Speed of Sound	344 m/s
Mass Density	1.21 kg/m^3
Boundary Admitance	1
Reference Pressure	20×10^{-6} Pa

Table 4.15: Material properties of the FSI elements used in the FE models of the simplified aircraft interior.

4.6.1 Acoustic Analysis

As mentioned in section 3.5.1, two acoustic models are studied. One has the shape of a half circular tube and the second one has the same shape, but it contains chairs. The presence of the chairs produces significant changes in the acoustic behaviour of the fluid. As the sound is forced to go around the chairs, the sound wave is no longer a plane wave. Furthermore, as the chairs are considered to be rigid and

reflective, the reflection of the sound waves is fairly large in the vicinity of the chairs, which also creates several differences in the acoustic behaviour of this model.

For the first model, the geometry and meshes are presented in figure 4.23.

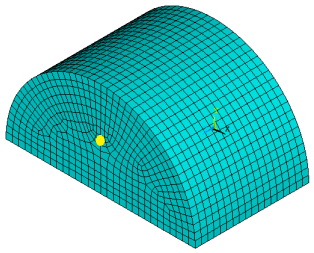

Figure 4.23: Geometry and meshes of the acoustic FE model of the aircraft interior (no chairs).

The maximum length of the elements is set to 0.175 m, which is equivalent to having around 20 FE per wavelength at a reference frequency of 100 Hz. The modal analysis extracts the mode shapes between 0 and 200 Hz. This is a coarse mesh to analyse this frequency range (36 FEs per wavelength should be used) however, using this number of elements per wavelength would require a considerable amount of computational power to perform the transmissibility analysis in Matlab®. Besides this, to verify if the transmissibility analysis is working properly, one has only to ensure that the results obtained using the transmissibility concept match the ones obtained from ANSYS harmonic analysis, and this is independent of the mesh refinement. As long as the same mesh is used in both models, if the models are working correctly, the results should be similar.

For the harmonic analysis, a pressure of 1 Pa is imposed to the node located at coordinates (0;1.25;3) (m), marked with an yellow dot in figure 4.23. The pressure response is measured at the mid-section of the acoustic cavity at the node with coordinates (0;2.5,1.5) (m). The transmissibility function between these two nodes is obtained in the harmonic analysis by dividing the pressure response by the imposed pressure. The results obtained in ANSYS are then compared with the ones obtained in Matlab® using the MDOF transmissibility concept. As the imposed pressure has a constant amplitude and is equal to 1 Pa, the transmissibility function is equal to the pressure response. In figure 4.24 are presented the results obtained from both methods for the pressure response.

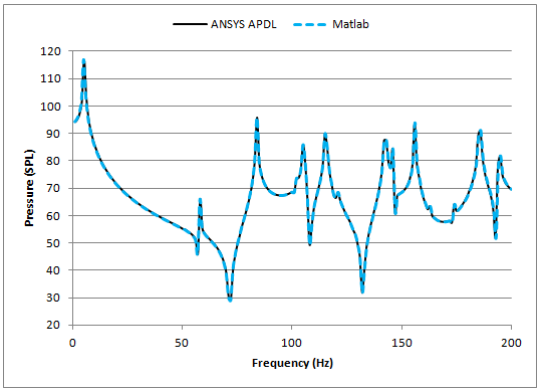

Figure 4.24: Pressure responses obtained using Matlab®'s transmissibility analysis and the FEM applied to the acoustic model of the aircraft interior without chairs.

As expected, the results are ”perfectly” matched. This proves that the transmissibility concept is able to estimate unknown pressures in the fluid domain, knowing the imposed pressure.

The model of the cavity with the chairs is created by subtracting the volumes of the chairs to the half circular tube. As mentioned before, the maximum length of the FEs is set to 0.25 m in all areas, and, since the geometry of this problem does not allow swept meshes, a free mesh is created. The material properties of the FLUID30 FEs are presented in table 4.14, and the geometry and meshes of the fully discretized model are presented in figure 4.25.

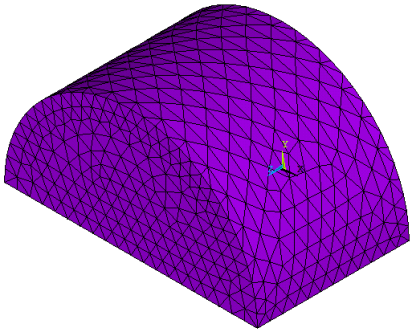

Figure 4.25: Geometry and meshes of the acoustic FE model of the aircraft interior (model with chairs).

In the harmonic analysis, the imposed pressure of 1 Pa is applied to the node with coordinates (0;1.25;3) (m), and the pressure response is measured at the node with coordinates (0.75;1.25;1.5) (m) (node 3427 in ANSYS). This last node is placed in an area where the head of a seated passenger would be. As in the previous case, the modal analysis extracts the natural modes between 0 and 200 Hz, which means that, as before, the used mesh is a coarse mesh. To account the wave distortion and increasing reflections around the chairs, the mesh is more refined in these areas.

Similarly to what was done in the previous case, the results of the harmonic analysis are compared with those obtained in Matlab® using the transmissibility concept. The results for the pressure response obtained from both methods are presented in figure 4.26.

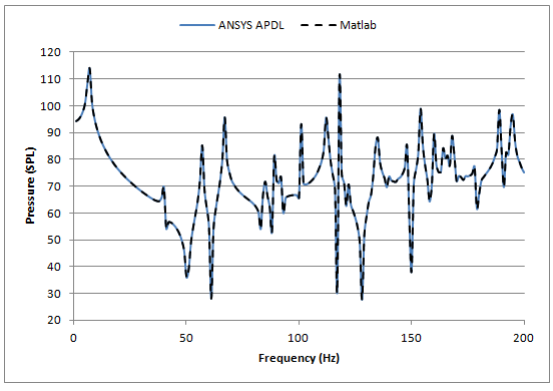

Figure 4.26: Pressure responses obtained using Matlab®'s transmissibility analysis and the FEM applied to the acoustic model of the aircraft interior with chairs.

It can be seen in figure 4.26 that the results obtained from both methods are similar. Again, the transmissibility concept proved to be accurate in predicting unknown pressure responses in this system.

The results presented in figures 4.24 and 4.26 prove that the transmissibility analysis is working properly. Now, it is necessary to evaluate if the transmissibility concept is able to identify the correct source of the disturbance for these last two models.

The Matlab® routine for source localization takes a significant amount of time to run and present the results. These last two models require the analysis of thousands of possible sources, which could take many hours. In order to speed up the process, not all the possible sources are analysed. Furthermore, the error function is computed over a smaller range of frequencies.

For the model without chairs, approximately 80 random nodes containing the correct source are selected, and the error function is analysed between 100 Hz and 109 Hz. The obtained results are presented in figure 4.27.

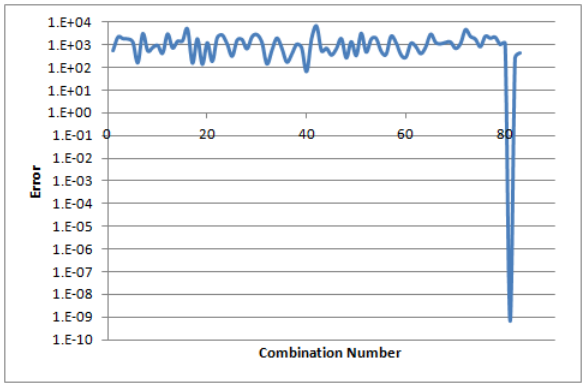

Figure 4.27: Results obtained in the identification of a single source in the acoustic model of an aircraft interior without chairs.

The previous figure shows that the minimum error occurs at the combination number 80, which corresponds to equation 8003. The mapping file states that equation 8003 matches node 31, which corresponds to the node where the pressure is imposed. This means that the program is able to pick the correct source from a set of possible locations.

Once the model with chairs contains less nodes, it is possible to study a larger set of possible sources. In this case, 1375 possible sources are studied and the error function is studied between 100 and 109 Hz. The obtained results are presented in figure 4.28.

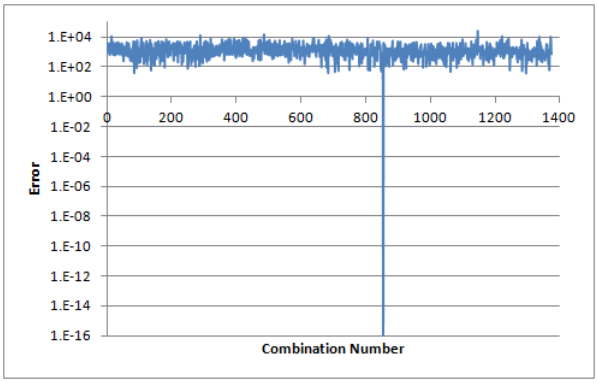

Figure 4.28: Results obtained in the identification of a single source in the acoustic model of an aircraft interior with chairs.

The minimum error occurs for combination 854, which corresponds to equation number 1710. The mapping file states that equation 1710 corresponds to node number 1218, which is the node where the pressure is imposed.

Since in the previous analyses not all the nodes are analysed, one cannot guarantee that the transmissibility matrix that solves the problem is unique. The model without chairs has symmetry in relation to the plane that passes through the mid-section (Z=1.5 m). This means that a load applied at the symmetric node might produce the same results as the ones obtained. This problem appears in the vibro-acoustic analysis and the importance of finding an optimum position for the sensor is discussed there.

4.6.2 Single Source Vibro-Acoustic Analysis

The model without chairs is remeshed with FLUID30 acoustic FEs with a maximum length of 0.5 m. This new mesh is quite coarse, which means that the range of frequencies under analysis has to be reduced. The model is now being analysed between 0 and 50 Hz, which gives around 28 FEs per wavelength at a reference frequency of 25 Hz.

Before studying the vibro-acoustic behaviour of the model with chairs, three different vibro-acoustic models are created from the acoustic model without chairs:

- A model with the shell inserted in the two vertical walls, at Z=0 m and Z=3 m;
- A model with the shell inserted in the two vertical walls and on the floor (Y=0 m);
- A model with the shell inserted around the entire domain.

The shell is discretized with SHELL181 FEs with the material properties defined in table 4.13. The elements touching the shell elements are set to FSI elements using the material properties in table 4.15, and the remaining acoustic elements keep the same properties as before. The displacement and rotation DOFs are fixed on the shell's edges, and the dynamic load is imposed at the node with coordinates (0;1.25;3) (m), along the Z direction. The amplitude of the dynamic load is equal to 1 N, and the node where it is applied is the same for all the three models described earlier.

Modal and harmonic analyses are conducted for all the three models. In the first two models, the pressure response is measured at the node with coordinates (0;2.5;1.5) (m). In the third model, the pressure response is measured at the node with coordinates (0;1.25;1.5) (m).

The transmissibility is obtained in the harmonic analysis by dividing the pressure response amplitude with the amplitude of the imposed displacement. Using the MDOF transmissibility concept, the results for the transmissibility are also obtained in Matlab® using the methodologies described in section 3.5. The results obtained with both methods for the three models described are presented in the following figures.

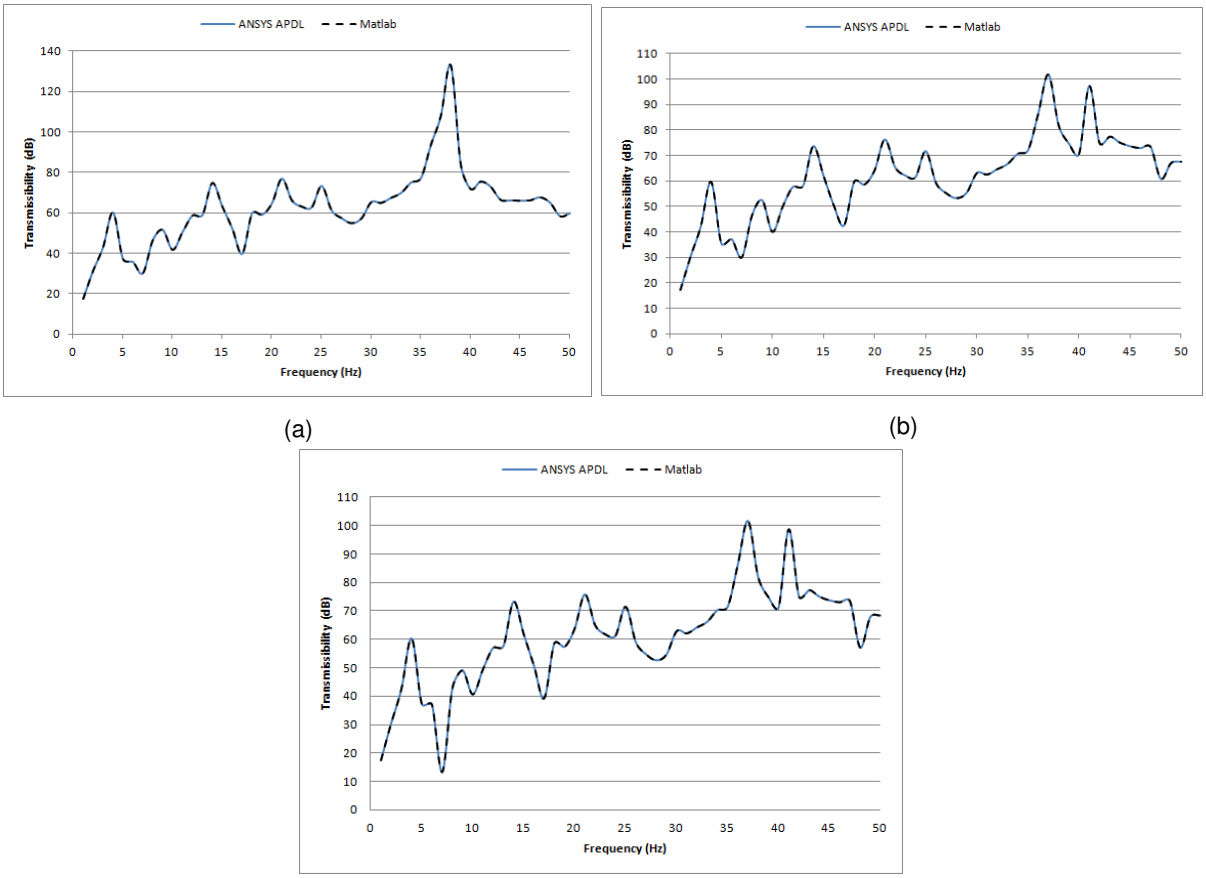

Figure 4.29: Results obtained using Matlab®'s transmissibility analysis and the FEM applied to the several vibro-acoustic models of the aircraft interior without chairs: the model with two vertical walls (a); the model with the vertical walls and floor (b); the model with the shell around the entire fluid domain (c).

The plots in figure 4.29 show that the transmissibility functions obtained with the transmissibility concept are coincident with the transmissibility functions obtained from the harmonic analysis. This proves that, for a certain known displacement on the structural shell of a vibro-acoustic system, the transmissibility concept is able to estimate unknown pressures at certain locations of the system.

The meshes of the model with chairs are maintained, and shell elements are inserted around the entire fluid domain. The material properties of the FEs used in this model are the same as in the previous examples. The displacement and rotation DOFs are constrained on the edges of the structural shell, and the dynamic load is applied at node 30 with coordinates (0;0;1.5) (m), along the Y direction. The pressure response is measured at node 737 with coordinates (0.75;1.25;1.5) (m).

The modal and harmonic solutions are conducted in ANSYS and the transmissibility analysis is done in Matlab®. The obtained results are presented in figure 4.30.

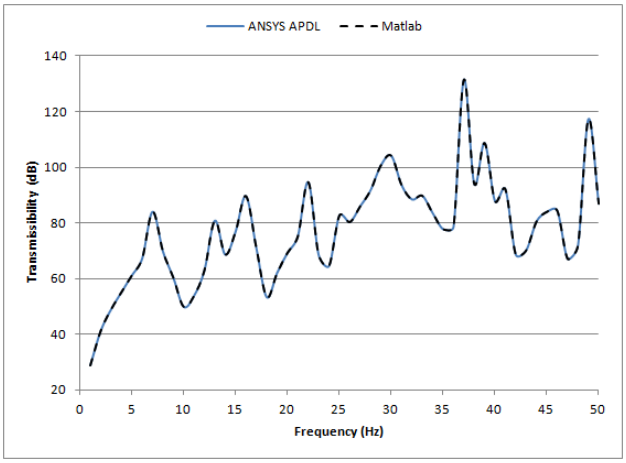

Figure 4.30: Results obtained using Matlab®'s transmissibility analysis and the FEM applied to the vibro-acoustic model of the aircraft interior with chairs.

The plots in figure 4.30 prove, once more, that the transmissibility functions obtained from both methods are similar.

The source localization algorithm is also applied to these vibro-acoustic systems. Using a coarser mesh in the vibro-acoustic systems without chairs, makes the analysis of all the nodes possible. The results for the model without chairs and with two vertical walls are presented in figure 4.31.

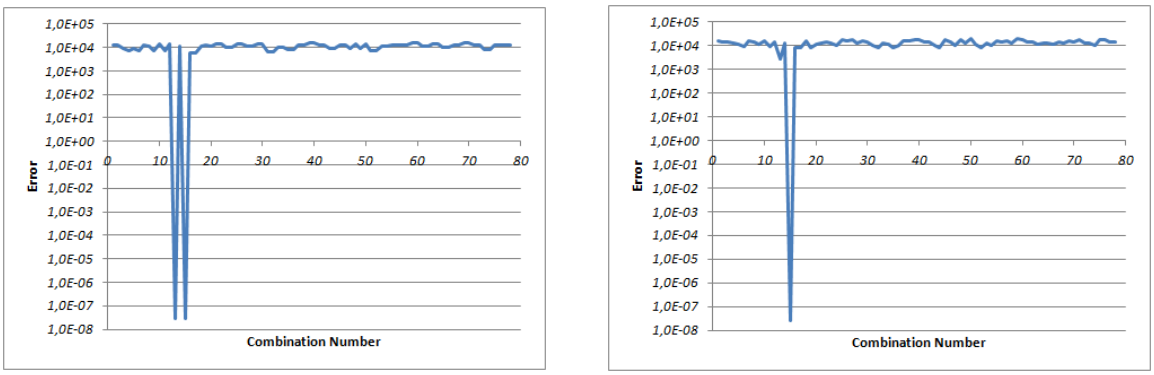

(a) (b)

Figure 4.31: Results obtained with the source localization algorithm applied to the vibro-acoustic model of the aircraft interior with two vertical walls. The results obtained with the sensor located at point (0;2.5;1.5) (m) are presented in (a), and the results obtained with the sensor located at point (0;2.5;2) (m) are presented in (b).

In this case, when the sensor is placed at point (0;2.5;1.5) (m) the program detects two sources. This happens because the source localization problem is an inverse problem that is usually ill-conditioned, and might lead to multiple solutions. In this case, the problem has symmetry with relation to the plane Z=1.5 m, that passes through the point where the sensor is placed. As a consequence, when the load is imposed in the symmetrical position (at the same place but in the other wall), the results for the pressure response are similar. This simple example calls for a better placement of the sensor when performing source localization. The problem of optimum sensor placement is a complex problem, and is described in more detail in [57]. When the sensor is placed at point (0;2.5;2) (m), only one source is identified.

The combination number 15 is identified by the program as the one that minimizes the error. This combination corresponds to node 5 in ANSYS, which is the node where the dynamic load is imposed. In the studied case, there is only one plane of symmetry, yet some cases might appear where the loading situation has many possible symmetries. This scenario may deceive the program and lead it to identify many sources. From the analysis of this example, one may conclude that the sensor must be placed, if possible, at a point that avoids such symmetries.

When the floor is added to the vibro-acoustic system, one must apply the source localization algorithm to the displacement DOFs along the Z and Y directions. As a consequence, two analyses are necessary: one to study the displacements along the Z direction, and a second one to study the displacements in the Y direction. The results of the analysis of the displacements in the Z direction are presented in figure 4.32, and the results of the analysis of the displacements in the Y direction are presented in figure 4.33.

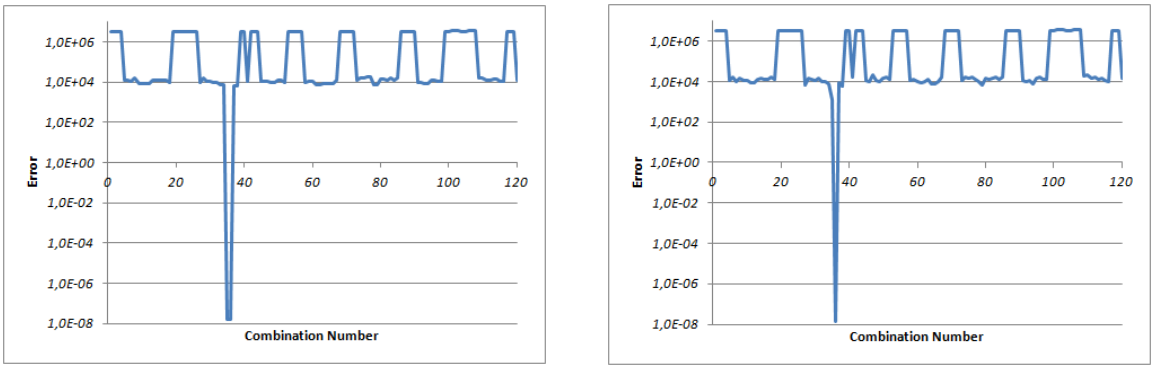

(a) (b)

Figure 4.32: Results obtained with the source localization algorithm applied to the vibro-acoustic model of the aircraft interior with walls and floor. The results obtained with the sensor located at point (0;2.5;1.5) (m) are presented in (a), and the results obtained with the sensor located at point (0;2.5;2) (m) are presented in (b).

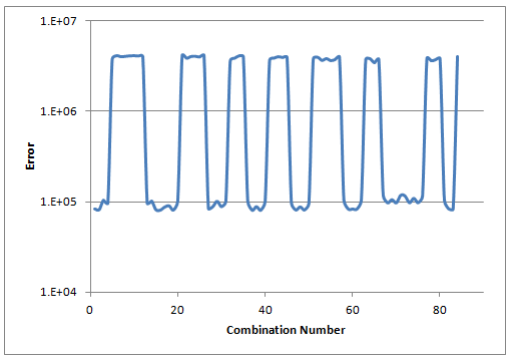

Figure 4.33: Results obtained with the source localization algorithm for the UY DOFs in the vibro-acoustic model of an aircraft interior with walls and floor. These results were obtained with the sensor located at point (0;2.5;2) (m).

Analysing the two previous figures, one can take several conclusions:

- When the sensor is placed at point (0;2.5;1.5) (m) the program picks, once more, two sources. The

cause of this was already explained earlier in this section, and this problem is solved by moving the sensor to point (0;2.5;2) (m);

- In the plots, one can see that there are some combinations in which the error increases significantly. These combinations correspond to displacements that are not normal to the surface of the shell. As the coupled vibro-acoustic FEM is defined for normal displacements, these points are not valid.
- The displacement at the source is in the Z direction therefore, the analysis in the Y direction was not able to identify any source.

According to the results in figure 4.32, the source is located in combination number 36, which corresponds to node number 5 in the ANSYS model. This is the node where the dynamic load was applied. Therefore, the program is able to identify the correct source.

The next system has shell elements around the entire fluid domain. To analyse all possible sources of displacement one should analyse the displacements in the Z direction, in the Y direction and then, solve the problem again but in cylindrical coordinates, in order to analyse the displacements normal to the cylindrical shell that makes the ceiling of the enclosure. Since trying all these scenarios would take considerable time, one decided to analyse only the sources of displacement in the Z direction. The results obtained for two possible sensor placements are presented in figure 4.34.

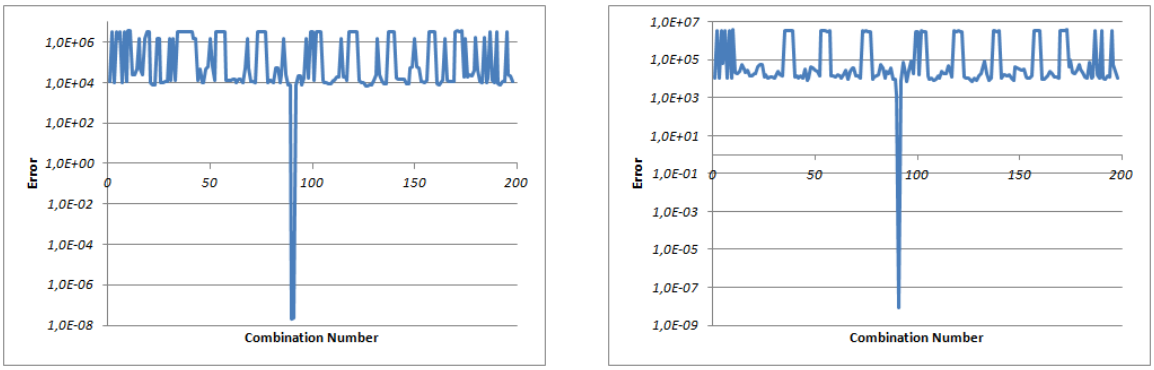

(a) (b)

Figure 4.34: Results obtained with the source localization algorithm applied to the vibro-acoustic model of the aircraft interior with shell around the entire fluid domain. The results obtained with the sensor located at point (0;1.25;1.5) (m) are presented in (a), and the results obtained with the sensor located at point (0;1.25;2) (m) are presented in (b).

Looking at the results, it is possible to see that the algorithm picks two sources when the sensor is located at point (0;1.25;1.5) (m), and only one source when the sensor is located at point (0;1.25;2) (m). Again, it goes to show that proper sensor placement is key for obtaining correct results. The minimum error occurs in combination number 91, which corresponds to the UZ DOF at node 5. The actual displacement is applied at this node.

The source localization algorithm for the vibro-acoustic system with chairs is the same as for the previous system. In order to get a complete analysis of the problem, one should test the possible displacement sources in the Z direction, in the Y direction and then, repeat the analysis in cylindrical

coordinates to analyse the displacements normal to the cylindrical shell. This procedure would take, like in the previous example, a significant amount of time. Therefore, the analysis is only conducted in the UY DOFs (displacements in the Y direction). Once the dimensions of the matrices of this system are quite large, studying only the possible sources of displacement in the Y direction takes a long time. To overcome this issue, only a set of 123 possible sources (containing the correct one) are studied. The frequencies are analysed between 35 and 39 Hz. The obtained results are presented in figure 4.35.

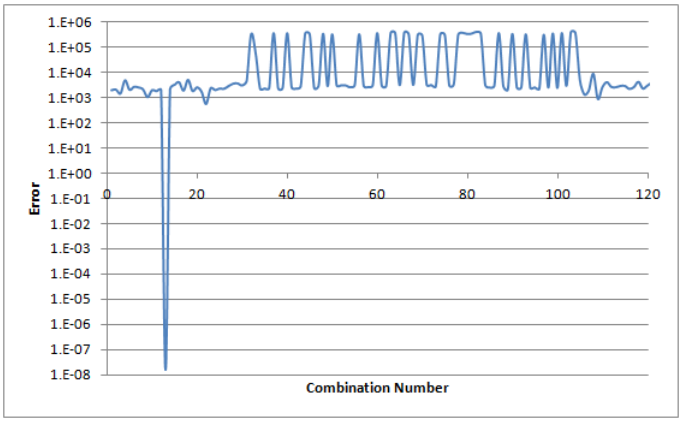

Figure 4.35: Results obtained with the source localization algorithm for the vibro-acoustic aircraft interior with chairs.

In this case there was no need to test different sensor placements. Given the position of the applied load, there are no possible symmetries in the system. The addition of the chairs undoes the symmetry that existed in the previous examples. However, this does not mean that the position of the sensor is optimal. If the source was located at a different point in the system, the identification of multiple sources could still be a problem. When choosing a position for the sensor, one has to carefully study the geometry and mode shapes of the system to make an informed decision. Yet, as previously stated, the problem of optimum sensor placement is complex and out of the scope of this work.

Like in the previous cases, the program retrieves points where the error is fairly large. In the developed Matlab® code, the type of DOF to analyse is inserted by the user. The program then selects all these DOFs in the mapping file and analyses them. Only looking at the mapping file, it is not possible to evaluate if the displacement is normal to the structural shell. This makes the elimination of these nodes quite difficult. One problem that arises from this, is that the same nodes are tested many times for different DOFs, reducing the overall performance of the implemented algorithm.

Looking at the results presented in figure 4.35, the minimum error can easily be identified. It is located in combination number 13. This combination corresponds to an imposed displacement at node 30 along the Y direction. This is the correct loading situation.

It is important to notice that in a real life situation, one would have to evaluate all the sources in order to find the correct one. In these examples, the location of the source is well known and, therefore, one can only test a few possible locations to prove that the concept works.

4.6.3 Multiple Source Vibro-Acoustic Analysis

In this analysis, the last system is modified to have only two vertical walls at both ends of the acoustic domain. Then, two dynamic loads (1 N) are applied, one in each wall, at coordinates (0,1.35,3) (m) (node 1218) and at coordinates (0,1.35,0) (m) (node 1365). A harmonic analysis is conducted with the given loads, and the pressures are measured in nodes 2183 and 696 with coordinates (0,1.25,1.5) (m) and (-0.1,1.25,1.5) (m) respectively. The transmissibility analysis is conducted in Matlab® and the results from both analyses are obtained.

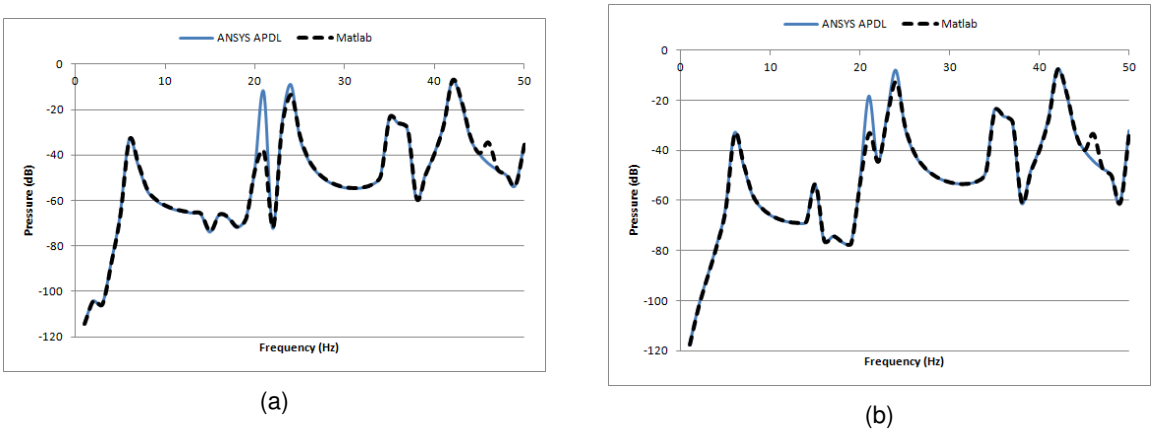

(a) (b)

Figure 4.36: Comparison between the results obtained in the vibro-acoustic aircraft interior with chairs, using ANSYS harmonic analysis and Matlab®'s multi-point transmissibility analysis for a measured pressure at: a) node 2183; b) node 696.

The results in figure 4.36 present some deviations between the results obtained from ANSYS and Matlab® . However, the transmissibility concept can still produce an accurate estimate in the majority of the analysed frequency range. The presented deviation might be due to the presence of cross-talk between both sources. This means that in the present case, despite being 3 meters apart, these two sources still influence each other in such a way that the transmissibility concept cannot accurately predict.

Transmissibility analysis in the presence of cross-talk can be challenging, since it is not easy to determine the level of cross-talk between both sources. In addition, the level of cross-talk between the two sources appears to vary with the frequency. Although some ways to quantify the presence of cross-talk in transmissibility analyses are presented in [22], the cross-talk compensation in these analyses is still quite undeveloped. As a consequence, the presence of cross-talk is still a limitation in multiple source transmissibility analysis.

5 Conclusions

The main purpose of this work is to develop a simple methodology for the identification of sources in simple vibro-acoustic systems using the transmissibility concept. To do so, one started by studying the applications of the transmissibility concept in the fields of vibration, acoustics, and vibro-acoustics, and after verifying some of the methodologies developed by previous authors, these were adapted to the problem of source identification. However, the methodologies developed throughout this work did not focus only on the identification of sources, but also on reducing the computational effort, and, therefore, the simulation time that is required for solving these problems.

The algorithms developed for the identification of sources in vibro-acoustic systems made possible the identification of one or more sources of displacement, as long as there is no cross-talk between multiple sources. The methodology used in the analysis of these problems requires the extraction of the global matrices from ANSYS. Even though there is some uncertainty on how these matrices are retrieved by the FE program, some advances are made. It is now known that for obtaining the vibro-acoustic transmissibility matrix in vibro-acoustic systems, one must use equation 3.12 instead of equation 2.103. This does not mean that equation 2.103 is wrong, it means that this equation must be adapted to suit ANSYS global matrices. By unraveling this detail concerning the global matrices, it is now possible to use the transmissibility concept in vibro-acoustic problems with more than one source of displacement.

Another complication that is pointed out by previous authors in this area (for example in [16]), is the simulation time required to perform the transmissibility analyses, an issue that was also present in this work. As a consequence, a methodology for extracting only the required entries of the receptance matrix is proposed. The results obtained throughout the present work using this new methodology prove its effectiveness. In fact, using the proposed methodology, one was capable of reducing significantly the simulation time, something that enabled the analysis of more complex problems with larger and/or more refined numerical models.

The numerical analysis of several vibro-acoustic systems proved that it is possible to estimate unknown pressures at some points of the fluid domain, using the measurements of certain displacements on the elastic shell. It also proved that the solution for the vibro-acoustic source localization might not be unique. Since the source identification problem is an inverse problem that is usually ill-conditioned, sometimes, the program might identify multiple sources. The present work presented some examples of this, and concluded that such problems may be solved by finding a more suitable position for the

sensor. In fact, the placement of sensors in symmetries or nodal lines can be counter-productive, once it may originate this problem. Finding an optimal sensor placement can be exhaustive. However, this work proves that avoiding symmetries may be a good starting point to avoid an ill-conditioned inverse problem.

The experimental results presented throughout this work exhibited significant differences when compared with the results of the numerical models. Such differences did not allow the comparison between experimental and numerical transmissibilities. However, by using more adequate materials in the experimental setup and by updating the numerical models, one may be capable of improving these results.

Summarizing, one may conclude that the objectives outlined in the beginning of this work were accomplished. Furthermore, the author hopes that his advances may contribute for some of the challenges that noise and vibration engineers are currently facing.

Future works in this area may address:

- The study of fluid-structure vibro-acoustic transmissibility, including the estimation of unknown displacements using measurements of the known pressures. The study of these systems may also include the problem of source identification.
- The study of cross-talk cancellation in acoustic and vibro-acoustic systems.
- Possible updates in the used FE models and experimental procedures. Applying the vibro-acoustic source localization algorithm should be one of the next steps in further research.
- The development of SEA based methodologies for transmissibility analysis in ”high frequency problems”.

The areas of acoustic and vibro-acoustic transmissibility offer many possible applications in current OTPA technologies. As a consequence, producing advances and knowledge in this area may be an important contribution to the engineering community.

References

[1] M. M. Neves and N. M. M. Maia. Estimation Of Applied Force Using The Transmissibility Concept. *Proceedings of ISMA2010 Including USD2010*, Pages 3887-3898, 2010.

[2] R. Jiao, J. Zhang. Vibro-acoustic modeling of a rectangular enclosure with a flexible panel in broad range of frequencies and experimental investigations. Journal of Vibroengineering, Pages 2683-2692, DOI: 18. 10.21595/jve.2016.16888, 2016.

[3] J. Wijker. Statistical Energy Analysis. In: Random Vibrations in Spacecraft Structures Design. Solid Mechanics and Its Applications, vol 165, Springer, Dordrecht, DOI: 10.1007/978-90-481-2728-3_4, 2009.

[4] V. M. N. Martins. Estimating Vibration, Acoustic and Vibro-Acoustic responses using Transmissibility Functions. Master Thesis, Instituto Superior Técnico, 2019.

[5] N. M. M. Maia, A. P. V. Urgueira, and R. A. B. Almeida. Whys and Wherefores of Transmissibility. In D. F. Beltran-Carbajal, editor, *Vibration Analysis and Control - New Trends and Developments*, chapter 10, Pages 187-216, ISBN 978-953-307-433-7, September 2011.

[6] Y. E. Lage, M. M. Neves, N. M. M. Maia, and D. Tcherniak. Force transmissibility versus displacement transmissibility. *Journal of Sound and Vibration*, Pages 5708-5722, ISSN 10958568, DOI: 10.1016/j.jsv.2014.05.038, 2014.

[7] Y. Lage, N. Maia, M. M. Neves. Force Magnitude Reconstruction Using the Force Transmissibility Concept. Shock and Vibration, Volume 2014, Pages 1-9, DOI: 10.1155/2014/905912, 2014.

[8] N. M. M. Maia, Y. E. Lage, M. M. Neves. Recent Advances on Force Identification in Structural Dynamics. In D. F. Beltran-Carbajal, editor, *Advances in Vibration and Structural Dynamics*, chapter 6, Pages 103-132, ISBN 978-953-51-0845-0, DOI: 10.5772/3421, December 2012.

[9] Y. Lage, N. Maia, M. M. Neves, A. Ribeiro. A Force Identification Approach for Multiple Degree of Freedom Systems. Conference Proceedings of the Society for Experimental Mechanics, Series 4, DOI: 10.1007/978-1-4419-9831-6_7, 2010.

[10] N. M. M. Maia, M. M. Neves, T. A. N. Silva. Transmissibility versus damage detection. In D. Moens, W. Desmet, B. Pluymers, & W. Rottiers (Eds.), Proceedings of ISMA 2018 - International Conference on Noise and Vibration Engineering and USD 2018 - International Conference on Uncertainty in Structural Dynamics (Pages 3901-3911), KU Leuven, Departement Werktuigkunde, 2018.

[11] R. Sampaio, N. Maia, A. Ribeiro, J. Silva. Damage Detection Using the Transmissibility Concept. Proceedings of the Sixth International Congress on Sound and Vibration (ICSV 6), Pages 2559-2568, 1999.

[12] A. Ribeiro, N. Maia, J. Silva. Experimental Evaluation of the Transmissibility Matrix. In IMAC XVII Orlando - Florida, Pages 1126-1129, 1999.

[13] A. Ribeiro, M. Fontul, J. Silva, N. Maia. Transmissibility Matrix in Harmonic and Random Processes. Shock and Vibration, Pages 563-571, DOI: 10.1155/2004/438986, 2014.

[14] C. Devriendt, F. Presezniak, G. De Sitter. Operational acoustic modal analysis using transmissibility measurements. In Proceedings of the ICSV 16, Krakow, 2009.

[15] C. Devriendt, P. Guillaume. The use of transmissibility measurements in output-only modal analysis. Mechanical Systems and Signal Processing, 21 (7), Pages 2689 - 2696, DOI: 10.1016/j.ymssp.2007.02.008, 2007.

[16] C. D. V. Guedes. Localização de Fontes Acústicas em Interiores de Avião Usando o Conceito de Transmissibilidade. Master Thesis (In Portuguese), Instituto Superior Técnico, 2016.

[17] C. D. V. Guedes and M. M. Neves. A model-based acoustic source localization using the MDOF transmissibility concept. In *Proceedings of the EuroRegio 2016, June 13-15*, Pages 1-10, Porto, Portugal 2016.

[18] D. Tcherniak, A. P. Schuhmacher. Application of Transmissibility Matrix Method to NVH Source Contribution Analysis. In IMAC XXVII, A Conference and Exposition on Structural Dynamics, Orlando, Florida USA, 2009.

[19] A. Schuhmacher. Techniques for Measuring the Vibro-Acoustic Transfer Function. Sound & vibration, Pages 6-12, March 2010.

[20] A. J. F. Cartaxo. Caracterização de Filtros Acústicos Baseada no Método dos Elementos Finitos. Master Thesis (In Portuguese), Instituto Superior Técnico, 2007.

[21] A. G. Cartaxo, M. M. Neves, S. N. Y. Gerges, J. L. B. Coelho. Verification and Validation of a Fluid-Structure Interaction Model used to characterize Sound Attenuation by a periodically spaced array of Cylinder Elements. *In Proceedings of ICSV 16, 5-9 July, edited by M.Pawelczyk and D. Bismor*, Krákow, Poland 2009.

[22] M. M. Neves, H. Policarpo, N. Maia, D. Tcherniak. A Note on the Use of Vibro-Acoustic Transmissibility to Estimate Vibro-Acoustic Responses. Proceedings of the International Conference on Structural Engineering Dynamics (ICEDyn 2019), Viana do Castelo, 2019.

[23] N. Sharma, T. R. Mahapatra, S. K. Panda. Numerical Study of Vibro-Acoustic Responses of Un-Baffled Multi-Layered Composite Structure under Various End Conditions and Experimental Validation. Latin American Journal of Solids and Structures, Pages 1547-1568, DOI: 10.1590/1679-78253830, 2017.

[24] M. J. Han, C. H. Lee, T. W. Park. Vibro-Acoustic Response in Vehicle Interior and Exterior Using Multibody Dynamic Systems Due to Cleat Impacts. International Journal of Automotive Technology, Vol 21, No. 3, Pages 591-602, DOI: 10.1007/s12239-020-0056-1, 2020.

[25] M. Barcan, I. Chirica, E. F. Beznea. Numerical Vibro-Acoustic Analysis of a Ship Compartment Structure. ITM Web of Conferences 29 02015, DOI: 10.1051/itmconf/20192902015, 2019.

[26] H. Yenerer, A. C. Stan, P. Sendur, I. Basdogan. Vibro-Acoustic Analysis of a Heavy Duty Truck Cabin. ASME 2014 12th Biennial Conference on Engineering Systems Design and Analysis, ESDA 2014. 2, DOI: 10.1115/ESDA2014-20559, 2014.

[27] E. Carletti, G. Miccoli, F. Pedrielli, G. Parise. Vibroacoustic Measurements and Simulations Applied to External Gear Pumps. An Integrated Simplified Approach. Archives of Acoustics. Vol. 41, No. 2, Pages 285–296, DOI: 10.1515/aoa-2016-0028, 2016.

[28] P. Czech, Z. Stanik, J. Warczek, M. Witaszek, K. Witaszek. Vibroacoustic evaluation of technical condition of the combustion engine water pump. In XII Konferencja naukowo-techniczna, Pages 2855-2862, 2015.

[29] M. Weber, T. Kletschkowski, S. Delf. Identification of noise sources by means of Inverse Finite Element Method using measured data. The Journal of the Acoustical Society of America, Pages 411-416, DOI: 10.1121/1.2932813, June 2008.

[30] M. Weber, T. Kletschkowski and B. Samtleben. Identification of Noise Sources by Means of Inverse Finite Element Method. In Proceedings of the COMSOL Conference Hannover, 2008.

[31] I. L. Hidalgo, A. Nabarrete, M. Santos. Structure-borne transmissibility evaluation through modeling and analysis of aircraft vibration dampers. Journal of Aerospace Technology and Management, Vol 3, No. 2, Pages 147-158, DOI: 10.5028/jatm.2011.03021611, 2011.

[32] R. Pirk, C. Souto, G. Guimarães, L. Goes. Acoustics and Vibro-Acoustics Applied in Space Industry, Pages 479 - 512, Chapter 20, Publisher IntechEditors, Marco G. Beghi, DOI: 10.5772/49966, August 2013.

[33] P. Bouillard, J. Almeida, V. Decouvreur, T. Mertens. Some challenges in computational vibro-acoustics: Verification, validation and medium frequencies. Article In Computational Mechanics, Pages 1-3, DOI: 10.1007/s00466-006-0153-7, January 2008.

[34] Siemens PLM Software. What is transfer path analysis. URL https://www.plm.automation.siemens.com/en_us/Images/ What_is_transfer_path_analysis_tcm1023-220904.pdf. Accessed March 2020.

[35] M. V. Van der Seijs, D. de Klerk, D. J. Rixen. General framework for transfer path analysis: History, theory and classification of techniques. Mechanical Systems and Signal Processing 68-69, Pages 217-244, DOI: 10.1016/j.ymssp.2015.08.004, 2015.

[36] P. Gajdatsy, K. Janssens, L. Gielen, P. Mas, H. Van der Auweraer. Critical assessment of operational path analysis: Mathematical problems of transmissibility estimation. The Journal of the Acoustical Society of America, Pages 5463-5468, DOI: 10.1121/1.2935749, June 2008.

[37] K. Janssens, P. Gajdatsy, L. Gielen, P. Mas, L. Britte, W. Desmet, H. Van der Auweraer. OPAX: A new transfer path analysis method based on parametric load models. Mechanical Systems and Signal Processing, Pages 1321-1338, DOI: 10.1016/j.ymssp.2010.10.014, 2015.

[38] H. F. D. Policarpo. Experimental and numerical acoustic and vibro-acoustic characterization of a wooden cavity, Research fellowship on the framework of Laboratório Associado de Energia, Transportes e Aeronáutica-EMS/50022 UID/EMS/50022/2013 Technical Report September, Instituto Superior Técnico, Lisbon, Portugal, 2017.

[39] Ph 136 abc. Applications of Classical Physics. Version 1212.1.K. URL http://www.pmaweb.caltech.edu/Courses/ph136/yr2012/1212.1.K.pdf. Accessed May 2020. September 2012.

[40] Equations Of Linear Elasticity, URL:

https://courses.math.ox.ac.uk/node/download_material/2306.pdf. Accessed May 2020. January 2017.

[41] Finite Element Analysis, Formulation of a Spring Element. URL: http://ocw.ump.edu.my/pluginfile.php/9794/mod_resource/content/2/3_Spring_Element_Formulation.pdf. Accessed March 2020.

[42] J. M. Silva, N. Maia. “Vibrações e Ruído”. AEIST – Associação dos Estudantes do Instituto Superior Técnico, Lisboa, Portugal, 2001.

[43] Base Excitation of Dynamic Systems. URL :https://www.slideshare.net/SondiponAdhikari/base-excitation-of-dynamic-systems. Accessed March 2020.

[44] F. J. P. Lau. Elementos de Aeroacústica. 2017.

[45] I. Rousseau. How Weather Affects Sound. Kama Industries, URL: https://www.kama.co.za/how-weather-affects-sound/. Accessed May 2020. October 2, 2019.

[46] L. Zhang. The Finite Difference Method for the Helmholtz Equation with Applications to Cloaking. URL: https://math.missouristate.edu/Assets/Math/li.pdf, Accessed March 2020.

[47] W. Desmet, D.Vandepitte. Finite Element Method in Acoustics. Proceedings of the ISAAC13 - International Seminar on Applied Acoustics, Leuven, ISBN 90-73802-73-3, 2002.

[48] T. Lodygowsky, W. Sumelka. Limitations in Application of Finite Element Method in Acoustic Numerical Simulation. In Journal of Theoretical and Applied Mechanics, Pages 849-865, Warsaw 2006.

[49] Theory Reference for the Mechanical APDL and Mechanical Applications. 3304(April):724-746, 2009.

[50] Mechanical APDL Command Reference. URL http://www.mm.bme.hu/gyebro/files/ans_help_v182/ans_cmd/Hlp_C_CmdTOC.html. Accessed March 2020.

[51] J. Burkardt. Harwell-Boeing Sparce Matrix File converted to Matlab Sparce Matrix. URL https://people.sc.fsu.edu/~{}jburkardt/m_src/hb_to_msm/hb_to_msm.html. Accessed March 2020, 2014.

[52] C.Howard. Coupled Structural-Acoustic Analysis Using ANSYS. Internal Report, The University of Adelaide, Department of Mechanical Engineering, Pages 1-15, 2000.

[53] I. S. Duff, R. G. Grimes, and J. G. Lewis. User's guide for the Harwell-Boeing sparse matrix collection (Release I). Published by RAL, Chilton, URL: https://cds.cern.ch/record/246109, 1992.

[54] LabView Software Description. URL: https://www.ni.com/pt-pt/shop/labview.html. Accessed October 2020.

[55] N. Martins. Apontamentos de Algebra Linear. Departamento de Matemática do Instituto Superior Técnico. URL: https://www.math.tecnico.ulisboa.pt/~nmartins/ALT17182S.pdf. Accessed April 2020. February 2018.

[56] Dylan Zwick. Math 2270 - Lecture 27: Calculating Determinants. URL: https://www.math.utah.edu/~zwick/Classes/Fall2012_2270/Lectures/Lecture27.pdf. Accessed April 2020, Fall 2012.

[57] H. M. Alqam, A. K. Dhingra. Motion Transmissibility for Load Identification Based on Optimum Sensor Placement. Shock and Vibration, Volume 2019, Article ID 7810686, DOI: 10.1155/2019/7810686, 2019.